Correlations in multiparticle production

Ringnér, Markus

1998

Document Version:
Publisher's PDF, also known as Version of record

Correlations in Multiparticle Production

Markus Ringnér

Department of Theoretical Physics
Lund University

1998

ISBN 91-628-3190-9

Correlations in Multiparticle Production

Markus Ringnér

Department of Theoretical Physics
Lund University, Sweden

Thesis for the degree of Doctor of Philosophy

Thesis Advisor: Bo Andersson

Faculty Opponent: James D. Bjorken

To be presented, with the permission of the Faculty of Mathematics and Natural Sciences of Lund University, for public criticism in Lecture Hall A of the Department of Physics on Wednesday, the 25th of November 1998, at 10.15 a.m.

Organization **LUND UNIVERSITY** Department of Theoretical Physics Sölvegatan 14A 223 62 LUND	**Document Name** **DOCTORAL DISSERTATION** **Date of issue** October 1998 **CODEN:** LUNFD6/(NFTF-1039)/1-18 (1998)
Author(s) Markus Ringnér	**Sponsoring organization**

Title and subtitle

Correlations in multiparticle production

Abstract

Different aspects of the strong interaction in particle collisions are studied. Most of the work is based on the Lund string fragmentation model for hadron production. A model which incorporates interference between identical bosons in the string model is presented. With this model the consequences for the Bose-Einstein effect are investigated in detail. What happens at the end of the QCD cascades is also addressed. It is shown that, with just a few reasonable assumptions, the emission of soft gluons is constrained to produce an ordered field in the form of a helix. A signature of the helix field which should survive fragmentation is presented. Inspired by the Feynman-Wilson gas analogy a partition function for the string model is derived and its properties are investigated.

Key words

QCD, String fragmentation, Bose-Einstein interference, Colour interference, Correlations.

Classification system and/or index terms (if any)

Supplementary bibliographical information	**Language** English
ISSN and key title	**ISBN** 91-628-3190-9
Recipient's notes	**Number of pages** 128 **Price** **Security classification**

Distribution by (name and address)

Markus Ringnér, Dept. of Theoretical Physics,
Sölvegatan 14 A, S-223 62 LUND

Signature _____ **Date** 1998-10-01

To my friends

This thesis is based on the following publications:

I B. Andersson, G. Gustafson, M. Ringnér and P. Sutton
The Feynman–Wilson gas and the Lund model
LU TP 98-15
(accepted for publication in the *European Physical Journal* **C**)

II B. Andersson and M. Ringnér
Bose–Einstein correlations in the Lund model
Nuclear Physics **B 513**, 627-644 (1998)

III B. Andersson and M. Ringnér
Transverse and longitudinal Bose–Einstein correlations
Physics Letters **B 421**, 283-288 (1998)

IV J. Häkkinen and M. Ringnér
Bose–Einstein and colour interference in W-pair decays
European Physical Journal **C 5**, 275-281 (1998)

V B. Andersson, G. Gustafson, J. Häkkinen, M. Ringnér and P. Sutton
Is there screwiness at the end of the QCD cascades?
Journal of High Energy Physics **09**, 014 (1998)

Contents

Introduction

This thesis deals mainly with the properties of final state particles produced in high energy particle processes, in which the strong interaction is active. It is divided into two parts – this introduction followed by five papers.

To give an example of multiparticle production in high energy particle processes this introduction starts off with a schematic picture of the various stages in hadronic e^+e^- events. Most of the work in this thesis is based on the Lund string fragmentation model which will be briefly described. Following this is a motivation for studying correlations. The basic phenomenon of Bose–Einstein correlations is presented using a treatment analogous to quantum optics. This introduction ends with a short summary of the five papers.

The first paper is an investigation of the analogy between multiparticle production in the Lund string fragmentation model and the multiparticle distributions of a classical gas. The following three papers describe a model for incorporating Bose–Einstein correlations in the string model. In the final paper a scenario at the end of the parton cascades is suggested and its consequences for fragmentation are discussed.

Hadron production

Essentially we investigate the high energy process $q\overline{q} \rightarrow$ hadrons. One type of experiment in which this occurs is the collision of electrons and positrons, also called e^+e^- annihilation. The process $e^+e^- \rightarrow \gamma^*, Z^0 \rightarrow q\overline{q} \rightarrow$ hadrons is shown schematically in Fig.(1). The electron and the positron are accelerated and when they collide they may annihilate into a photon or a Z^0. The γ^* or the Z^0 may then split into a quark and an anti-quark. This possibility is described by the theory for electro-weak interactions, which in particular gives the probability for such an event. The $q\overline{q}$-pair is however not directly observed in the experimental detector. Instead a large number of hadrons are

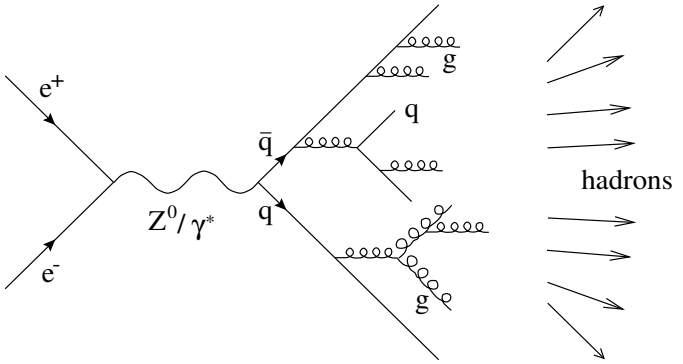

Figure 1: The various stages in a high energy particle process, in which the strong interaction is active. Firstly, the electron and the positron come from the accelerator and they collide. In the collision they may annihilate into a photon or a Z^0, which may split into a quark and anti-quark pair. This first part is governed by the electro-weak interaction. Then the quark and anti-quark radiate gluons, which may radiate further quarks and gluons, in a so-called parton cascade. Finally, there is hadronization, in which the gluons and quarks turn into the hadrons which are observed in the detector. The parton cascade and the hadronization are governed by the strong interaction.

measured. This final step in the process is governed by the strong interaction and it can be divided into two parts. Firstly, there is the parton cascade, where the quark and the anti-quark radiate gluons. The emitted gluons may then radiate more gluons or split into new $q\overline{q}$-pairs, and so on. Secondly, there is the hadronization, in which the produced partons, i.e. the quarks and gluons, turn into the observed particles.

The theory for the strong interaction is called quantum chromo dynamics (QCD). The force field between partons due to QCD is called a colour field and the partons carry what is called colour charge. That free quarks or gluons have never been seen suggests that colour charge is confined. QCD is such that approximate methods have to be used to get predictions and results from the theory.

At short distances and over short times the quarks and gluons can be considered as free particles and the perturbative approximation of QCD (perturbative QCD) works well. The parton cascade is a good example of a process which is well described by perturbative QCD. At larger distances, roughly 10^{-15}m, the perturbative approximation breaks down and one has to use other approaches.

Hadronization is an example of the strong interaction which cannot be cal-

culated using perturbative QCD. As the parton cascade evolves the distance scales become larger. When hadronization sets in the distances are too large for perturbative approximations. One model to describe hadronization which has been very successful when compared with experimental data is the Lund string fragmentation model [1].

The Lund string fragmentation model

At the end of the parton cascade there is a colour force field stretched between the partons. The QCD vacuum surrounding the partons contains both $q\overline{q}$-pairs and gluons. This vacuum will make it energetically favoured to press the colour field between two partons into a tube and the field can be thought of as a string going from parton to parton. This confining of the field is very different from the electro-magnetic field between two electrically charged particles where the field spreads over all space.

Let us consider the simplest case of a quark and an anti-quark going out in opposite directions with a colour field spanned between them. In the Lund string model the colour field is approximated with a massless relativistic string with constant energy-density. This means that as the quark and anti-quark move apart, more and more energy will be stored in the string-like field between them. To observe a free quark in an experiment would imply that it has been completely separated from its partner. The cost of separating a quark rises due to the constant energy-density linearly with the distance and it would therefore cost an infinite amount of energy to release a quark. In this way, the string picture provides an intuitive picture for why quarks not are observed directly in an experiment. When the quarks run out of energy they will be dragged back by the field and they will approach each other again. A $q\overline{q}$-pair will thus yo-yo back and forth and what is finally produced is particles made up of quarks instead of individual quarks.

In a typical experiment the energy of the $q\overline{q}$-pair is so large that the energy stored in the field between them is large enough to produce new $q\overline{q}$-pairs as shown in Fig.(2). There will then be a region between a newly produced quark and anti-quark where the total colour field due to all the quarks and anti-quarks cancels. Since there is no colour field this means that the string breaks into two independent string pieces. One going from the first quark to the new anti-quark and one going from from the new quark to the initial anti-quark. If these new pieces have enough energy they will also break-up. This process will continue into smaller and smaller pieces until only ordinary hadrons remains, as shown in Fig.(2).

The primary hadrons produced in the break-up process may be unstable and

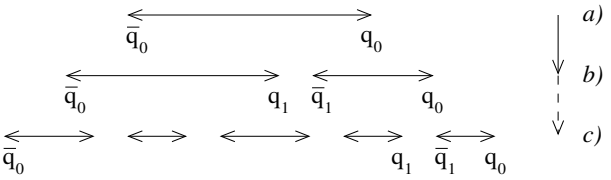

Figure 2: The fragmentation of the string. *a)* The initial quark–anti-quark pair. *b)* The first break-up where a new quark–anti-quark pair is produced. *c)* After several break-ups a set of quark–anti-quark pairs that can be treated as hadrons remains.

decay into stable hadrons. Consequently, what is finally measured is lots of hadrons produced from an initial $q\bar{q}$-pair. However, in the end these particles come out essentially aligned along the initial partons and the parton configuration can in general be reconstructed. Experimental data can in this way be used to learn about the dynamics of quarks and gluons.

In the Lund fragmentation model the hadrons get small transverse momenta, with respect to the string axis. Producing a $q\bar{q}$-pair which is not massless costs energy. This means that they cannot be produced in a point but have to be separated by some distance, consequently the string piece in between them vanishes and its energy is used for the pair production. Such a mechanism can be described by quantum mechanical tunneling and it results in a Gaussian distribution for the transverse momenta.

One of the nice features of the Lund string fragmentation model is that it can be formulated stochastically as an iterative process and it is therefore well-suited for computer implementation.

Correlations

To discriminate between various theoretical predictions and models it is often profitable to go further in the analysis than just simply analysing single-particle spectra. Studying the correlations between the produced hadrons can be important for learning about both parton cascades and hadronization. With the large number of events generated at the LEP accelerator at CERN it has become possible to test various models in more detail.

The correlation studies in this thesis covers aspects of both parton cascades and hadronization. Bose-Einstein correlations is in the case of hadron production a quantum-mechanical effect. The model for it in this thesis is based on the Lund

string fragmentation model, which is essentially semi-classical. The incorporation of quantum-mechanical effects in the Lund model can provide further knowledge about hadronization. The work on what happens at the end of the QCD cascades is an example of where correlation studies of the hadrons give information on the dynamics at parton level. The remaining part of this section is an effort to give some background to the phenomenon of Bose–Einstein correlations, before going into the details of the model in this thesis.

Bose–Einstein correlations

The Bose–Einstein effect, sometimes called the Hanbury-Brown–Twiss (HBT) effect, occurs because the production amplitude for a set of particles should be symmetrised for identical bosons. It was first used in astronomy, where one uses the interference pattern of photons to get information about the size of the photon emitting region, i.e. the size of a particular star [2]. In a high energy collision most of the particles produced are pions and their interference pattern can be analysed in a similar way [3]. Experimentally the Bose–Einstein (BE) effect can be observed as an enhancement of the two-particle correlation function when the two particles are identical bosons and they have very similar energy-momenta. I will in this section give a simplified description of the BE effect analogous to classical optics, to give some flavour of how it arises in the production of identical final state bosons in a high energy collision.

Suppose we have a source producing pions with a space-time dependent wave-function $f(x)$. The total amplitude for emitting a pion with energy-momentum k_1 is then given by

$$A(k_1) = \int dx_i e^{-ik_1 x_i} f(x_i) \tag{1}$$

and the joint amplitude for emitting two pions with k_1 and k_2 is

$$A(k_1, k_2) = A(k_1)A(k_2) = \int dx_i e^{-ik_1 x_i} f(x_i) \int dx_j e^{-ik_2 x_j} f(x_j) \ . \tag{2}$$

It should be noted that Eq.(2) is symmetric with respect to the exchange of the two pions, i.e. it is BE symmetric. The integrals are taken over the space–time distribution of the source which is finite both in time and space.

The normalised two-particle correlation function $C_2(k_1, k_2)$ is defined as

$$C_2(k_1, k_2) = \frac{\langle P(k_1, k_2) \rangle}{\langle P(k_1) \rangle \ \langle P(k_2) \rangle} = \frac{\langle A(k_1)A(k_2)A^*(k_1)A^*(k_2) \rangle}{\langle A(k_1)A^*(k_1) \rangle \ \langle A(k_2)A^*(k_2) \rangle} \ . \tag{3}$$

The chaotic limit

The basic assumption of the BE effect is the chaotic limit. It corresponds to assuming that the phases of the production amplitudes fluctuate wildly for each point in space. The two-particle probability

$$\langle P(k_1,k_2)\rangle = \int dx_i dx_j dx_k dx_l \langle f(x_i)f(x_j)f^*(x_k)f^*(x_l)\rangle e^{-ik_1(x_i-x_k)} e^{-ik_2(x_j-x_l)} \tag{4}$$

will in this limit, if the production amplitudes are Gaussian, only get contributions from two cases: $x_i = x_k, x_j = x_l$ and $x_i = x_l, x_j = x_k$, reducing it to

$$\langle P(k_1,k_2)\rangle = \int dx_i dx_j |f(x_i)|^2 |f(x_j)|^2 \left(1 + e^{i(k_2-k_1)(x_i-x_j)}\right) \ . \tag{5}$$

For the one-particle probability we get in the same limit

$$\langle P(k_1)\rangle = \int dx_i dx_j \langle f(x_i)f^*(x_j)\rangle e^{-ik_1x_i} e^{ik_1x_j} = \int dx_i |f(x_i)|^2 \ . \tag{6}$$

If we introduce the normalised intensity density of the source $\rho(x)$ and its Fourier transform $\tilde{\rho}(k)$

$$\rho(x) = \frac{|f(x)|^2}{\int dx |f(x)|^2} \quad \text{and} \quad \tilde{\rho}(k) = \int dx \rho(x) e^{-ikx} \tag{7}$$

then the normalised two-particle correlation function can be written as

$$C_2 = 1 + |\tilde{\rho}(\Delta k)|^2 \tag{8}$$

where $\Delta k = k_2 - k_1$. We note in particular that $C_2 \to 2$ as $\Delta k \to 0$.

The coherent case

To show the importance of chaotic phases I will consider the complete coherent case where there are well defined phases between different production amplitudes. If we let ϕ_i and f_i denote the phase and the amplitude at the production point x_i respectively, we get

$$\begin{aligned} \langle P(k_1)\rangle &= \int dx_i dx_k f(x_i) f^*(x_k) e^{-ik_1(x_i-x_k)} \\ &= \int dx_i dx_k e^{i(\phi_i-\phi_k)} f_i f_k e^{-ik_1(x_i-x_k)} \end{aligned} \tag{9}$$

and for the joint probability

$$\begin{aligned} \langle P(k_1,k_2)\rangle &= \int dx_i dx_j dx_k dx_l e^{i(\phi_i+\phi_j-\phi_k-\phi_l)} f_i f_j f_k f_l e^{-ik_1(x_i-x_k)} e^{-ik_2(x_j-x_l)} \\ &= \langle P(k_1)\rangle \ \langle P(k_2)\rangle \ . \end{aligned} \tag{10}$$

We note that in the coherent case we find $C_2 = 1$.

Some remarks

At this point it should be clear that chaotic emission of bosons is needed to give rise to the BE effect, i.e. emission of identical bosons is not sufficient. Note however that $\langle P(k_1, k_2)\rangle$ is oscillating with $\Delta k \Delta x$ even in the coherent case, but that the product of the single probabilities contains the same oscillations in this case.

The results are based on plane-wave propagation of the bosons after production, which is reasonable only if there are no final state interactions. This means that the effects of final state interactions have to be taken into account to provide quantitative interpretations from the experimentally measured correlation functions.

If we make a simple model for the source and assume that it is a sphere of emitters with a Gaussian intensity density, described by a radius parameter σ

$$\rho(\mathbf{x}) = \rho(0) e^{-\frac{\mathbf{x}^2}{2\sigma^2}} \tag{11}$$

it corresponds in the chaotic limit to the following C_2

$$C_2(\Delta k) = 1 + e^{-|\Delta \mathbf{k}|^2 \sigma^2} \quad . \tag{12}$$

To extract the radius parameter from experiment

$$C_2(Q) = 1 + \lambda e^{-Q^2 \sigma^2} \tag{13}$$

is usually fitted to the data. $Q^2 = -(\Delta k)^2$ and λ is a parameter introduced to accommodate the fact that the measured two-particle correlation not always is 2 for $\Delta k = 0$. The parameter λ has sometimes been interpreted as the degree of incoherence in the source.

Another assumption in the derivation is that there is no correlation between momentum and the production point in the source of the emitted particles. This is obviously not the case in the string model where the production point of a particle and its momentum are strongly correlated. Such a correlation means that the f-amplitudes are k-dependent and that the 'Bose–Einstein' term

$$\propto \int dx_i dx_j \langle f(x_i, k_1) f^*(x_i, k_2)\rangle \ \langle f(x_j, k_2) f^*(x_j, k_1)\rangle e^{-i\Delta k (x_i - x_j)} \tag{14}$$

will only be sensitive to a part of the source, since for a fixed small Δk the overlap of $f(x_i, k_1)$ and $f^*(x_j, k_2)$ will vanish rapidly as $\Delta x = x_i - x_j$ increases.

It is therefore the distance in production points for which the momentum distributions of the produced particles overlap which will be measured using the BE effect. Thus the Bose–Einstein term is sensitive to something which not necessarily corresponds to the overall size of the source.

The papers

The number of particles produced in a typical event is so large that straightforward calculation of their properties soon becomes prohibitive. The work in this thesis therefore depends on computer implementations of the models. In these, Monte-Carlo (MC) programs, events are generated and their properties can be compared with real experimental events. The MC program based on the Lund string fragmentation model is widely used and it is called JETSET [4].

Paper I

In this paper we use an analogy invented by Feynman that is usually called the Feynman–Wilson gas (FWG) [5]. This analogy links multiparticle production cross-sections to the multiparticle distributions of a classical gas.

Inspired by the FWG analogy, we derive a partition function for the Lund string fragmentation model. Furthermore, we calculate the first two terms in the virial expansion in the density of particles. Our partition function then yields an equation of state which is similar to that of a Van der Waal's gas. The gas is one-dimensional in rapidity. Particles with zero (transverse) mass do not take up any volume in rapidity and in this case the equation of state reduces to that of an ideal gas.

The partition function of the gas is in a simple way related to the multiplicity distribution of its constituent particles. This provides us with a method of investigating the partition function. For a fixed rapidity 'volume', our partition function corresponds to a multiplicity distribution which is very close to a binomial distribution.

The partition function is derived assuming that the particles are ordered in rapidity. This is true for the string break-up vertices. Therefore, we expect that the vertices provide the optimal case to investigate the properties of the partition function. We find that the multiplicity distribution of the vertices is well described by the partition function. Finally, we analyse how this is modified for the particles, both with and without decays of unstable particles.

Paper II

A model for incorporating Bose–Einstein correlations in the Lund model is presented. BE interference between identical bosons produced in hadronic interactions is of a purely quantum mechanical nature. This poses two problems. Firstly, the probability for a string to decay into a set of hadrons is based on semi-classical arguments and the process therefore has to be provided with a quantum mechanical framework. Secondly, the MC implementations of hadronization models are formulated in the language of stochastical processes, i.e. they are based on probabilities, while quantum mechanics is based on amplitudes.

Based on the similarity between the probability for a string to decay into a set of hadrons and Fermi's golden rule, we present two quantum mechanical processes providing similar matrix elements for the production process.

We show that the interference between identical particles can be incorporated into the probability based MC program if each event is assigned a weight. The weight for a given event, where the particles are produced in the order $\mathcal{P}$ is given by

$$w = 1 + \sum_{\mathcal{P}' \neq \mathcal{P}} \frac{2\mathrm{Re}(\mathcal{M}_{\mathcal{P}} \mathcal{M}^*_{\mathcal{P}'})}{|\mathcal{M}_{\mathcal{P}}|^2 + |\mathcal{M}_{\mathcal{P}'}|^2}, \tag{15}$$

where $\mathcal{M}_{\mathcal{P}}$ is the matrix element for the production of the given configuration. The sum goes over all other configurations $\mathcal{P}'$ in which identical bosons are exchanged. As emphasized in the description of the BE effect, a crucial ingredient to get an enhancement in the correlation function is the chaoticity of the phases of the emission-amplitudes. In this model the chaoticity of the phase of the matrix element corresponds to the sum over very many interference terms in the calculation of the event weight.

For n identical bosons the number of configurations is $n!$. We describe a scheme to include only the configurations which contribute to the sum in Eq.(15). In this way it is possible to reduce the computation time to levels where a complete multiparticle symmetrisation of $\mathrm{q\overline{q}}$ events at LEP energies is manageable.

The model provides an interpretation of the correlation length as a reasonable estimate of the space–time distance, along the colour field, between the production points of two identical bosons.

Paper III

The transverse and longitudinal properties of the particles stem in the Lund string fragmentation model from two different production mechanisms. This is

manifested in the event weight used to implement the BE correlations and it results in a difference in the correlation length along the string and transverse to it.

Two-dimensional correlation functions are studied and the two-particle correlation length is found to be roughly a factor of two larger along the string. The transverse momentum part of the weight provides damping and summed over many particles it introduces Gaussian noise. We therefore find that the difference in correlation lengths is even more apparent when we analyse genuine three-particle correlations. We conclude that two-dimensional three-particle correlations are a sensitive tool to investigate the longitudinal stretching of the string field.

Paper IV

In this paper, we study effects on the W mass measurements at LEP2 from BE and colour interference during the hadronization phase.

In the reaction $e^+e^- \to W^+W^- \to (q_1\overline{q}_2)(Q_1\overline{Q}_2)$ we expect that normally the two singlet systems $(q_1\overline{q}_2)$ and $(Q_1\overline{Q}_2)$ hadronize independently into two strings. If the strings don't interact with each other then the final state is given by the superposition of two independently fragmenting strings. However, if the two systems interact, either through perturbative gluon exchange or in the hadronization phase, it naturally may have implications for the final state.

The pairs $(q_1\overline{Q}_2)$ and $(Q_1\overline{q}_2)$ also form colour singlets with probability $1/N_c^2$ and this probability could be further enhanced by gluon exchange. We therefore expect that the hadronization can give "recoupled" colour strings between these quark–anti-quark pairs. A model for colour recoupling in the hadronization phase of W-pair decays is presented in [6]. The work on colour interference in paper IV is based on an improved version of this model. We find that the possible experimental signal proposed in [6] is ruled out for small recoupling probabilities.

The typical separation in space–time between the W^+ and the W^- decay vertices is much smaller than 0.1 fm at LEP2 energies. Since this distance is much smaller than typical hadronic sizes and the correlation lengths associated with BE interference, bosons from different W's can be subject to BE symmetrisation. This was first proposed in [7]. The model for BE correlations in the Lund model presented in paper II provides an interpretation of the correlation length between identical bosons as the distance along the colour field between their production points. We therefore argue that there are no BE correlations between bosons coming from different W's.

In summary, we conclude that the theoretical uncertainties in the W mass determination, from interference effects during the hadronization phase, should be smaller than the experimental statistical error.

Paper V

A scenario for the end of the QCD cascades is presented. The basic idea is that the constraint imposed by helicity conservation in the emission of gluons will lead to each gluon being surrounded by an exclusion region for further gluon emission. This restricts the maximum number of gluons in a given total phase space. If there is a tendency to emit as many gluons as possible then the azimuthal degree of freedom has to be utilized. The most close-packed configuration in rapidity–azimuthal-angle space corresponds to the gluons being on a helix. This does not necessarily mean that the colour field is wound into a helix since there are very many ways to colour-connect a given set of gluons.

This has been investigated in a toy model containing the relevant features. We find that the sub-optimal configurations do not swamp the optimal one and an ordered field with the characteristics of a helix emerges.

We have modified the Lund fragmentation scheme to incorporate a correlation between the rapidity and the azimuthal angle of the string break-up vertices. This modification yields results which are consistent with current experimental measurements, but predicts at least one signature which should be observable. Our observable for the helix colour field, which we call screwiness, is defined as follows

$$\mathcal{S}(\omega) = \sum_{e} \left| \sum_{j=1}^{n} \exp(i(\omega y_j - \phi_j)) \right|^2 . \tag{16}$$

The first sum is over all the events in the analysis and the second goes over the particles in an event.

To understand how screwiness behaves we note that each term in the inner sum can be viewed as a step in the complex plane having unit length. If the phase of each step is fluctuating wildly the sum of several steps will have the properties of a random walk. The average length of a sum of n steps is then in particular $\sqrt{n}$. We conclude that screwiness for a fixed ω will, in the case of random phases, be $N\langle n\rangle$, where N denotes the number of analysed events. For $\omega = 0$ the inner sum is the sum of the directions of the particles transverse momenta. If the number of particles in the event is not too small we expect that the local conservation of transverse momenta will lead to screwiness being small for ω close to zero. On the other hand if there is a correlation between rapidity and

azimuthal angles, screwiness will be enhanced for the corresponding ω. In the maximum case, all the steps are in the same direction and screwiness takes the value $N\langle n\rangle^2$.

We therefore expect screwiness to be small for $\omega \simeq 0$, have a peak for the ω corresponding to the close-packing of the gluons and finally fall off to a plateau for large ω, corresponding to the case of random phases.

We find that this observable can survive particle production and subsequent resonance decays.

Acknowledgments

First, I want to thank Bo for his continuous efforts and excellent guidance. I would also like to thank Patrik for numerous explanations and for surviving in the noisy office we share. A fair share of gratitude goes to Jari and Carsten for trying to keep up with my frequent coffee-breaks. I thank Patrik, Jari and Peter for reading this introduction. Finally, I want to thank everyone at the department who has contributed to a great atmosphere during my stay.

References

[1] B. Andersson, G. Gustafson, G. Ingelman and T. Sjöstrand, *Phys. Rep.* **97**, 31 (1983)

[2] R. Hanbury-Brown and R.Q. Twiss, *Nature* **178**, 1046 (1956)

[3] G. Goldhaber, S. Goldhaber, W. Lee and A. Pais, *Phys. Rev.* **120**, 300 (1960)

[4] T. Sjöstrand, *Comp. Phys. Comm.* **82**, 74 (1994)

[5] K.G. Wilson, *Cornell preprint* CLNS-131, (1970)
Later published in the *Proc. of the XIVth Scottish Universities Summer School in Physics (1973)*, eds R.L. Crawford and R. Jennings, Academic Press, New York (1974)

[6] G. Gustafson and J. Häkkinen, *Z. Phys.* **C64**, 659 (1994)

[7] L. Lönnblad and T. Sjöstrand, *Phys. Lett.* **B351**, 293 (1995)

The Feynman–Wilson gas and the Lund model

Paper I

The Feynman–Wilson gas and the Lund model

Bo Andersson, Gösta Gustafson, Markus Ringnér and Peter Sutton

Department of Theoretical Physics, Lund University,
Sölvegatan 14A, S-223 62 Lund, Sweden

We derive a partition function for the Lund fragmentation model and compare it with that of a classical gas. For a fixed rapidity "volume" this partition function corresponds to a multiplicity distribution which is very close to a binomial distribution. We compare our results with the multiplicity distributions obtained from the JETSET Monte Carlo for several scenarios. Firstly, for the fragmentation vertices of the Lund string. Secondly, for the final state particles both with and without decays.

1.1 Introduction

The cross-sections of QCD multiparticle production processes at high energies have many similarites with the multiparticle distributions of a classical gas, an analogy which was first noted by Feynman and Wilson [1]. This gas is essentially one dimensional in rapidity space. In this paper we use the gas analogy to derive a partition function for the Lund string fragmentation model [2]. We perform a virial expansion to the second order in the density of particles. Our partition function then yields an equation of state for a Van der Waal's gas. Furthermore, it reduces to that of an ideal gas when the produced particles are massless.

The partition function of the gas is related in a simple way to the multiplicity distribution of its constituent particles. This provides us with a method of investigating the partition function. We show that for a fixed rapidity "volume" our partition function corresponds to a multiplicity distribution which is very similar to a binomial distribution.

For large rapidity intervals the major fluctuations in multiplicity stem from gluon radiation. We will, however, neglect gluon emission. In this paper we are only interested in comparing the Lund fragmentation model with the properties of a classical gas.

We analyse the multiplicity distributions obtained from the JETSET Monte Carlo [3] for several scenarios. Firstly, we investigate the string break-up vertices, then the primary particles and finally we include decays. We find that all cases are remarkably well described by distributions from the binomial family. In the derivation of our partition function we assume that the particles are ordered in rapidity. Since this is true for the vertices, we expect the distributions of vertices to be the optimal case. Indeed, these distributions are well described by our partition function.

The transition from vertices to particles introduces some smearing in rapidity. This results in a wider multiplicity distribution, where the width is sensitive to the transverse mass of the produced particles. We obtain an ordinary binomial for the primary particles. However, the strong smearing from decays ensures that, for the final state particles, this distribution becomes a negative binomial distribution.

We shall begin with a short presentation of the basic ideas of the Feynman–Wilson gas (FWG). This is followed by an introduction to the Lund model and its relationship to the FWG. We next turn to the multiplicity distributions for the vertices and lastly how they are modified for the final state particles.

1.2 The Feynman–Wilson gas

The original discussion of the FWG can be found in [1]. Here we summarize the main features of the model. We consider a multiparticle production process where the two primary particles have four momenta p_1 and p_2 and large invariant $s = (p_1+p_2)^2$. The n secondary particles have four momenta $k_1, k_2, \ldots, k_n$, and each is on the mass shell. In the FWG model the three remaining degrees of freedom in each k_i correspond to the "spatial" co-ordinates of a gas particle via

$$\begin{aligned} \tilde{x} &= k_x \\ \tilde{y} &= k_y \\ \tilde{z} &= \ln[(k_z + k_0)/m_\perp] \end{aligned} \tag{1.1}$$

where the transverse mass is defined by

$$m_\perp = \sqrt{m^2 + k_x^2 + k_y^2} \ . \tag{1.2}$$

Note that in this picture $\tilde{z}$ corresponds to the rapidity of the relevant particle. We will assume here that each produced particle is of the same type (each has the same mass) but the extension to different species is straightforward.

We can write the total cross section for the production process using these spatial variables. We first note that the invariant phase space d^3k/k_0 becomes $d^3\tilde{r}$. The energy momentum conserving delta functions are first written in terms of $p = p_1 + p_2 - k_1 - \ldots - k_n$.

$$\delta(p_0)\delta^3(p) = 2\delta(p_+)\delta(p_-)\delta^2(p_\perp) \tag{1.3}$$

with $p_\pm = p_0 \pm p_z$. This can be expressed in terms of $\tilde{r}$ variables using the relationship $k_0 \pm k_z = m_\perp e^{\pm\tilde{z}}$.

The delta functions have the effect of introducing a fixed volume for the gas. The transverse momenta are limited and constrain the gas to a narrow tube of radius ~ 300 MeV. We shall instead focus on the $\tilde{z}$ co-ordinate. We first introduce W_+ and W_- via

$$W_\pm \equiv (p_1 + p_2)_\pm \tag{1.4}$$

so that we can write

$$\delta(p_\pm) = \delta(W_\pm - \sum m_{\perp i} \exp(\pm\tilde{z}_i)) \ . \tag{1.5}$$

In the following we use the Lorentz frame where $W_\pm = \sqrt{s}$. The two delta distributions contain the requirement that the "gas volume" should be of the

order of $\ln s$. To see this we may integrate out the rapidities of the first and the last particles to obtain

$$\begin{aligned} d\tilde{z}_1 d\tilde{z}_n\, \delta(\cdots)\delta(\cdots) &\simeq 1/s \\ \tilde{z}_1 \simeq -\tilde{z}_n &\simeq \ln(\sqrt{s})\,. \end{aligned} \tag{1.6}$$

We may in this approximation choose a number s_0 in such a way that

$$\Delta\tilde{z} \equiv \tilde{z}_1 - \tilde{z}_n = \ln(s/s_0) \tag{1.7}$$

and assume that all the particles are kept inside this rapidity "volume". If the spatial co-ordinates of the primary particles are R_1 and R_2 respectively then the cross section can be written as

$$\sigma_T(R_1,R_2) = \sum_{n=2}^{\infty}\left[\left(\prod_i^n \int d^3\tilde{r}_i\right)\, 2\delta(p_+)\delta(p_-)\delta^2(p_\perp)\;\sigma_n(\tilde{r}_1,\ldots,\tilde{r}_n,R_1,R_2)\right]\,. \tag{1.8}$$

For fixed R_1, R_2 then σ_T corresponds, in the FWG analogy, to the partition function of the gas and the functions σ_n are the n particle distribution functions for the gas. Our aim is to connect these ideas to particle production within QCD as represented by the Lund model.

1.3 The Lund model and the Feynman–Wilson gas

1.3.1 The Lund model

In this section we briefly review some features of the Lund model fragmentation scheme. We will mostly be concerned with the simple situation when the colour force field from an original quark-antiquark pair (produced by e^+e^- annihilation, for example) decays into a set of final state hadrons.

In the Lund model, the colour force field is approximated by a massless relativistic string with a quark (q) and an antiquark ($\overline{\mathrm{q}}$) at the endpoints. The gluons are treated as internal excitations on the string field. This means that there is a constant force field, $\kappa \simeq 1$ GeV/fm, corresponding to a linearly rising potential, spanned between the original pair. After being produced the q and the $\overline{\mathrm{q}}$ are moving apart and the energy in the field can be used to produce new $\mathrm{q}\overline{\mathrm{q}}$-pairs. When a new pair is created the string is split into two pieces.

The production rate of a pair with combined internal quantum numbers corresponding to the vacuum is, from quantum mechanical tunneling in a constant

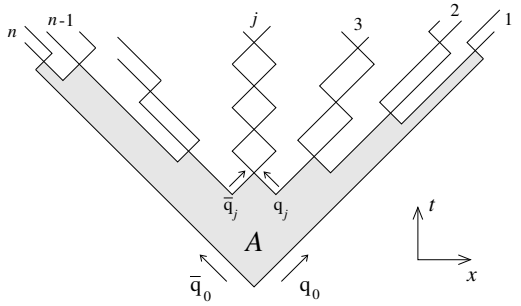

Figure 1.1: The break-up in space–time of a Lund string into n hadrons. The fragmentation area is denoted by A.

force field, given by

$$P(\mu_\perp) = \exp\left(-\frac{\pi\mu_\perp^2}{\kappa}\right). \tag{1.9}$$

Here the quarks in the pair have transverse mass $\mu_\perp = \sqrt{\mu^2 + \vec{k}_\perp^2}$, mass μ and transverse momentum $\pm\vec{k}_\perp$. The final state mesons in the Lund model correspond to isolated string pieces containing a q from one breakup vertex and a $\overline{\mathrm{q}}$ from the adjacent vertex together with the produced transverse momentum and the field energy in between. The break-up of the string is illustrated in Fig.(1.1).

One necessary requirement is that to obtain real positive (transverse) masses all the vertices must have spacelike difference vectors. Together with Lorentz invariance this means that all the vertices in the production process must be treated in the same way [4]. Another consequence is that it is always the slowest mesons that are produced first in any Lorentz frame (corresponding to the fact that time-ordering is frame dependent). Furthermore each vertex has the property that it will divide the event into two causally disconnected jets, the mesons produced along the string field to the right and those produced to the left of the vertex. This can be seen in Fig.(1.1).

A convenient ordering along the force field of the produced particles is rank ordering. Two particles have adjacent rank if they share a q$\overline{\mathrm{q}}$ pair created at a vertex . The first rank meson contains the internal quantum numbers of the original q together with those of the $\overline{\mathrm{q}}$ produced at the vertex closest to the endpoint q. Similarly the second rank meson contains the internal quantum numbers of the q from this "first" vertex and the $\overline{\mathrm{q}}$ of the "second" etc. In this way rank ordering corresponds to an ordering along a light-cone. Alternatively

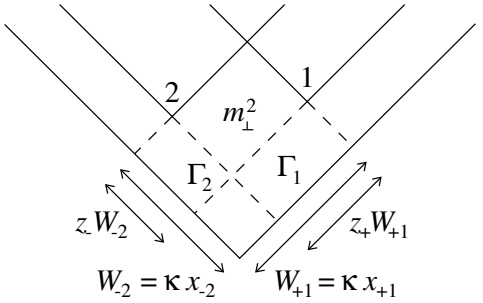

Figure 1.2: The production, in energy–momentum space, of a particle with transverse mass $m_\perp$. The particle is produced between the vertices 1, with the squared proper-time $\tau_1^2 = \Gamma_1/\kappa^2$, and 2, with $\tau_2^2 = \Gamma_2/\kappa^2$. The particle has fractional light-cone components z_+ and z_-.

it is also possible to rank order in the direction from the original $\overline{\mathrm{q}}$.

The basic Lund model fragmentation process then stems from the following two assumptions

1. In the centre of phase space (i.e. far from the endpoints) the string decay process will reach a steady state. The probability to find a vertex is, after many production steps along the light-cone, a finite distribution in the proper time of the vertex. This is also the case when the total string field energy becomes very large.
2. The decay process is the same whether it is ordered along the positive or along the negative light-cone.

If we consider Fig.(1.2), this means that we assume that the probability to reach the space-time point 1 at (x_{+1}, x_{-1}), after many steps along the positive light-cone, and to produce a meson with transverse mass $m_\perp$ by one further step to the vertex 2 at (x_{+2}, x_{-2}), is equal to the probability to reach the point 2, after many steps along the negative light-cone, and by one further step to 1 produce the meson with $m_\perp$.

Changing variables to the squared Lorenz invariant proper time $\tau^2 = x_+ x_-$ and the rapidity $y = 1/2 \ln(x_+/x_-)$ the probability to reach the point 1 is $H(\tau_1^2) d\tau_1^2 dy_1$. The probability to produce one further particle with mass $m_\perp$ and fractional light-cone component z_+ is $f(z_+, m_\perp) dz_+$. A particle with fractional light-cone component z_+ has the positive light-cone energy-momentum component $p_+ = z_+ \kappa x_{+1}$ and has, in order to stay on the mass-shell, the neg-

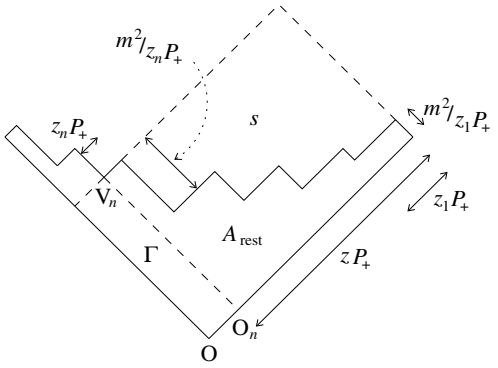

Figure 1.3: The decay, in energy-momentum space, of an n-particle cluster with invariant squared mass s. The fragmentation area of the cluster is $A_{\rm rest}$. $\Gamma = \kappa^2\tau^2$ is with respect to the proper-time τ of the last vertex.

ative component $p_- = m_\perp^2/p_+ = z_-\kappa x_{-2}$. This means that we obtain the equation:

$$H(\tau_1^2)d\tau_1^2 f(z_+, m_\perp)dz_+ = H(\tau_2^2)d\tau_2^2 f(z_-, m_\perp)dz_- \ . \tag{1.10}$$

It is a nice and surprising feature of the assumptions above that there is a unique process that fulfills Eq.(1.10) [4],

$$\begin{aligned} H_j &= C_j\Gamma^{a_j}\exp(-b\Gamma) \quad \text{with} \ \ \Gamma = \kappa^2\tau^2 \ , \\ f_{jk} &= \hat{N}_{jk} z^{a_j-1}\left(\frac{1-z}{z}\right)^{a_k}\exp(-bm_\perp^2/z) \ . \end{aligned} \tag{1.11}$$

The numbers C_j and $\hat{N}_{jk}$ are normalisation constants and the particle is assumed to be produced in a step from a vertex with flavour j to a vertex with flavour k. If n_f denotes the number of $q\overline{q}$-flavours, the process has $n_f + 1$ parameters. Although the parameter a is, in principle, flavour dependent, there has been no need to utilize this in the Lund model as implemented in the JETSET Monte Carlo; except for the first rank particle in a heavy quark jet [5]. The parameter b must be flavour independent.

It is possible to construct the probability to produce a finite energy cluster of rank-connected particles [4] from Eq.(1.11). Such a cluster is shown in Fig.(1.3). This probability distribution is in a natural way subdivided into two parts, the probability to obtain the cluster and the probability that the cluster decays in a particular way. In the following we order the particles along the positive light-cone. If the cluster has a total light-cone fraction z and a fixed total

squared cms energy s then the (non-normalised) probability to obtain such a cluster is

$$dP_{\rm ext} = \frac{dz}{z} z^{a_0} \left(\frac{1-z}{z}\right)^{a_n} \exp(-b\Gamma(s,z)) \quad \text{with} \quad \Gamma(s,z) = s\frac{1-z}{z} \,. \tag{1.12}$$

The cluster then starts at a vertex with flavour f_0 and ends with flavour f_n. The Γ value is that of the last vertex, as shown in Fig.(1.3). Thus a cluster is produced in the same way as a single particle between the vertices with a_0 and a_n. Similarly we find that the (non-normalised) probability for the cluster to decay into the particular channel with the particles $\{p\}_j$ is

$$dP_{\rm int} = \left[\prod \hat{N}_j dp_j \delta(p_j^2 - m_j^2)\right] \delta(\sum p_j - P_{\rm tot}) \exp(-bA_{\rm rest}) \tag{1.13}$$

where $A_{\rm rest}$ is the decay area of the cluster, as shown in Fig.(1.3). Equation (1.13) is for simplicity written in the ordinary Lund model fashion with a single a-parameter (this parameter is not explicit in the formula) and we note the appearance of the phase space for the final state particles multiplied by the exponential area decay law. The quantity $P_{\rm tot}$ is the total energy momentum of the cluster so that $P_{\rm tot}^2 = s$. We may determine the finite energy version of the vertex distribution, $H(\Gamma)$, from Eq.(1.12) by exchanging z for Γ. This yields

$$H_s \propto \frac{\Gamma^{a_n} s^{a_0 - a_n}}{(\Gamma + s)^{a_0+1}} \exp(-b\Gamma) \,. \tag{1.14}$$

The function H_s in Eq.(1.14) is exponentially decreasing in Γ so that the power dependence in the denominator only plays a role for small values of Γ and then it is hardly noticable for large values of s. In this way the assumption 1. above is fulfilled. That is to say when s becomes very large there is (after normalisation) a finite distribution in the proper-time size of the decay vertices.

1.3.2 The connection between the Lund model and the FWG

We will now exhibit the decay distribution of a cluster, as given by Eq.(1.13), in terms of the partition function which is studied in statistical physics. For simplicity we write the formulas for a single particle transverse mass $m_\perp$ and a single flavour and we let j denote the rank of a particle. The phase space factor can in analogy with the result in section 1.2 be written with the particle energy momentum vectors $p_j \equiv m_\perp(\exp(y_j), \exp(-y_j))$ as

$$d\Psi \equiv \left[\prod \hat{N} dp_j \delta(p_j^2 - m_j^2)\right] \delta(\sum p_j - P_{tot})$$

$$= \left[\prod_1^n \hat{N} dy_j\right] \delta(\sum m_\perp \exp(y_j) - P_+)\delta(\sum m_\perp \exp(-y_j) - P_-)$$
$$\simeq \frac{\hat{N}^2}{s} \prod_2^{n-1} \hat{N} dy_j \ . \tag{1.15}$$

We have in the last line integrated out the first and the last rapidities in the delta function and from now on we assume that the remaining particles are placed in rapidities between $\Delta y/2$ and $-\Delta y/2$ with $\Delta y = \ln(s/s_0)$ and s_0 is some suitable scale. If all the particles are ordered in rapidity we may integrate out the phase space factor and obtain

$$\int d\Psi = \frac{\hat{N}^2(\hat{N}\Delta y)^{n-2}}{s(n-2)!} \ . \tag{1.16}$$

We next consider the decay area of the cluster. Figure (1.4) shows that it can be written in terms of the rapidities of the particles

$$A = m_\perp^2 \sum_{j=1}^n \sum_{k=j}^n \exp(y_k - y_j) \ . \tag{1.17}$$

From this equation and Eq.(1.15) we note that the decay distribution in Eq.(1.13) has similarities with a partition function, Z_n, and we therefore define a grand partition function Z as

$$\begin{aligned} Z &= \sum_n Z_n \\ &= s \sum_n \left[\left(\prod_{j=1}^n \hat{N} dy_j \right) \delta(\ldots)\delta(\ldots) \exp\left(-b m_\perp^2 \sum_{j=1}^n \sum_{k=j}^n \exp(y_k - y_j) \right) \right] \\ &\equiv s \sum_n \left[\left(\prod_{j=1}^n \hat{N} dy_j \right) \delta(\ldots)\delta(\ldots) \exp\left(-\frac{1}{kT} \sum_{j=1}^n \sum_{k=j}^n V(y_j - y_k) \right) \right] \end{aligned} \tag{1.18}$$

(The factor of s is required in order to have a dimensionless partition function.) In this way we see that the decay distribution in Eq.(1.13) may be interpreted as the partition function for a system of n particles with co-ordinates y_j interacting with exponential two-body potentials in a one-dimensional volume equal to Δy. We note that whilst all the particles interact in this way ("long-range interactions") the exponential decrease of the potentials ensures that the effective interaction is rather short ranged.

If the particles are imagined as making up a gas in rapidity space and are

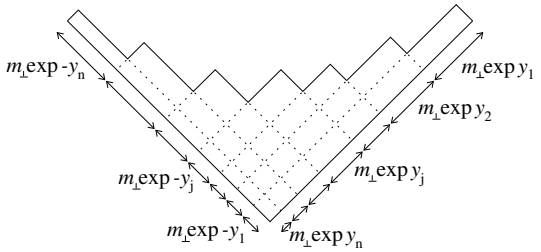

Figure 1.4: The fragmentation area partitioned into two-particle regions reveals how the area can be expressed as in Eq.(1.17).

interacting via two-body potentials, then the Hamiltonian is

$$H = \sum_j T(\pi_j) + \sum_{j,k} V(y_j - y_k) \ . \tag{1.19}$$

The phase space volume element is $\prod(dy_j d\pi_j)$, with π_j denoting the quantities canonically conjugate to the co-ordinates y_j. The kinetic energy factors T are integrated out in Eq.(1.18) and incorporated into the constants $\hat{N}$. These constants then play the role of fugacities.

We shall now attempt to obtain a simplifed expression for the partition function, Z_n. We have already seen that in the strong ordering limit the phase space may be easily integrated according to Eq.(1.16). Using this limit may seem drastic since two neighbours in rank may well have a different rapidity order. However, if many pairs are not well ordered then many of the exponential potentials in the in the partition function will be strongly increasing, i.e. the area suppression in the Lund model will make these contributions small.

We can easily find an expression for the exponential in our partition function if we approximate the fragmentation area. Assuming that each particle lies along the hyperbola with $< \sqrt{\Gamma} >= \gamma$ then each takes up a rapidity length $\delta = m_\perp/\gamma$. Consequently all the n particles take up the rapidity length $\Delta y = n\delta = nm_\perp/\gamma$ and the total area is $\gamma^2 \Delta y = n^2 m_\perp^2/\Delta y$. Since the particles are produced around the average hyperbola, we expect that this result may be modified by a constant, c_2, of order unity giving

$$bA \simeq \frac{bc_2 m_\perp^2 n^2}{\Delta y} = \frac{c_3 n^2}{\Delta y} \ , \tag{1.20}$$

where we have introduced $c_3 = bm_\perp^2 c_2$. In this way we obtain from Eq.(1.16) and Eq.(1.20) a description of the grand partition function in terms of the

multiplicity n. In the approximation that n is large, i.e. for large rapidity intervals Δy, we can write the partition function in terms of two parameters c_1 and c_3 as

$$Z_n \simeq \frac{(c_1 \Delta y)^n}{n!} \exp\left(\frac{-c_3 n^2}{\Delta y}\right) . \tag{1.21}$$

We will comment further on the parameters c_1 and c_3 when we investigate to what extent the partition function in Eq.(1.21) describes the particle production in the Lund model.

1.3.3 The partition function in the Gaussian approximation

We now investigate the grand partition function in the limit where the number of particles is large, but the density is low (as in an ordinary gas). In this case we expect that the grand partition function can be approximated by the maximal term in the sum. To find the multiplicity for which the partition function is maximal we first define Φ_n by writing Eq.(1.21) as

$$Z_n = \exp \Phi_n . \tag{1.22}$$

If we treat n as a continuous variable we can expand Φ_n in a Taylor series as

$$\Phi(n) \simeq \Phi(\overline{n}) + (n - \overline{n})\ \Phi'(\overline{n}) + \frac{(n-\overline{n})^2}{2}\ \Phi''(\overline{n}) . \tag{1.23}$$

Choosing $\overline{n}$ such that $\Phi'(\overline{n}) = 0$, we evidently have a Gaussian approximation for Z_n

$$Z_n \simeq \exp \Phi(\overline{n})\ \exp\left(-\frac{(n-\overline{n})^2}{2V}\right) \tag{1.24}$$

where the variance, V, is given by $V = -1/\Phi''(\overline{n})$. It is straightforward to obtain expressions for both $\overline{n}$ and V if we use Stirlings approximation for the factorial in $\Phi(n)$. We find

$$\begin{aligned} \overline{n} &= \frac{\Delta y}{2c_3}\ \ln(\frac{c_1 \Delta y}{\overline{n}}) \\ V &= \overline{n}\left(1 + \frac{2c_3\overline{n}}{\Delta y}\right)^{-1} . \end{aligned} \tag{1.25}$$

Notice that, since c_3 is positive, this implies that the variance of the distribution is less than the mean and the distribution is therefore narrower than a Poissonian. If we now introduce the density of particles in the rapidity volume, $R = \overline{n}/\Delta y$, then

$$\Phi(\overline{n}) = (R + c_3 R^2)\Delta y . \tag{1.26}$$

For large $\overline{n}$ we can approximate the grand partition function as $Z \sim Z_{\overline{n}}$ and so

$$Z \sim \left(\frac{s}{s_0}\right)^{a_R} \tag{1.27}$$

with

$$a_R = R + c_3 R^2 \ . \tag{1.28}$$

The grand canonical partition function, for a gas is related to the pressure, P, temperature, T and volume, $\ln(s/s_0)$, of the gas via

$$\begin{aligned} \Omega &\equiv -kT \ln Z \\ P &= -\frac{\partial \Omega}{\partial \ln(s/s_0)} \end{aligned} \tag{1.29}$$

where k is Boltzmann's constant. For the partition function in Eq.(1.27) we obtain the following equation of state for the gas

$$P = kT(R + c_3 R^2) \ . \tag{1.30}$$

Our expansion thus corresponds to the first two terms in the virial expansion in the particle density of the gas. We note that the equation of state in Eq.(1.30) is similar to that of a Van der Waal's gas. For particles with zero (transverse) mass we have $c_3 = 0$. In this case a particle does not take up any volume in rapidity and Eq.(1.30) reduces to the equation of state for an ideal gas.

1.4 The vertex distributions

The partition function is related to the multiplicity distribution, P_n, since

$$P_n = \frac{Z_n}{Z} \ . \tag{1.31}$$

In the remaining sections we shall use this relationship to further study our partition function. We begin here with a study of the vertices produced in the string fragmentation. These vertices are strongly ordered in rapidity and thus satisfy one of the assumptions used to derive our partition function. This is only an approximation in the case of the particles. Of course, the number of vertices corresponds directly to the number of primary particles.

In what follows we outline a simple model in which all particles have the same mass ($m = 0.8$ GeV) and there is no transverse momenta. The effects of relaxing those constraints will be considered in the next section where we return to the particles.

1.4.1 The distribution in rapidity

We begin by studying the separation between neighbouring vertices. In the Lund model the distribution of such separations for a fixed mass, m, is given by

$$P(\delta y) = N \int d\Gamma \Gamma^a e^{-b\Gamma} \int_0^1 dz \frac{(1-z)^a}{z} e^{-bm^2/z} \delta \left(\delta y - \frac{1}{2} \ln \left(\frac{\Gamma + m^2/z}{\Gamma(1-z)} \right) \right) . \tag{1.32}$$

The logarithm of this distribution is plotted in Fig.(1.5) for various values of the Lund model parameters a and b. We see from this figure that there are two main characteristics of the distribution. The first is an effective minimum separation between vertices which increases with bm^2, but is independent of a. Physically this separation arises because two vertices cannot be very close together in rapidity if they must produce a massive particle. The second characteristic is an exponential fall off for large separations, δy, which depends only on the parameter a.

We can consider a simple model which reproduces the above features very well. In this model the rapidity region is divided up into a series of N equal bins of size $\delta y_{\rm bin}$. The effective minimum separation between vertices can now be taken into account by demanding that no bin may contain more than a single vertex. Each bin is assigned a probability p to contain a vertex and a probability $1-p$ to be empty. This allows us to compute the probability of a separation, δy, between two vertices. If δy is discretised as $\delta y = n\delta y_{\rm bin}$ with n an integer then the probability of such a separation is given by a geometric series

$$\begin{aligned} P(\delta y) &= p(1-p)^{n-1} \qquad\qquad (n = 1, 2, \ldots) \\ &= \frac{p}{(1-p)} \exp(-\beta \delta y) \end{aligned} \tag{1.33}$$

with $\beta = -\ln(1-p)/\delta y_{\rm bin}$. We see that large δy separations are exponentially suppressed. The two main features of Fig.(1.5) are thus very well reproduced by this simple model, which corresponds to distributing the vertices according to a binomial distribution (appendix 1.A).

We can investigate the accuracy of the binomial approximation using the JETSET Monte Carlo (for consistency we use a fixed mass ($m = 0.8$ GeV) and have no transverse momentum generation). Here we generate 2-jet ($\mathrm{q\overline{q}}$) events and analyse the distribution of vertices within a rapidity range, Δy. The energy is chosen to be sufficiently large in order to avoid edge effects from the q and $\overline{\mathrm{q}}$ fragmentation contaminating the Δy region. The mean, $\langle n \rangle$, and the variance, V, of the resulting multiplicity distributions are used to calculate the binomial parameters N and p, as detailed in appendix 1.A. We will see later that binomial distributions with these N and p values do indeed reproduce the

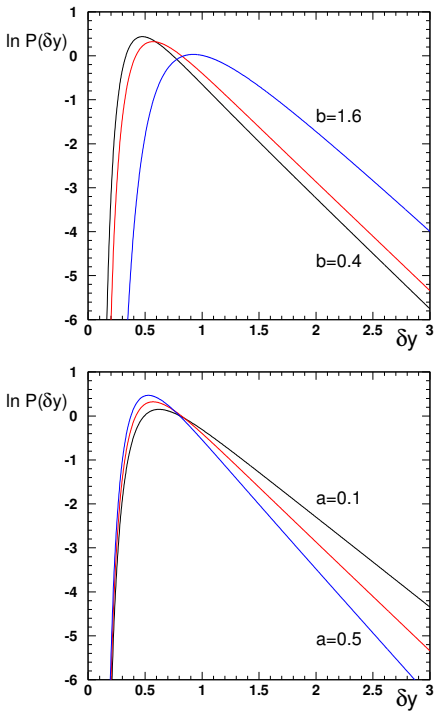

Figure 1.5: The logarithm of the distribution of the rapidity distance $P(\delta y)$ between adjacent vertices as predicted by the Lund model (Eq.(1.32)) for a fixed mass, $m = 0.8$ GeV, but different values of the Lund model parameters a and b. The upper plot shows fixed $a = 0.3$ and $b = 0.4,\ 0.58,\ 1.6$. The lower plot shows fixed $b = 0.58$ and $a = 0.1,\ 0.3,\ 0.5$.

multiplicity distributions very well. Figure (1.6) shows the results as a function of Δy, for various values of the parameter b. We see that for large rapidity volumes ($\Delta y \gtrsim 5$ units) the binomial assumptions seem to work very well. That is to say, the observed p parameter is effectively constant as a function of Δy, whilst the parameter N is linear with Δy. This corresponds to a constant bin size $\delta y_{\rm bin}$. (As expected the bin size is found to be proportional to bm^2.)

The behaviour of the effective JETSET N and p parameters at small values of Δy can easily be understood. When Δy becomes smaller than the normal bin size, $\delta y_{\rm bin}$, we have only one bin which is now of size Δy. In Fig.(1.6) all of

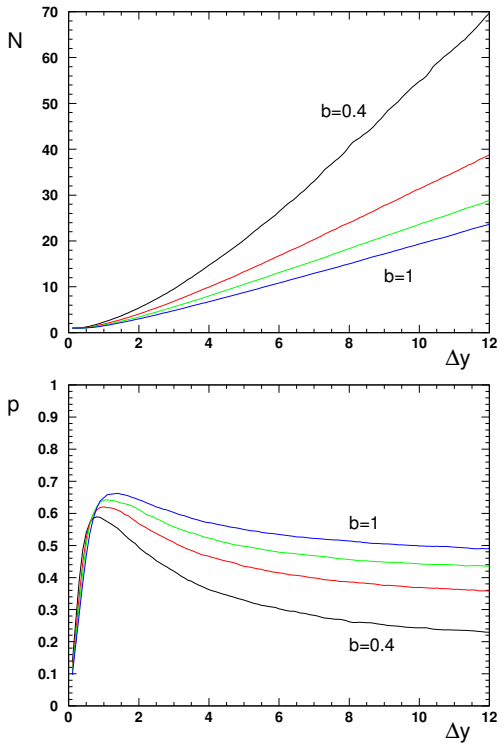

Figure 1.6: The values of N (upper plot) and p (lower plot) for the vertex distributions produced by JETSET (for a fixed mass and no transverse momentum generation) as a function of the rapidity volume, Δy. We show the results for fixed $a = 0.3$ and $b = 0.4$, 0.6, 0.8 and 1.

the N curves indeed tend to the limit $N = 1$. Meanwhile the observed p value is the probability to find a vertex in this single bin

$$p_{\rm obs} = p\,\frac{\Delta y}{\delta y_{\rm bin}} \qquad (\Delta y < \delta y_{\rm bin}) \ . \tag{1.34}$$

Thus the observed p becomes linear with Δy when Δy is smaller than the bin size. This effect can be seen in Fig.(1.6). Between the limits of large and small Δy the behaviour of N and p are not so well determined. Here correlations between closely spaced vertices will play a role.

We are now in a position to turn our attention back to the partition function. This formula should also generate a good description of the multiplicity

distribution for the vertices. We have

$$P_n \;=\; c_0 \,\frac{(c_1\Delta y)^n}{n!}\,\exp\left(\frac{-bm^2\;c_2 n^2}{\Delta y}\right) \tag{1.35}$$

Here c_0 is a normalisation parameter and so is determined in terms of the remaining parameters. We can relate the parameters c_1 and c_2 to the parameters N and p of the binomial distribution. The procedure is explained in detail in appendix 1.B. For large Δy, we obtain

$$\begin{aligned} c_1 &= \frac{Np}{\Delta y}\;\exp\left[\frac{p}{(1-p)}\right] \\ c_2 &= \frac{\Delta y}{2bm^2N(1-p)} \end{aligned} \tag{1.36}$$

In Fig.(1.7) we show the values of c_1 and c_2 which we obtain from our JETSET multiplicity distributions. For large rapidity volumes, Δy, they tend to constant values. We noted in section 1.3.3 that it is also possible to approximate Eq.(1.35) using a Gaussian distribution (with the appropriate mean and variance). If we express the mean and variance of Eq.(1.25) in terms of N and p and solve for c_1 and c_2, then we obtain the same expressions as Eq.(1.36). We note, however, that in the case of a Gaussian distribution one has a symmetric distribution. This is not true of either Eq.(1.35) or the binomial distribution since they both contain a term $n!$ in the denominator.

Finally in Fig.(1.8) we demonstrate how well the binomial and Eq.(1.35) reproduce the observed multiplicity distribution. We show three curves firstly the JETSET multiplicity distribution, secondly that obtained from the binomial distribution and finally the distribution obtained from Eq.(1.35). At $\Delta y = 5$ we see very good agreement and it is difficult to distinguish the different curves whilst at $\Delta y = 10$ all of the curves lie on top of each other. We thus see that the vertex multiplicity distributions produced by JETSET do indeed agree very well with our simple expression for the partition function, Z_n.

1.4.2 Distribution in proper time

So far we have discussed the distribution of the vertices in terms of the rapidity, y. If p_T is neglected then the position of the vertices is specified by one further variable Γ, which is related to the proper time of the vertex. In this section we will investigate how the vertices are distributed in Γ. As we discussed in section 1.3.1, we have for the vertices that

$$P(\Gamma) \propto \Gamma^a \exp(-b\Gamma) \tag{1.37}$$

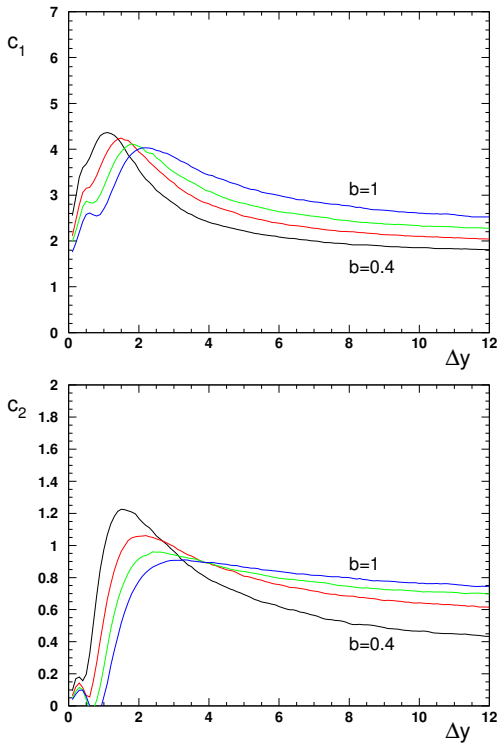

Figure 1.7: The values of c_1 (upper plot) and c_2 (lower plot) for the vertex distributions produced by JETSET (for a fixed mass and no transverse momentum generation) as a function of the rapidity volume, Δy. We show the results for fixed $a = 0.3$ and $b = 0.4$, 0.6, 0.8 and 1.

which has a mean $\langle \Gamma \rangle = (1 + a)/b$. Equation (1.37) is, however, an inclusive distribution. If we examine vertices within a rapidity range, $\Delta y \lesssim 2$, then we find that they are correlated. This means, for example, that if a vertex has a large Γ value then nearby vertices are also likely to have large Γ values.

We now examine how the vertices are distributed in Γ inside a rapidity range Δy for various multiplicities, n. Motivated by the finite energy vertex distribution, $H(\Gamma)$, which we considered earlier in Eq.(1.14), we parameterize the distributions as

$$H_n(\Gamma, \Delta y) = C \frac{\Gamma^{a_{\rm eff}(n,\Delta y)}}{(\Gamma + s_{\rm eff}(n, \Delta y))^{a+1}} \exp(-b\Gamma) \quad . \tag{1.38}$$

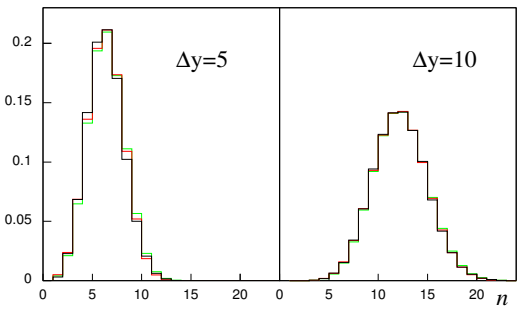

Figure 1.8: The multiplicity distributions for the vertices for various values of the rapidity volume Δy as obtained from JETSET (solid curve), the binomial distribution (medium grey curve) and Eq.(1.35) (light grey curve).

Note that taking the weighted average of H_n should reproduce the inclusive distribution of Eq.(1.37). In Fig.(1.9) we show distributions in Γ obtained from JETSET for $\Delta y = 6$. Each plot in the figure is for a different number of vertices, n, together with the corresponding fit according to Eq.(1.38). Here the parameters $a_{\rm eff}$ and $s_{\rm eff}$ have been fitted for each different n value. We see that one can find values of $a_{\rm eff}(n, \Delta y)$ and $s_{\rm eff}(n, \Delta y)$ for which a very reasonable description of the Γ distributions is obtained. We note that the large Γ behaviour is determined *only* by the Lund parameter b and not by n or Δy. Thus it is only dependent on the scale for the area law suppression. Next we examine the dependence of both $a_{\rm eff}$ and $s_{\rm eff}$ on the multiplicity and the rapidity interval. We have carried out fits to the Γ distribution obtained from JETSET for a set of values of n and Δy. We find that both of these functions depend only on the ratio $R = n/\Delta y$. This can be seen clearly in Fig.(1.10) where we plot the results of our fits for three different values of Δy, as a function of the density R.

This completes our study of the distribution of vertices produced in the Lund model of fragmentation. We can summarize our findings as follows. In rapidity the vertices are approximately distributed according to the partition function, whilst in proper time they are distributed according to Eq.(1.38). Importantly we find that the large Γ behaviour of the distribution in Γ is determined only by the area law. We also find that the functions $a_{\rm eff}$ and $s_{\rm eff}$ only depend on the density of vertices, R, which is itself the important quantity in the equation of state for the gas in rapidity.

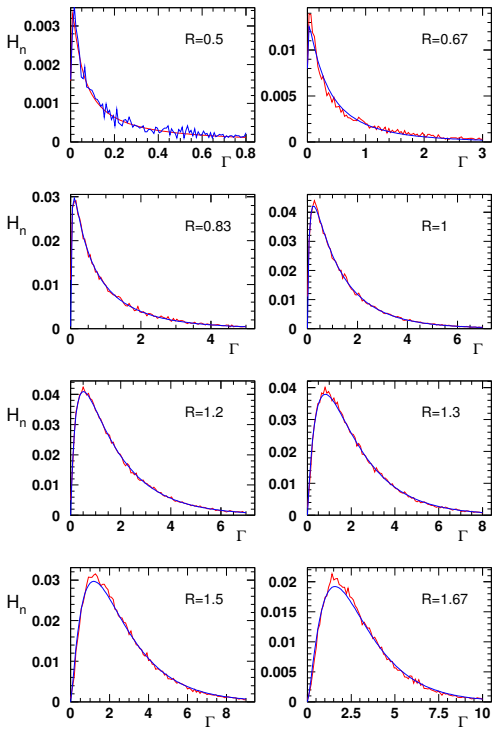

Figure 1.9: The distributions $H_n(\Gamma, \Delta y)$ obtained from JETSET for the default values of the Lund model parameters ($a = 0.3$ and $b = 0.58$). Also shown are the continuous curves obtained from our fits based on Eq.(1.38). In this example $\Delta y = 6$ and $n = 3 \ldots 10$. The corresponding R values are shown on each plot.

1.5 The particle distributions

For primary particles the mean multiplicity corresponds to the mean number of vertices. The effects of going over from vertices to particles essentially means some smearing in rapidity. Thus the rapidity ordering assumed for Eq.(1.21) will no longer be true. However, for large Δy it should still be a good approximation. The rapidity of a particle is distributed around the average rapidity of the two vertices from which the particle stems with a width of about one unit of rapidity. Therefore the particle multiplicity distribution for a finite rapidity interval Δy will have the same average as the vertices but a larger width. To understand this effect we return to our simple binomial model. As before we

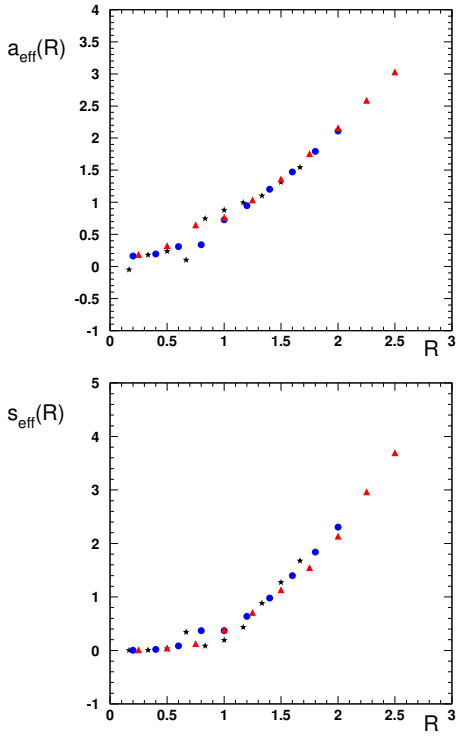

Figure 1.10: The functions $a_{\rm eff}(R)$ (upper plot) and $s_{\rm eff}(R)$ (lower plot) versus R. We show the results for three different rapidity ranges $\Delta y = 4$ (triangles), $\Delta y = 5$ (circles), and $\Delta y = 6$ (stars).

divide the rapidity range into N equal bins with the probability p to contain a vertex. Now we further assume that the presence of a vertex in any bin results in a particle in one of the two neighbouring bins with probability q or in the original bin with the remaining probability $1 - 2q$. In order to see how this smearing affects the mean and the variance we compute the generating function. The generating function for the original binomial distribution is given by

$$G(z) = [1 + p(z-1)]^N \; . \tag{1.39}$$

Some straightforward algebra then shows that the generating function for the above particle distribution is given by

$$G(z) = [1 + p(z-1)]^{(N-2)}[1 + p(z-1) + p^2(z-1)^2 q(1-q)]^2 \; . \tag{1.40}$$

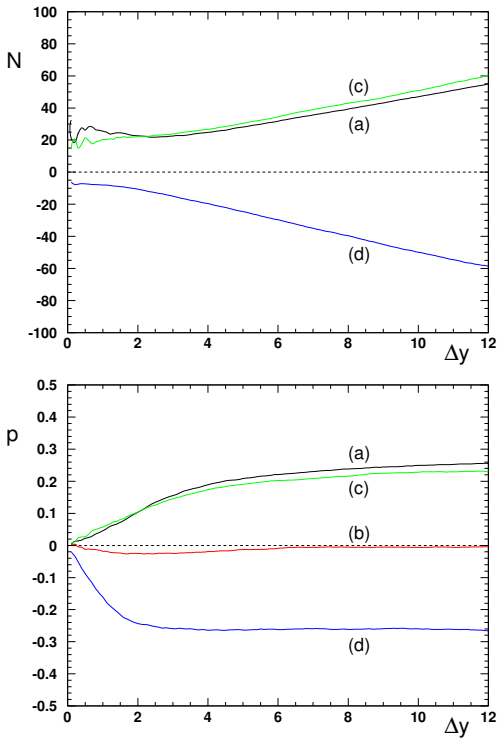

Figure 1.11: The values of N (upper plot) and p (lower plot) for the particle multiplicity distributions produced by JETSET. The four cases shown correspond to: (a) a single mass, no decays or $p_\perp$; (b) complete mass spectra, but no decays or $p_\perp$; (c) complete mass spectra, but no decays; and (d) complete mass spectra, charged final state particles.

Thus two factors of $(1+p(z-1))$ have been modified. The mean is unchanged and equal to Np, but the variance is increased from $V = \langle n\rangle(1-p)$ to

$$V = \langle n\rangle[1-p+4pq(1-q)/N]\,. \tag{1.41}$$

This distribution can be rather well approximated by another binomial distribution with the same mean and variance. This corresponds to effective p and N values

$$\begin{aligned} p_{\text{eff}} &= p[1-4q(1-q)/N] \\ N_{\text{eff}} &= \frac{Np}{p_{\text{eff}}}\,. \end{aligned} \tag{1.42}$$

Thus we see how a larger spread of the particles around the vertices (a larger q-value) corresponds to a larger width and a smaller effective p-value. From Eq.(1.42) p_{eff} must be larger than zero, but if we had allowed for a spread beyond the nearest bin then negative values of p_{eff} would be possible. This corresponds to a negative binomial distribution. Since the bin width is of the order of $bm_\perp^2$ the spread is certainly beyond neighbouring bins in the case of pion production.

We have investigated various cases of final state production. The multiplicity distributions can still be well approximated by binomial distributions with constant p-values for large rapidity intervals. In Fig.(1.11) we show N and p as a function of Δy for the various cases.

For a situation with only a single stable hadron, assumed to have the mass $m = 0.8$ GeV, and no transverse momentum generation, the result is as expected. Comparing the multiplicity distribution with the distribution for the vertices, we find that p is decreased and N is increased. The product of N and p is however the same for the two distributions.

If we include the standard mixture of different hadron masses p is further reduced. We obtain in this case a distribution that is very close to a Poissonian. Thus, as expected, the width of the multiplicity distribution greatly increases when light pions are produced.

Including transverse momentum generation increases p to positive values as shown in the figure. The transverse mass of the pions is thus, in the case of the standard mixture of hadrons, not small enough to give a negative p-value.

Finally, if we include the decays of unstable particles and analyse the final charged particles then the width increases substantially and p becomes negative (corresponding to a negative binomial distribution). Including the final uncharged particles in the analysis results in an even more negative p-value.

We can summarize our findings as follows. The width of the multiplicity distribution is very sensitive to the mass spectrum of the produced particles. Using default JETSET the average transverse mass is large enough to give a binomial multiplicity distribution. In this case the negative binomial distribution for the final state stems from the increased width due to decays.

1.6 Conclusions

Inspired by the Feynman–Wilson gas analogy we have derived an explicit form for the grand partition function of the Lund fragmentation model. This par-

tition function is described in terms of the multiplicity n. In particular, we derive an equation of state for the gas, corresponding to the first two terms in the virial expansion in the particle density.

The partition function is derived in the approximation that the particles are ordered in rapidity. This is true for the string break-up vertices and the number of vertices corresponds to the number of particles. Therefore, we have investigated the properties of the partition function using the vertices. For large rapidity intervals, we find that the average and the fluctuations of the multiplicity of vertices are described by the partition function.

The partition function gives a multiplicity distribution which is close to a binomial distribution. We find that the average transverse mass of the produced particles is sufficiently large to get a reasonable description from the approximation that the particles are ordered in rapidity. Thus the multiplicity distribution of the particles stemming from the string is described by an ordinary binomial. It is the decays of the unstable particles that results in a negative binomial distribution for the number of final charged particles.

The distribution of the vertices for different rapidity volumes and different multiplicities has also been investigated in terms of the proper-time. We find that the behaviour for large proper-times is determined only by the area-law and is independent of both the volume and the multiplicity. For smaller proper-times the distribution is described by a simple parametrisation. We find that the important quantity for the parametrisation is the density of vertices in rapidity, which in turn is described by the equation of state for the gas.

Acknowledgment

This work was supported in part by the EU Fourth Framework Programme 'Training and Mobility of Researchers', Network 'Quantum Chromodynamics and the Deep Structure of Elementary Particles', contract FMRX-CT98-0194 (DG 12 - MIHT).

1.A The binomial and negative binomial distributions

The binomial distribution is defined by

$$P(n) = \left(\begin{array}{c} N \\ n \end{array} \right) p^n (1-p)^{N-n} \quad . \tag{1.43}$$

The average, $\langle n \rangle$, and the variance $V = \langle n^2 \rangle - \langle n \rangle^2$ of this distribution are related to N and p via

$$\begin{aligned} \langle n \rangle &= Np \\ V &= Np(1-p) \quad . \end{aligned} \tag{1.44}$$

The binomial distributions form a family of distributions depending on the values of N and p. In the limit $p \to 0$ for constant $\langle n \rangle$, the distribution becomes a Poisson distribution. It is also possible to continue the expressions in Eq.(1.43) to negative p-values, which for constant $\langle n \rangle = Np$ implies also a negative N. In this case the distribution becomes a negative binomial distribution. Such a distribution is conventionally written in the form

$$P_k(n) = \left(\begin{array}{c} k+n-1 \\ k-1 \end{array} \right) \tilde{p}^k (1-\tilde{p})^n \tag{1.45}$$

where

$$\begin{aligned} \tilde{p} &= \left(\frac{1}{1-p} \right) \qquad (p < 0) \\ k &= -N \qquad\qquad (N < 0) \quad . \end{aligned} \tag{1.46}$$

Note that the relationships of Eq. (1.44) for the average and the variance remain true, even when p and N are both negative. Negative p-values correspond to distributions which are wider than a Poissonian. Thus the negative binomial distributions belong to the same larger family as the (ordinary) binomial and Poisson distributions. Within this family the width can vary from zero to infinity. Ordinary and negative binomials correspond to V smaller and larger than $\langle n \rangle$ respectively, with the Poisson distribution as the limiting case in between.

1.B The binomial approximation of the partition function

Our aim is to determine the c_1 and c_2 parameters of Eq.(1.35) from the N and p parameters of a binomial distribution. We begin by using Stirlings approxi-

mation to write the binomial distribution as

$$\begin{aligned}\ln(P) &= \frac{\ln N}{2} + N\ln N - (N-n)\ln(N-n) - n - \\ &\quad \frac{\ln(N-n)}{2} + N\ln(1-p) + n\ln\left(\frac{p}{1-p}\right) - \ln(n!) \end{aligned} \tag{1.47}$$

whilst the distribution in Eq.(1.35) can be written as

$$\ln(P_n) = \ln(c_0) - \frac{bm^2c_2n^2}{\Delta y} + n\ln(c_1\Delta y) - \ln(n!) \ . \tag{1.48}$$

We now express n as $n = \langle n\rangle + x$, where $\langle n\rangle$ is the mean. Next we subtract Eq.(1.47) from Eq.(1.48) and expand around $x = 0$ up to terms of order x^2. Equating the series coefficients to zero determines the parameters c_1 and c_2 in terms of N and p. We obtain

$$\begin{aligned} c_1\Delta y &= Np\ \exp\left[\frac{1-2p+2Np-2Np^2}{2N(1-p)^2}\right] \\ \frac{bm^2c_2}{\Delta y} &= \frac{2N(1-p)-1}{4N^2(1-p)^2} \ . \end{aligned} \tag{1.49}$$

Which for large Δy can be simplified to

$$\begin{aligned} c_1\Delta y &= Np\ \exp\left[\frac{p}{(1-p)}\right] \\ \frac{bm^2c_2}{\Delta y} &= \frac{1}{2N(1-p)} \ . \end{aligned} \tag{1.50}$$

If we insert these expressions into Eq.(1.35) then we finally obtain

$$P_n \sim \frac{(Np)^n}{n!}\exp\left[\frac{-n^2+n2Np}{2N(1-p)}\right] \ . \tag{1.51}$$

References

[1] K.G. Wilson,
Proc. Fourteenth Scottish Universities Summer School in Physics (1973),
eds R.L. Crawford and R. Jennings (Academic Press, New York, 1974).

[2] B. Andersson, G. Gustafson, G. Ingelman and T. Sjöstrand,
Phys. Rep. **97**, 31 (1983)
B. Andersson, The Lund Model, (*Cambridge University Press*, 1998)

[3] T. Sjöstrand, *Comp. Phys. Comm.* **82**, 74 (1994)

[4] B. Andersson, G. Gustafson and B. Söderberg, *Z. Phys.* **C20**, 317 (1983)

[5] M.B. Bowler, *Z. Phys.* **C11**, 169 (1981)
D.A. Morris, *Nucl. Phys* **B313**, 634 (1989)

Bose–Einstein correlations in the Lund model

Paper II

Bose–Einstein correlations in the Lund model

Bo Andersson and Markus Ringnér

Department of Theoretical Physics, Lund University,
Sölvegatan 14A, S-223 62 Lund, Sweden

Nuclear Physics **B 513**, 627-644 (1998)

By providing the Lund Model fragmentation process with a quantum-mechanical framework we extend the results of [6] to situations where there are very many identical bosons. We investigate the features of the weight distributions in some detail and in particular exhibit three-particle Bose–Einstein correlations, the influence on the ρ-spectrum and the difference between charged and neutral pion correlations.

2.1 Introduction

The Hanbury-Brown–Twiss (HBT) effect [1], often called the Bose–Einstein effect, originated in astronomy where one uses the interference pattern of the photons to learn about the size of the photon emission region, i.e. the size of the particular star, which is emitting the light. The effect can be described as an enhancement of the two-particle correlation function that occur when the two particles are identical bosons and have very similar energy-momenta. A well-known formula [2] to relate the two-particle correlation function (in four-momenta $p_j, j = 1, 2$ with $q = p_1 - p_2$) to the space–time density distribution, ρ, of (chaotic) emission sources is,

$$\frac{\sigma d\sigma_{12}}{d\sigma_1 d\sigma_2} = 1 + |\mathcal{R}(q)|^2 \tag{2.1}$$

where $\mathcal{R}$ is the normalized Fourier transform of the source density

$$\mathcal{R}(q) = \frac{\int \rho(x) dx \exp(iqx)}{\int \rho(x) dx} \quad . \tag{2.2}$$

This quantity is often, without very convincing reasons, parametrised in terms of a "source radius" R and a "chaoticity parameter" λ,

$$|\mathcal{R}(q)|^2 = \lambda \exp(-R^2 Q^2) \tag{2.3}$$

with $Q^2 = -q^2$. The source radii obtained by this parametrisation tend to be similar in all hadronic interactions (we exclude heavy ion interactions where the extensions of nuclear targets and probes will influence the result), with $R \sim 0.5 - 1$ fm, but the chaoticity varies rather much depending upon the particular data sample and the method of the fit. At present the knowledge of higher-order correlations is still limited in the experimental data, although in principle there should be such correlations.

The HBT effect between identical bosons produced in hadronic interactions, being of a purely quantum mechanical nature, is not easily included in the event generator programs used in high energy physics. Such simulation programs, like HERWIG [3] (based upon the Webber–Marchesini parton cascades and ending by cluster fragmentation) and JETSET [4] (based upon the Lund Model string dynamics [7]) are built in accordance with classical stochastical processes, i.e. they produce a probability weight for an event without any quantum mechanical Bose–Einstein interference effects.

Sjöstrand has introduced a clever device as a subroutine to JETSET, in which the HBT effect is simulated as a mean field potential attraction between identical bosons [5]. Thus, given a set of energy-momentum vectors of identical

bosons, $p_1, \ldots, p_n$, generated without any HBT effect, it is possible to reshuffle the set into another set where each pair on the average has been moved relatively closer to show a (chosen) HBT-correlation, while still keeping to energy-momentum conservation for the whole event.

In this paper we will develop a method devised in [6] to provide the Lund Model with a quantum mechanical interpretation. In particular there will be a production matrix element with well-defined phases. This will then be used to make a model of the HBT effect. Although this model stems from different considerations it will nevertheless contain predictions which are similar to those in the ordinary approach giving Eq.(2.1). The correlations in this model are implemented as weights assigned to events generated by JETSET.

In section 2.2 we survey those features of the Lund model, that are necessary for the following. We have in this work extended the method from [6] to situations where there are many identical bosons and in section 2.3 we will exhibit the general n-particle HBT-correlations in the model. The resulting expressions contain a sum of in general $n!$ terms, i.e. it is of exponential type from a computational point of view. It is possible to subdivide the expressions in accordance with the group structure of the permutation group. Although the higher order terms provide small contributions in general the computing times are still forbidding. In order to speed up the calculations we introduce instead in this paper the notion of *links* between the particles and we show that in this way it is possible to obtain expressions of power type from a calculational point of view, which are perfectly tractable in a computer.

In the last section we exhibit a set of results both in order to show the workings of the model and to provide predictions for experiments. Since we have extended the model to multiparticle permutations we show in particular that the model exhibit three-particle BE correlations. In agreement with our findings in section 2.3, that our general expression is sensitive to a reasonable estimate of the space–time difference between the production points of the identical bosons, we get a difference between charged and neutral pion correlations. The details of the general event weight distribution are analysed and we also investigate the influence on the ρ-spectrum

We will in this paper be satisfied to treat only two-jet events, i.e. we will neglect hard gluon radiation and we will come back to HBT effects in gluon events in another publication.

2.2 Some properties of the Lund model

Within the framework of perturbative QCD it is possible to obtain many useful formulas but all the results are expressed in a partonic language. In order to be able to compare to the hadronic distributions, which are observed in the experimental setups, it is necessary to supplement the perturbative results with a fragmentation process. We will in this paper be concerned with the Lund string model [7] and we start with a brief introduction to its main properties.

In the string model the confining colour field is approximated by a massless relativistic string. The endpoints of the string are identified with quark and anti-quark properties while the gluons are assumed to behave as transverse excitations on the string. The string can break up into smaller pieces by the production of $q\overline{q}$-pairs (i.e. new endpoints). Such a pair will immediately start to separate because of the string tension, which in the rest frame of a string segment corresponds to a constant force κ; phenomenologically $\kappa \simeq 1$ GeV/fm. Final state mesons are formed from a q and a $\overline{q}$ from adjacent vertices, as shown in Fig.(2.1).

Each breakup vertex will separate the string into two causally disconnected parts. From the causality, together with Lorentz covariance and straightforward kinematics, it is possible to derive a unique breakup rule for the string by means of (semi)classical arguments [8].

The unique breakup rule results in the following probability for a string to decay into hadrons $(p_1, \ldots, p_n)$.

$$dP(p_1,...,p_n) = \left[\prod_i (N dp_i \delta(p_i^2 - m_i^2))\right] \delta(\sum_j p_j - P_{tot}) \exp(-bA) \qquad (2.4)$$

where A is the area of the breakup region as indicated in Fig.(2.1) and N and b are two parameters.

The similarity of the result to Fermi's Golden Rule for the probability of a quantum mechanical transition, i.e. the size of the final state phase space multiplied by the square of a matrix element $|\mathcal{M}|^2$ expressed by the exponential area suppression, provides a reasonable starting point to try to derive a corresponding quantum mechanical process. There are at least two possible mechanisms, *viz.* a quantum mechanical tunneling process a la Schwinger and/or the possible relationship to the Wilson loop operators in a gauge field theory. We will find that they provide very similar answers to the problem.

Starting with the tunneling arguments, we note that while a massless $q\overline{q}$-pair without transverse momentum can be produced in a point-like way anywhere

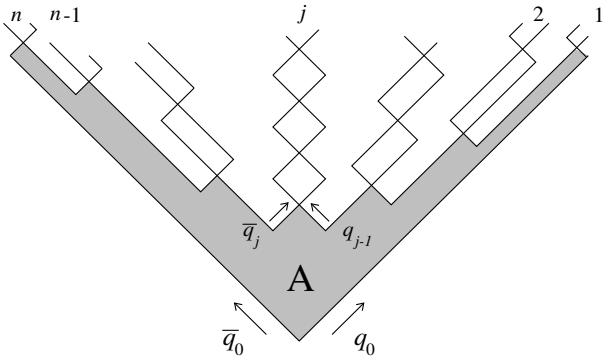

Figure 2.1: The decay of a Lund Model string.

along the string, a massive pair or a pair with transverse momentum must classically be produced at a distance so that the string energy between them can be used to fulfill energy-momentum conservation. If the transverse momentum is conserved in the production process, i.e. the $q\overline{q}$ with masses μ obtain $\pm\vec{k}_\perp$, respectively, then the pair may classically be realised at a distance $\delta x = 2\mu_\perp/\kappa$, where $\mu_\perp$ is the transverse mass $\sqrt{\mu^2 + \vec{k}_\perp^2}$.

The probability for a quantum mechanical fluctuation of a pair, occurring with $\mu_\perp$ at the (space-like) distance δx, is in a force-free region given by the free Feynman propagator squared:

$$|\Delta_F(\delta x, \mu_\perp)|^2 \sim \exp(-2\mu_\perp \delta x) = \exp\left(-\frac{4\mu_\perp^2}{\kappa}\right) \quad . \tag{2.5}$$

A corresponding quantum mechanical tunneling process in a constant force field will according to WKB methods give

$$\left|\exp\left(-2\int_0^{\delta x}\sqrt{\mu_\perp^2 - (\kappa x)^2}dx\right)\right|^2 = \exp\left(-\frac{\pi\mu_\perp^2}{\kappa}\right) \equiv P(\mu_\perp) \quad . \tag{2.6}$$

The difference is that in the force-free case we obtain an exponential suppression $4\mu_\perp^2/\kappa$ but when the constant force pulls the pair apart we obtain the somewhat smaller suppression $\pi\mu_\perp^2/\kappa$. Besides the mass suppression (which phenomenologically will suppress strange quark-pairs with a factor of ~ 0.3 compared to "massless" up and down flavored pairs) we obtain the transverse momentum Gaussian suppression

$$\exp\left(-\frac{1}{2\sigma^2}k_\perp^2\right) \quad \text{with} \quad 2\sigma^2 = \frac{\kappa}{\pi} \quad . \tag{2.7}$$

The value of σ as used in JETSET is a bit larger than the result in Eq.(2.7) but this can be understood as an effect of soft gluon generation along the string. The transverse momentum of a hadron produced in the Lund Model is then the sum of the transverse momenta of its constituents.

We may use the elementary result in Eq.(2.6) to calculate the persistence probability of the vacuum, $\mathcal{P}$, as it is defined in [9]. It is the probability that the no-particle vacuum will not break up, owing to pair-production, during the time T over a transverse region $A_\perp$, when a constant force κ is applied along the longitudinal x-direction over a region L:

$$\mathcal{P} = \prod_{t\in(0,T),x\in(0,L),\vec{k}_\perp,s,f} (1 - P(\mu_\perp)) = \exp\left(\sum_{t,x,\vec{k}_\perp,s,f} \log(1-P)\right) \quad . \tag{2.8}$$

We have then assumed that the field couples to (fermion) pairs with spin s and flavors f and we sum over all possibilities for the production. As each pair needs a longitudinal size $\delta x = 2\mu_\perp/\kappa$ and, according to Heisenberg's indeterminacy relation, will live during a time-span $2\pi/2\mu_\perp$ there is at most $\kappa LT/2\pi$ pairs possible over the space-time region LT. The transverse momentum summation can be done by Gaussian integrals from an expansion of $\log(1-P)$ and the introduction of the well-known number of waves available in a transverse region $A_\perp$: $(A_\perp/(2\pi)^2)d^2k_\perp$. In this way we obtain for the persistence probability

$$\mathcal{P} = \exp(-\kappa^2 LTA_\perp\Pi) \quad \text{with} \quad \Pi = \frac{n_f n_s}{4\pi^3}\sum_{n=1}^{\infty}\frac{1}{n^2}\exp\left(-\frac{n\pi\mu^2}{\kappa}\right) \tag{2.9}$$

where n_f, n_s is the number of flavor and spin states.

There are two remarks to this result. Firstly, although the method to treat the integration over time and longitudinal space, by close-packing reasonably sized boxes, may not seem convincing the final formula [9] coincides with the one obtained by Schwinger [10], for the case of a constant electric field $\mathcal{E}$. Then κ is identified with the force of the charges in the external field, i.e. $\kappa \to e\mathcal{E}$.

Secondly, the result is in evident agreement with the formula for the decay of the Lund string in Eq.(2.4) if we identify LT with the (coordinate space) area size A. In this way we also obtain the result that the parameter b is

$$b = \kappa^2 A_\perp \Pi \tag{2.10}$$

i.e. it corresponds to the transverse size of the (constant) force field, which we have modeled by the string. The quantity Π is $1/(12\pi)$ for two massless spin 1/2-flavors.

The second quantum mechanical approach is to note that a final state hadron stems from a q from one vertex j and a $\overline{\mathrm{q}}$ from the adjoining vertex $j+1$. In order to keep to gauge invariance it is then necessary that the production matrix element contains at least a gauge connector between the vertices: $\exp(i\int_j^{j+1} g\mathcal{A}^\mu dx_\mu)$, where g is the charge and $\mathcal{A}^\mu$ the gauge field. Consequently the total production matrix element must contain a Wilson loop operator:

$$\mathcal{M} = \exp(i \oint g\mathcal{A}^\mu dx_\mu) \tag{2.11}$$

with the integration around the region A (note that the field is singular along the border line and we are therefore not allowed to distort the integration contour inwards). The operator in Eq.(2.11) was predicted (and inside lattice gauge calculations also found) to behave as

$$\mathcal{M} = \exp(i\xi A) \tag{2.12}$$

with the real part of ξ, $Re(\xi) = \kappa$. In the present situation where the force field region decays we expect an imaginary part, corresponding to the pair production rate according to the well-known Kramers-Kronig [11] relationship for the dielectricity in matter, in this case the QCD vacuum.

The two interpretations of the area law, i.e. the Schwinger tunneling in Eq.(2.9) and the Wilson loop operator result in Eq.(2.12) can be related if we note that according to Gauss' law the integral over the extension of the force field should correspond to the charge. For a thin string we should then obtain for the area falloff rate $b \propto \kappa^2 A_\perp \propto \kappa\alpha$. Although Gauss' law is more complicated for a non-abelian field with triplet and octet color-charges and similarly octet fields it is possible to make a case for an identification of the parameter b as

$$b = \frac{\kappa n_f \bar{\alpha}}{12} \tag{2.13}$$

which is what we should expect from the expected imaginary part of the dielectricity in Eq.(2.12). $\bar{\alpha} = 3g^2/(4\pi)$ is then the effective QCD coupling, including the color factors. The result is also phenomenologically supported if we consider a partonic cascade down to a certain transverse momentum cutoff $k_{\perp c}$ and then use the Lund model hadronization formulas to obtain the observed properties of the final state. In that way we may determine the parameters in the model as functions of the partonic cascade cutoff. A remarkably good fit to the b-parameter is given by $C/\log(k_{\perp c}^2/\Lambda^2)$ with C given by Eq.(2.13) and $\Lambda \simeq 0.5$ GeV [12], according to the QCD coupling.

Independently of the precise identification of b, we obtain a possible matrix element from Eq.(2.12)

$$\mathcal{M} = \exp(i\kappa - b/2)A \tag{2.14}$$

which not only will provide us with the Lund decay probability in Eq.(2.4), but also can be used in accordance with [6] to provide a model for the Hanbury-Brown–Twiss effect for the correlations among identical bosons.

2.3 A model for Bose–Einstein correlations

We will from now on work in energy-momentum space in agreement with the usual treatment of the Lund model formulas. Further we will make use of a light-cone metric with $p_\pm = e \pm p_\ell$ where ℓ denotes the longitudinal direction along the string. The two metrics differ by a factor of two, i.e. $2dedp_\ell = dp_+dp_-$. Note in particular that compared to the considerations in the earlier section this means that the area $A \to 2\kappa^2 A$ and the parameter $b \to b/(2\kappa^2)$.

We now consider a final state containing (among possibly a lot of other stuff) n identical bosons. There are $n!$ ways to produce such a state, each corresponding to a different permutation of the particles. According to quantum mechanics the transition matrix element is to be symmetrised with respect to exchange of identical bosons. This leads to the following general expression for the production amplitude

$$\mathcal{M} = \sum_{\mathcal{P}} \mathcal{M}_{\mathcal{P}} \tag{2.15}$$

where the sum goes over all possible permutations $\mathcal{P}$ of the identical bosons. The cross section will then contain the square of the symmetrised amplitude $\mathcal{M}$

$$|\mathcal{M}|^2 = \sum_{\mathcal{P}} (|\mathcal{M}_{\mathcal{P}}|^2 (1 + \sum_{\mathcal{P}' \neq \mathcal{P}} \frac{2\mathrm{Re}(\mathcal{M}_{\mathcal{P}} \mathcal{M}^*_{\mathcal{P}'})}{|\mathcal{M}_{\mathcal{P}}|^2 + |\mathcal{M}_{\mathcal{P}'}|^2})) \ . \tag{2.16}$$

The phenomenological models used to describe the hadronization process are formulated in a probalistic language (and not in an amplitude based language). This implies that interference between different ways to produce identical bosons is not included. In this case the probability for producing the state is

$$|\mathcal{M}|^2 = \sum_{\mathcal{P}} |\mathcal{M}_{\mathcal{P}}|^2 \tag{2.17}$$

instead of the probability in Eq.(2.16). Comparing Eq.(2.16) and Eq.(2.17) it is seen that a particular production configuration leading to the final state $\mathcal{P}$ can be produced according to a probalistic scheme and that the quantum mechanical interference from production of identical bosons can be incorporated by weighting the produced event with

$$w = 1 + \sum_{\mathcal{P}' \neq \mathcal{P}} \frac{2\mathrm{Re}(\mathcal{M}_{\mathcal{P}} \mathcal{M}^*_{\mathcal{P}'})}{|\mathcal{M}_{\mathcal{P}}|^2 + |\mathcal{M}_{\mathcal{P}'}|^2} \ . \tag{2.18}$$

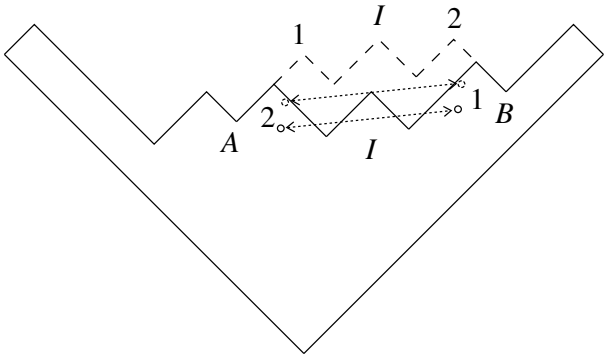

Figure 2.2: The two possible ways, $(\ldots,1,I,2,\ldots)$ and $(\ldots,2,I,1,\ldots)$, drawn with solid and dashed lines respectively, to produce the entire state when two of the bosons are identical. The open circles show the two different production points for each identical boson and the arrows indicate the space-time difference, δx, between the two production points for the two production configurations. A and B denote the two vertices surrounding the identical bosons.

The outer sum in Eq.(2.16) is as usual taken care of by generating many events.

In order to see the main feature of symmetrising the hadron production amplitude in the Lund Model we consider Fig.(2.2), in which two of the produced hadrons, denoted $(1,2)$, are assumed to be identical bosons and the state in between them is denoted I. We note that there are two different ways to produce the entire state corresponding to the production configurations $(\ldots,1,I,2,\ldots)$ and $(\ldots,2,I,1,\ldots)$, i.e. to exchanging the two identical bosons. The two production configurations are shown in the figure and the main observation is that they in general correspond to different areas!

The area difference, ΔA, depends only on the energy momentum vectors p_1, p_2 and p_I, but can in a dimension-less and intuitively useful way be written

$$\frac{\Delta A}{2\kappa} = \delta p \delta x \tag{2.19}$$

where $\delta p = p_2 - p_1$ and $\delta x = (\delta t; 0, 0, \delta z)$ is a reasonable estimate of the space-time difference, along the surface area, between the production points of the two identical bosons. We note that the space-time difference δx is always space-like. In Fig.(2.2) δx, for the two production configurations, is indicated by arrows, together with open circles showing the corresponding production points. The production points are defined by the centres of the particles space–

time rectangles.

We go on to consider the effects of transverse momentum generation in the $q\overline{q}$-vertices. First we note that the total transverse momenta of the sub-state $1, I, 2$ in Fig.(2.2) stem from the q and $\overline{q}$ generated at the two surrounding vertices, A and B. This is, owing to momentum conservation, fixed by the properties of the hadrons generated outside of the sub-state. Using this we find that there is a unique way to change the transverse momenta in the vertices surrounding the intermediate state I such that every hadron has the same transverse momenta in both production configurations.

Suppose as an example that we have generated $\pm\mathbf{k}_{\perp A}$ in the vertex A and $\pm\mathbf{k}_{\perp B}$ in the vertex B (i.e. so that $-\mathbf{k}_{\perp A}$ and $\mathbf{k}_{\perp B}$ defines the sub-state). Then to conserve the transverse momenta of the observed hadrons when changing production configuration from $(1, I, 2)$ to $(2, I, 1)$ it is necessary to change the generation of transverse momenta in the two vertices surrounding I as follows (in an easily understood notation):

$$\begin{aligned} \pm\mathbf{k}_{\perp I} &\rightarrow \pm(\mathbf{k}_{\perp A} + \mathbf{k}_{\perp B} - \mathbf{k}'_{\perp I}) \\ \pm\mathbf{k}'_{\perp I} &\rightarrow \pm(\mathbf{k}_{\perp A} + \mathbf{k}_{\perp B} - \mathbf{k}_{\perp I}) \ . \end{aligned} \tag{2.20}$$

This means that exchanging two bosons with different transverse momenta will result in a change in the amplitude as given by Eq.(2.7) for some of the vertices.

From the amplitudes in Eq.(2.14) and Eq.(2.7) we get that the weight in the Lund Model can be written

$$w = 1 + \sum_{\mathcal{P}' \neq \mathcal{P}} \frac{\cos\frac{\Delta A}{2\kappa}}{\cosh\left(\frac{b\Delta A}{2} + \frac{\Delta(\sum p^2_{\perp \mathrm{q}})}{2\sigma^2_{p_\perp}}\right)} \tag{2.21}$$

where Δ denotes the difference with respect to the configurations $\mathcal{P}$ and $\mathcal{P}'$ and the sum of $p^2_{\perp \mathrm{q}}$ is over all vertices. We have introduced $\sigma_{p_\perp}$ as the width of the transverse momenta for the generated hadrons, (i.e. $\sigma^2_{p_\perp} = 2\sigma^2$).

Using Eq.(2.19) for a single pair exchange one sees that the area difference is, for small δp, governed by the distance between the production points and that ΔA increases quickly with this distance. We also note that ΔA vanishes with the four-momentum difference and that the contribution to the weight from a given configuration, $\mathcal{P}'$, vanishes fast with increasing area difference ΔA. From these considerations it is obvious that only exchanges of pairs with a small δp and a small δx will give a contribution to the weight. In this way it is possible to relate to the ordinary way to interpret the HBT effect, cf. Eq.(2.2).

It is straightforward to generalise Eq.(2.19) to higher order correlations. One

notes in particular that the area difference does not vanish if more than two identical bosons are permuted and only two of the bosons have identical four-momenta.

Models for BE correlations have been suggested, e.g. [13], with similar weight functions, but it is important to note that the weight in our model has a scale both for the argument to the cos-function as well as for the function which works as a cut-off for large δp and δx (in our case a cosh-function). Further the two scales in our model are different and well-defined, at least phenomenologically. We will come back to the influence of the two scales in section 2.5.

2.4 MC implementation

To calculate the weight for a general event, with multiplicity n, one has to go through $n_1!n_2!...n_N! - 1$ possible production configurations, where n_i is the number of particles of type i and there are N different kinds of bosons. For a general e^+e^- event at 90 GeV this is not possible from a computational point of view.

We know however that the vast majority of configurations will give large area differences and they will therefore not contribute to the weight. One of our aims with this work has been to find a way to approximate the sum in Eq.(2.21) with *a sum over configurations with significant contributions to the weight.* From basic group theory we know that every group can be partitioned into its classes. Let $11111\ldots1$ denote the class containing only the identity element, where all particles are unchanged, $m_1m_2111\ldots1$ denote the class of group-elements where m_1 particles are cyclically permuted, m_2 other particles are cyclically permuted and the rest are unchanged, and so on. We can define the order, k, of a class as $k = \sum_i (m_i - 1)$. The useful feature of this ordering of classes is that for all group-elements contained in order k the minimum of the summed size (in positions) of the cyclically permuted clusters , Δr, is k, i.e. the minimum length over which particles are moved increases with the order. From the discussion at the end of section 2.3 it is then obvious that the contribution to the weight from a configuration will decrease with its order. All classes up to order 4 are shown in Table 2.1.

We have found that for essentially all events the weight does not change when including the fifth order. But we have also found that lots of lower-order configurations give no contributions to the weight. This is not acceptable when taking computing time into account and we have therefore abandoned using a cut in order.

Order	0	1	2	3	4
Classes	11111...1	21111...1	22111...1	22211...1	22221...1
			31111...1	32111...1	32211...1
				41111...1	33111...1
					42111...1
					51111...1
Δr	0	≥ 1	≥ 2	≥ 3	≥ 4

Table 2.1: The classes of the permutation group order by order up to the fourth order. Δr is the minimum length over which particles are permuted.

In this work we have instead approximated the sum in Eq.(2.21) with a sum over configurations of all orders with significant contributions to the weight. This has been done by introducing *exchange-links* between particles. We have only taken into account interference with configurations where all particles are produced in positions from which there is a link to a particle's original production position. Defining a link matrix, $\mathcal{L}$, as follows

$$\mathcal{L}_{ij} = \begin{cases} 1 & \text{if there is a link between particles } i \text{ and } j. \\ 0 & \text{otherwise} \end{cases}$$

one gets a simple representation of the configurations to be considered. The function of a link, $\mathcal{L}_{ij}$, is to enable moving particle i to particle j's position. It is important to note that a general link matrix enables higher order permutations even though the links are defined between pairs only. If all elements in $\mathcal{L}$ are 1, it corresponds to considering all n! permutations, while only the original configuration is considered if $\mathcal{L}$ is the identity matrix.

ΔA for a pair exchange increases, as previously discussed, with the four-vector difference δp and with the size of the state in between. Since we know from Eq.(2.21) that the contribution to the weight for a given configuration vanishes fast with increasing area difference ΔA, it is useful to introduce the concept of link-size, defined below as the invariant four-momentum difference together with the invariant mass of the particles produced in between the pair (in rank). By only accepting links between particles if the size of the link between them is smaller than some cut-off link-size, δ_c, we get a prescription for the exchange matrix of an event. In this way, by specifying the allowed two-particle exchanges, we get, to all orders, which configurations to take into account. We have found that for a given δ_c one includes all configurations that provide a contribution larger than some ϵ to the weight. Taken together this means that we get all the important contributions to the weight if we chose δ_c so large that the neglected terms smaller than ϵ give a negligible change for every weight.

We have used a cut-off link-size such that there is a link between identical bosons if one of the following conditions is fulfilled.

- $Q^2 = -(p_i - p_j)^2 < Q^2_{\rm max} \simeq 1$ GeV^2.
- the invariant mass of the particles produced in between (along the string) the pair is less than $m^2_{\rm max} \simeq (20$ GeV$)^2$.

Including links larger than this give no contribution to the weight for essentially all events. There are a few special events for which the weights have not converged with this δ_c. They are very rare and have in common that they have a cluster of particles such that exchanging any pair in the cluster will give a large area-difference, but there are cyclic permutations which give a small area-difference. Increasing δ_c to include these configurations give no noticeable effect in any observable known to us (except the computing time in the simulation!).

Including decays

A large fraction of all final-state bosons stem from decays of short-lived resonances with lifetimes comparable to the time scale in string decay. Therefore they may contribute to the Bose–Einstein effect. To include their decay amplitudes and phase space factors and symmetrise the total amplitude is very difficult and it is furthermore not known how to do that in a model-consistent way. We have included resonance decays in the following simple way

> Particles with width larger than $\Gamma_{\rm min}$ are assumed to decay before Bose–Einstein symmetrisation sets in and the matrix elements are evaluated with their decay products regarded as being produced directly, ordered in rank. We have used $\Gamma_{\rm min} = 0.02$ GeV.

The signal in the two-particle correlation function goes down very much if we neglect all the pions from resonance decays when symmetrising the amplitudes. But our signals are fairly independent of $\Gamma_{\rm min}$ as long as it is small enough for the ρ's to decay before the symmetrisation.

An elaborate discussion on the treatment of resonances in connection with BE correlations can be found in [14].

2.5 Results

In our simulations we have used the Lund string model [7] implemented in the JETSET MC [4] to hadronize $q\overline{q}$-pairs (i.e. no gluons are considered). The MC implementation of our model is available from the authors.

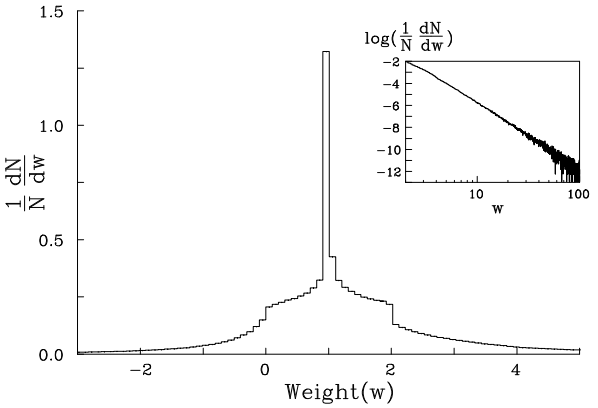

Figure 2.3: The distribution of Bose–Einstein weights for two-jet states in JETSET. The tail of positive weights is shown in the insert.

2.5.1 The weight distribution and two-particle correlations

The majority of the weights are close to and centered around unity, as seen in Fig.(2.3). There is however a tail of weights far away from unity in both directions. The tail of positive weights is shown as an insert and the distribution looks like a power. However if we subdivide the events into sets with similar number of links and study the weight distributions for these sets separately, we find that the weight distribution for each set is basically Gaussian. The width of these Gaussians increases with the number of links in the corresponding set, as shown in Fig.(2.4). The power like behaviour of the weight distribution is therefore merely a consequence of summing over events with different number of links. It should be emphasized that the negative weights only are a technical problem. Summing over many events results in positive probabilities for all physical observables, which is obvious from Eq.(2.16).

We have taken the ratio of the two-particle probability density of pions, ρ_2, with and without BE weights applied as the two-particle correlation function, R_2, i.e.

$$R_2(p_1, p_2) = \frac{\rho_{2w}(p_1, p_2)}{\rho_2(p_1, p_2)} \tag{2.22}$$

where the w denotes weighted distributions.

As discussed in connection with Eq.(2.19) the correlation length in Q depends inversely on the (space-like) distance between the production points of the

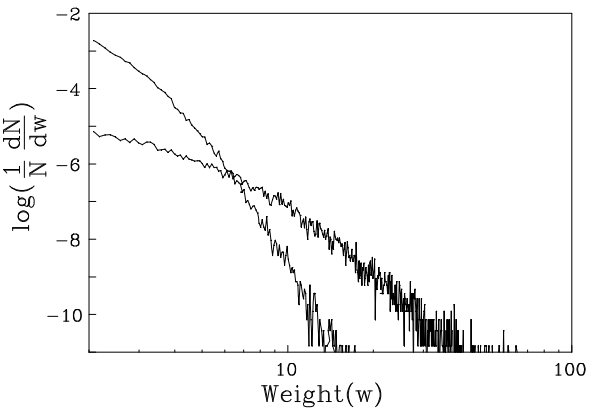

Figure 2.4: The distribution of Bose–Einstein weights for two-jet events subdivided into sets with different number of links, n_l. Two samples for $3 \leq n_l \leq 5$ and $10 \leq n_l \leq 12$ are plotted.

identical bosons and the Bose–Einstein correlation length, that is dynamically implemented, in this model can most easily be described as the flavour compensation length, i.e. the region over which a particular flavour is neutralised. Identically charged particles cannot be produced as neighbours along the string in the Lund model while neutral particles can. This implies that identically charged pions which always must have a non-vanishing state in between will have a more narrow correlation distribution in Q compared to neutral pions. This has been found as can be seen in Fig.(2.5) where the correlation distributions for pairs of particles used in the symmetrisation are shown. The correlation functions have been normalised to unity in the region $1.0 \leq Q \leq 2.5$. The correlation distribution for charged pions can be approximated by the LUBOEI algorithm [5] with radii $\simeq$ 1 fm and $\lambda \simeq 0.8$ as input parameters (Note that the input parameters are not exactly reproduced in the resulting correlation function). This is in reasonable agreement with the LEP experiments, which measure sizes of the order of $0.5 - 1$ fm, [15, 16, 17], even though they tend towards values smaller than 1 fm. The correlation function depends on the daughters of resonances and especially the decay products of η' play a large role. The production rate of η' used in JETSET was questioned in [14], in connection with BE correlations. We have used reduced production rates for η and η' by setting the extra suppression factors in JETSET to 0.7 and 0.2 respectively, in accordance with the DELPHI tuning [18]. For a more elaborate quantative comparison with data our BE Monte Carlo has to be tuned further and the resulting events have to be subjected to the same corrections as in the

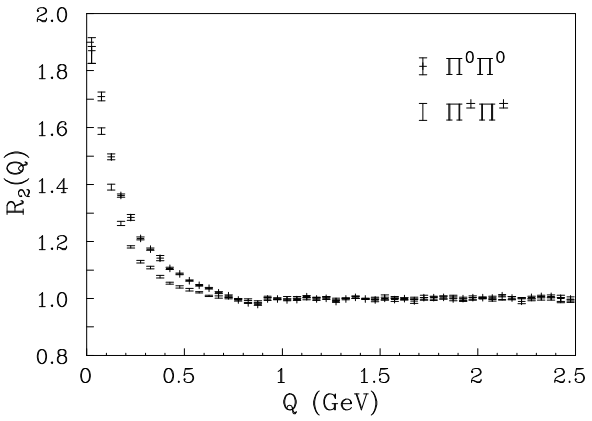

Figure 2.5: The ratio $R(Q)$ of the number of pairs with invariant relative four-momentum Q with and without Bose–Einstein weights applied. The sample consists of the particles used in the symmetrisation.

experimental analysis.

The general findings for the parameter dependence of the weight function in Eq.(2.21) is that due to the smallness of b as compared to $1/\kappa$, it is for most of the terms in the sum the decrease of the cos-function with increasing ΔA that governs the behaviour. For larger ΔA it is the transverse momentum contributions to the cosh-function which takes over to damp the contribution to the weight. Note that the argument of the cos-function contains κ as the basic scale and that the transverse momentum contributions also are governed essentially by κ (see Eq.(2.7)). Going over to correlation functions we find as expected from the conclusions for the weight function that the correlation function is not affected when the b-parameter is changed $\pm 20\%$. The slope of the correlation function for small Q values and therefore the correlation length is very sensitive to κ and it is also sensitive to the width of the transverse momenta. The transverse momentum generation acts as noise in the model so that all weights approach unity and consequently all correlations vanish with increasing $\sigma_{p_\perp}$. It is however this noise which makes the weight calculations tractable. Consequently, the main parameter is the string tension, κ, in this model for Bose–Einstein correlation weights as well as for the correlation length.

Since the BE weights are depending on the space-like distance between the production points we have studied the two-particle correlation function as a function of the invariant space-time distance $\Delta x = \sqrt{-\delta x^2}$ where $\delta x = (\delta t; 0, 0, \delta z)$

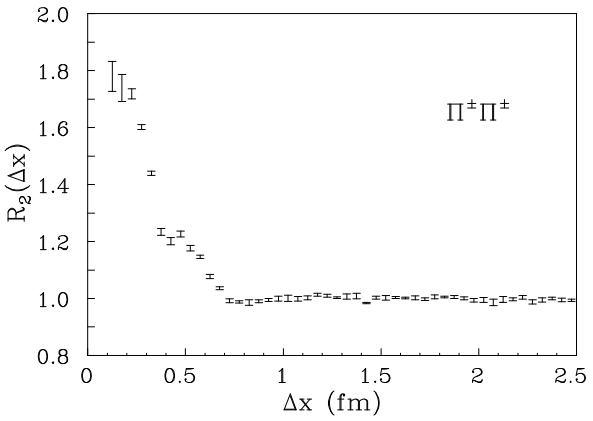

Figure 2.6: The ratio $R_2(\Delta x)$ of the number of pion pairs with invariant relative distance Δx with and without Bose–Einstein weights applied. The sample consists of the particles used in the symmetrisation, i.e. pions that are initially produced or stemming from short lived resonances as defined in section 2.4.

as defined in Eq.(2.19). In Fig.(2.6) $R_2(\Delta x)$, which has been normalised to unity in the region $1.0 \leq Q \leq 2.5$, is plotted. The figure illustrates that the effect of the Bose–Einstein symmetrisation , i.e. to pack identical bosons closer together in phase-space, is manifest up to production point separations of about 0.7 fm. It should however be noted that many configurations where pairs are exchanged over significantly larger distances give significant contributions to the weight.

We have also found that the higher order contributions to the sum in Eq.(2.21) is of importance for the two-particle correlations. That is using more than two-particle exchanges when calculating the weights does not only affect the weight distribution but also the two-particle correlation function, $R_2(Q)$.

In heavy-ion collision experiments one has found that the extracted correlation length has an approximate $1/\sqrt{m_t}$ dependence [19], where m_t is the transverse mass, $\sqrt{m^2 + p_t^2}$. This is in agreement with hydrodynamical models describing the source evolution in heavy-ion collisions. Recently a similar m_t dependence has been found for Z^0 hadronic decays in e^+e^- annihilation at LEP [24], when the transverse directions are defined with respect to the jet axis. In the Lund Model the average space-like distance between pairs of identical pions increases with m_t and one would therefore not expect a correlation length which falls off with m_t. For initially produced particles we get a correlation length which

is essentially independent of m_t. However when analysing all final particles we find for increasing m_t that the correlation length falls off and that the λ parameter increases, as in [24]. From this we conclude that the observed m_t dependence of the correlation length in data is, in our model, compatible with the vanishing of contributions from decay products with increasing m_t.

2.5.2 Residual Bose–Einstein correlations

Bose–Einstein correlations acting between identical bosons may have significant indirect effects on the phase space for pairs of non-identical bosons. We have studied mass distributions of $\pi^+\pi^-$ systems to see how our model affects systems of unlike charged pions. Many analyses use $\pi^+\pi^-$ distributions to quantify the Bose–Einstein correlations, using the unlike-charged distributions as reference samples with which to compare the like-charged pion distributions. We have found that the assumption that the two-particle phase space densities for $\pi^+\pi^-$ systems are relatively unaffected by Bose–Einstein symmetrisation is fairly good. Taking the ratio of the $\pi^+\pi^-$ mass distributions with and without Bose–Einstein symmetrisation applied gives that the mass distribution is not altered much by the symmetrisation, and that the effect is smaller than 5% in the entire mass range.

It has however been observed experimentally that the Breit-Wigner shape for oppositely charged pions from the decay of the ρ resonance [20, 21, 22] is distorted. We have therefore analysed $\pi^+\pi^-$ distributions when the pair comes from the decay of a ρ^0. These $\pi^+\pi^-$ mass distributions, with and without BE weights applied, are shown together with the difference of the two in Fig.(2.7). From the difference it is clearly seen that the weighting depletes the region around the ρ mass and shifts the masses towards lower values as well as it slightly increases the width of the distribution. The figure clearly shows the potential of our model to affect the mass spectrum of the ρ^0.

2.5.3 Three-particle correlations

The existence of higher order dynamical correlations, which are not a consequence of two-particle correlations, is of importance for the understanding of BE correlations. There are very few experimental studies of genuine three-particle correlations, mainly because of the problem of subtracting the consequences of two-particle correlations and the need for high statistics of large multiplicity events. Genuine short-range three-particle correlations have been observed in e^+e^- annihilations by the DELPHI experiment. They conclude that they can be explained as a higher order Bose–Einstein effect [23].

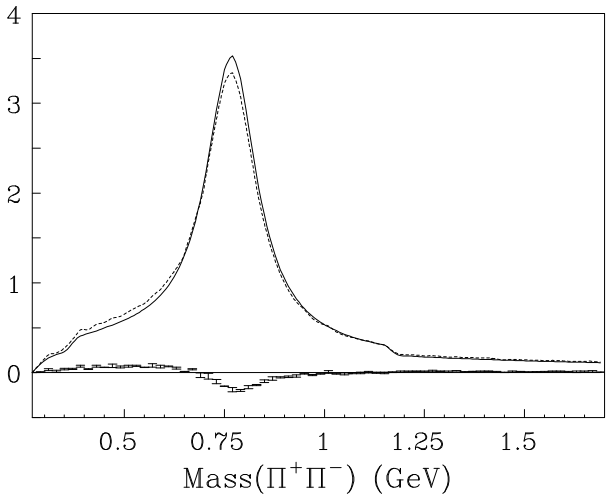

Figure 2.7: ρ^0 meson mass shift induced by the Bose–Einstein correlations in our model. The solid curve shows the Breit-Wigner as generated by JETSET while the dashed curve is obtained after applying BE weights to the events. The curve with error bars is the difference of the two (dashed-solid). The areas under the two mass distributions are normalised to unity in the shown mass range.

To reduce problems with pseudo-correlations due to the summation of events with different multiplicities we have used three-particle densities normalised to unity separately for every multiplicity in the following way

$$\tilde{\rho}_3^{(a,b,c)}(p_1,p_2,p_3) = \sum_{n\geq 8} P(n_a,n_b,n_c)\tilde{\rho}_3^{(n_a,n_b,n_c)}(p_1,p_2,p_3) \tag{2.23}$$

$$\tilde{\rho}_3^{(n_a,n_b,n_c)}(p_1,p_2,p_3) = \frac{1}{n_a(n_b-\delta_{ab})(n_c-\delta_{ac}-\delta_{bc})}\frac{1}{\sigma_{(n_a,n_b,n_c)}}\frac{d^3\sigma_{(n_a,n_b,n_c)}}{dp_1dp_2dp_3} \tag{2.24}$$

where n is the charged multiplicity, σ_{n_a,n_b,n_c} is the semi-inclusive cross section for events with n_i particles of species i, and

$$P(n_a,n_b,n_c) = \frac{\sigma_{(n_a,n_b,n_c)}}{\sum_{n_a,n_b,n_c}\sigma_{(n_a,n_b,n_c)}} \quad . \tag{2.25}$$

We have aimed to study the genuine normalised three particle correlation function, $\tilde{R}_3$, defined as

$$\begin{aligned}\tilde{R}_3 \quad = \quad & [\tilde{\rho}_3(p_1,p_2,p_3) - \tilde{\rho}_2(p_1,p_2)\tilde{\rho}_1(p_3) - \tilde{\rho}_2(p_1,p_3)\tilde{\rho}_1(p_2) - \tilde{\rho}_2(p_2,p_3)\tilde{\rho}_1(p_1) \\ & +2\tilde{\rho}_1(p_1)\tilde{\rho}_1(p_2)\tilde{\rho}_1(p_3)]/(\tilde{\rho}_1(p_1)\tilde{\rho}_1(p_2)\tilde{\rho}_1(p_3)) + 1\end{aligned} \tag{2.26}$$

where we have used an abbreviated notation for the $\tilde{\rho}_3$ from Eq.(2.23), and $\tilde{\rho}_1$ and $\tilde{\rho}_2$ are the corresponding one- and two-particle densities, normalised in accordance with Eq.(2.23) and Eq.(2.24). $\tilde{R}_3$ is equal to one if all three-particle correlations are consequences of two-particle correlations.

In order to calculate the $\tilde{\rho}_2\tilde{\rho}_1$ and $\tilde{\rho}_1\tilde{\rho}_1\tilde{\rho}_1$ terms in Eq.(2.26) the common experimental procedure is to mix tracks from different events. Using a mixing procedure in our model means weighting triplets of particles with products of event weights. This results in large statistical fluctuations and to get them under control, with our event weights, requires generation of very many events. We have therefore taken another approach, in order to minimise the computing time. We have used combinations of charged pions in the following way to approximate Eq.(2.26)

$$\tilde{R}_3 \equiv \frac{\tilde{\rho}_{3w}^{(\pm,\pm,\pm)} - 3(\tilde{\rho}_{3w}^{(\pm,\pm,\mp)} - \tilde{\rho}_3^{(\pm,\pm,\mp)})}{\tilde{\rho}_3^{(\pm,\pm,\pm)}} \tag{2.27}$$

where w, as previously, denotes weighted distributions. There are a couple of things to note in connection with Eq.(2.27). If there are genuine positive three-particle correlations for $(++-)$ and $(--+)$ combinations, as observed by the DELPHI collaboration [23] they will if they come from BE symmetrisation contribute to the $\tilde{R}_3$ in Eq.(2.27), but they will reduce the signal. Secondly, we note that there is a possible bias from two-particle correlations from $(+-)$ combinations but that it is small as discussed previously. We also note that using the normalisation in Eq.(2.24) reduces problems with contributions from like- and unlike-charge combinations having different multiplicity dependence. It should also be observed that the $\tilde{R}_3$ in Eq.(2.27) can be studied experimentally since getting the $\tilde{\rho}_{3w}$'s of course is achieved by analysing single events and the $\tilde{\rho}_3$ samples can be made by mixing events.

We have analysed the three-particle correlations as a function of the kinematical variable

$$Q = \sqrt{q_{12}^2 + q_{13}^2 + q_{23}^2} \quad \text{with} \quad q_{ij}^2 = -(p_i - p_j)^2 \ . \tag{2.28}$$

Fig.(2.8) shows $\tilde{R}_3$, the genuine three-particle correlation function for like-sign triplets, as approximated in Eq.(2.27). A strong correlation is observed for small Q-values. There is a dip in the curve for Q-values around 1 GeV which is compatible with the depletion of ρ^0's around its mass and gives an indication of the error from using unlike-charged pions in the approximation of $\tilde{R}_3$.

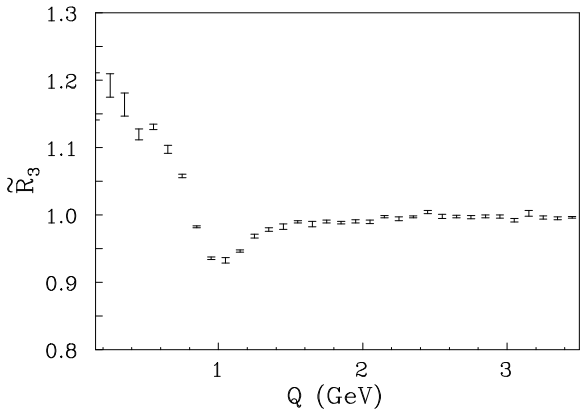

Figure 2.8: The Q-dependence of the genuine three-particle correlation function $\tilde{R}_3$, defined in the text.

Acknowledgments

We thank T. Sjöstrand for very valuable discussions and B. Söderberg for discussions about permutations.

References

[1] R. Hanbury-Brown and R.Q. Twiss, *Nature* **178**, 1046 (1956)

[2] M.G. Bowler, *Z Phys.* **C29**, 617 (1985)

[3] HERWIG 5.9; G. Marchesini, B.R. Webber, G. Abbiendi, I.G. Knowles, M.H. Seymour and L. Stanco, *Comp. Phys. Comm.* **67**, 465 (1992)

[4] T. Sjöstrand, *Comp. Phys. Comm.* **82**, 74 (1994)

[5] L. Lönnblad and T. Sjöstrand, *Phys. Lett.* **B351**, 293 (1995)

[6] B. Andersson and W. Hofmann, *Phys. Lett.* **B169**, 364 (1986)

[7] B. Andersson, G. Gustafson, G. Ingelman and T. Sjöstrand, *Phys. Rep.* **97**, 31 (1983)

[8] B. Andersson, G. Gustafson and B. Söderberg, *Z. Phys.* **C20**, 317 (1983)

[9] N.K. Glendenning and T. Matsui, *Phys. Rev.* **D28**, 2890 (1983)

[10] J. Schwinger, *Phys. Rev.* **82**, 664 (1951)

[11] R. Kronig, *J. Amer. Optical Soc.* **12**, 547 (1926)
H.A. Kramers, *Atti del Congress Internationale de Fisici Como* (1927)

[12] B. Andersson, G. Gustafson, A. Nilsson and C. Sjögren, *Z. Phys* **C49**, 79 (1991)

[13] S. Todorova, *Private communications*

[14] M.G. Bowler, *Phys. Lett* **B180**, 299 (1986)

[15] D. Decamp et al. (ALEPH Coll.), *Z. Phys.* **C54**, 75 (1992)

[16] P. Abreu et al. (DELPHI Coll.), *Z. Phys.* **C63**, 17 (1994)

[17] P.D. Acton et al. (OPAL Coll.), *Phys. Lett.* **B267**, 143 (1991)

[18] K. Hamacher and M. Weierstall, *DELPHI 95-80 PHYS 515* (1995)

[19] T. Alber et al., (NA35 Coll.), *Z. Phys.* **C66**, 77 (1995)
H. Bøggild et al. (NA44 Coll.), *Phys. Rev. Lett.* **74**, 3340 (1995)

[20] P.D. Acton et al. (OPAL Coll.), *Z. Phys.* **C56**, 521 (1992)
P. Abreu et al. (DELPHI Coll.), *Z. Phys.* **C65**, 587 (1995)

[21] P. Abreu et al. (DELPHI Coll.), *Z. Phys.* **C63**, 17 (1994)

[22] G. Lafferty, *Z. Phys.* **C60**, 659 (1993)

[23] P. Abreu et al. (DELPHI Coll.), *Phys. Lett.* **B355**, 415 (1995)

[24] B. Lörstad and O.G. Smirnova, *Proceedings of the 7th International Workshop on Multiparticle Production 'Correlations and Fluctuations', Nijmegen, The Netherlands* (1996)

Transverse and longitudinal Bose–Einstein correlations

Paper III

Transverse and longitudinal Bose–Einstein correlations

Bo Andersson and Markus Ringnér

Department of Theoretical Physics, Lund University,
Sölvegatan 14A, S-223 62 Lund, Sweden

Physics Letters **B 421**, 283-288 (1998)

We show how a difference in the correlation length longitudinally and transversely, with respect to the jet axis in e^+e^- annihilation, arises naturally in a model for Bose–Einstein correlations based on the Lund string model. In genuine three-particle correlations the difference is even more apparent and they provide therefore a good probe for the longitudinal stretching of the string field. The correlation length between pion pairs is found to be rather independent of the pion multiplicity and the kaon content of the final state.

3.1 Introduction

The Hanbury-Brown–Twiss (HBT) effect (popularly known as the Bose–Einstein effect) corresponds to an enhancement in the two identical boson correlation function when the two particles have similar energy-momenta. A well-known formula [1] to relate the two-particle correlation function (in four momenta $p_j, j = 1, 2$ with $q = p_1 - p_2$) to the space-time density, ρ, of (chaotic) emission sources is

$$\frac{\sigma d^2\sigma_{12}}{d\sigma_1 d\sigma_2} = 1 + |\mathcal{R}(q)|^2 \tag{3.1}$$

where $\mathcal{R}$ is the normalised Fourier transform of the source density

$$\mathcal{R}(q) = \frac{\int \rho(x) \exp(iqx)}{\int \rho(x) dx} \quad . \tag{3.2}$$

The commonly used event generators HERWIG and JETSET are based upon classical stochastical processes and do not include HBT-effects (although Sjöstrand, in JETSET, has introduced an ingenious method to simulate any given distribution by means of a kind of mean-field potential attraction between the bosons in the final state).

In this letter we will further investigate some features of the methods developed in [3] (an extension of [2] to multi-boson final states). We will show that the model predicts, due to the properties of string fragmentation, a difference between the correlation length along the string and transverse to it. In practice this means that if we introduce the longitudinal and transverse components of the vector q (defined with respect to the thrust direction) then we obtain a noticeable difference in the correlation distributions. This becomes even more noticeable when we go to the three-particle HBT effect (which was predicted in [3]) because in this case even more of the longitudinal stretching of the string field becomes obvious. Finally we will investigate the influence of the kaon and baryon content of the states on the HBT effects between the pions.

3.2 Longitudinal and transverse correlation lengths

The starting point of our Bose–Einstein model [2, 3] is an interpretation of the (non-normalised) Lund string area fragmentation probability for an n-particle state (cf Fig.(3.1))

$$dP(p_1, p_2, \ldots, p_n) = \left[\prod_1^n N dp_j \delta(p_j^2 - m_j^2)\right] \delta(\sum p_j - P_{tot}) \exp(-bA) \tag{3.3}$$

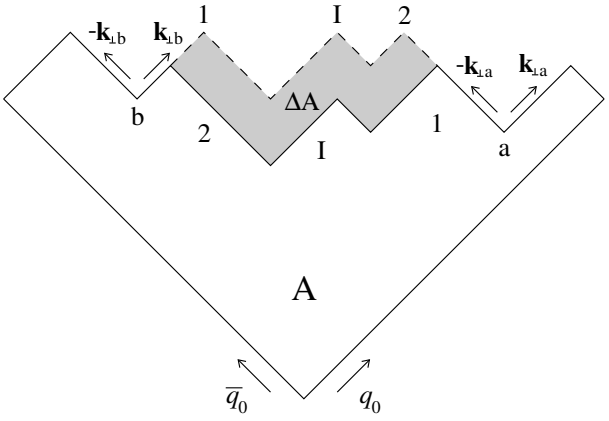

Figure 3.1: The decay of a Lund Model string spanning the space–time area A. The particles 1 and 2 are identical bosons and the particle(s) produced in between them is denoted by I. The two possible ways, $(\ldots, 1, I, 2, \ldots)$ and $(\ldots, 2, I, 1, \ldots)$, to produce the state are shown and the area difference between the two cases, ΔA, is shaded. The two neighbouring vertices of the state with the two identical bosons are denoted by a and b, and the transverse momenta of the quarks produced in the neighbouring vertices are $\pm\mathbf{k}_{\perp a}$ and $\pm\mathbf{k}_{\perp b}$, respectively.

in accordance with a quantum mechanical transition probability containing the final state phase space multiplied by the square of a matrix element $\mathcal{M}$. In [2] and in more detail in [3] a possible matrix element is suggested in accordance with (Schwinger) tunneling and the (Wilson) loop operators necessary to ensure gauge invariance. The matrix element is

$$\mathcal{M} = \exp(i\kappa - b/2)A \tag{3.4}$$

where the area A is interpreted in coordinate space, κ is the string constant (phenomenologically $\kappa \simeq 1\,\mathrm{GeV/fm}$) and $b \simeq 0.3\,\mathrm{GeV/fm}$ is the decay constant. Note that the parameter b is much smaller than κ. From now on we will, as is usual in the Lund model, go over to the energy momentum space. Then the area $A \to 2\kappa^2 A$, while $b \to b/2\kappa^2$, as explained in [3].

The transverse momentum properties are in the Lund model taken into account by means of a Gaussian tunneling process. In this way the produced $\mathrm{q\overline{q}}$-pair in each vertex will obtain $\pm\mathbf{k}_\perp$ and the hadron stemming from the combination of a $\overline{\mathrm{q}}$ from one vertex and a q from the adjacent vertex obtains $\mathbf{p}_\perp = \mathbf{k}_{\perp j+1} - \mathbf{k}_{\perp j}$.

In case there are two or more identical bosons the matrix element should be

symmetrised and in general we obtain the symmetrised production amplitude

$$\mathcal{M} = \sum_{\mathcal{P}} \mathcal{M}_{\mathcal{P}} \tag{3.5}$$

where the sum goes over all possible permutations of the identical particles. The squared amplitude occurring in Eq.(3.3) will then be

$$|\mathcal{M}|^2 = \sum_{\mathcal{P}} |\mathcal{M}_{\mathcal{P}}|^2 \left(1 + \sum_{\mathcal{P}' \neq \mathcal{P}} \frac{2\mathrm{Re}(\mathcal{M}_{\mathcal{P}} \mathcal{M}^*_{\mathcal{P}'})}{|\mathcal{M}_{\mathcal{P}}|^2 + |\mathcal{M}_{\mathcal{P}'}|^2} \right) \quad . \tag{3.6}$$

JETSET will provide the outer sum in Eq.(3.6) by the generation of many events but it is evident that the model predicts a quantum mechanical interference weight, $w_{\mathcal{P}}$, for each given final state characterised by the permutation $\mathcal{P}$:

$$w_{\mathcal{P}} = 1 + \sum_{\mathcal{P}' \neq \mathcal{P}} \frac{2\mathrm{Re}(\mathcal{M}_{\mathcal{P}} \mathcal{M}^*_{\mathcal{P}'})}{|\mathcal{M}_{\mathcal{P}}|^2 + \mathcal{M}_{\mathcal{P}'}|^2} \quad . \tag{3.7}$$

In the Lund Model we note in particular for the case exhibited in Fig.(3.1), with two identical bosons denoted 1 and 2 having a state I in between, that the decay area is different if the two identical particles are exchanged. It is evident that the interference between the two permutation matrices will contain the area difference, ΔA, and the resulting general weight formula will be

$$w_{\mathcal{P}} = 1 + \sum_{\mathcal{P}' \neq \mathcal{P}} \frac{\cos \frac{\Delta A}{2\kappa}}{\cosh \left(\frac{b \Delta A}{2} + \frac{\Delta (\sum \mathbf{k}^2_{\perp j})}{2\kappa} \right)} \tag{3.8}$$

where Δ stands for the difference between the configurations described by the permutations $\mathcal{P}$ and $\mathcal{P}'$ and the sum is taken over all the vertices. In our MC implementation of the weight we replace the string constant κ in the transverse momentum generation with the default (in JETSET) transverse width, $2\sigma^2$ (which is of the order of κ). The calculation of the weight function for n identical bosons contains $n! - 1$ terms and it is therefore from a computational point of view of exponential-type. We have in [3] introduced approximate methods reducing it to power-type instead and we refer for details to this work.

We have seen that the transverse and longitudinal components of the particles momenta stem from different generation mechanisms. This is clearly manifested in the weight in Eq.(3.8) where they give different contributions. In the following we will therefore in some detail analyse the impact of this difference

on the transverse and longitudinal correlation lengths, as implemented in the model.

In order to understand the properties of the weight in Eq.(3.8) we again consider the simple case in Fig.(3.1). The area difference of the two configurations depends upon the energy momentum vectors p_1, p_2 and p_I and can in a dimensionless and useful way be written as

$$\frac{\Delta A}{2\kappa} = \delta p \delta x_L \tag{3.9}$$

where $\delta p = p_2 - p_1$ and $\delta x_L = (\delta t; 0, 0, \delta z)$ is a reasonable estimate of the space-time difference, along the surface area, between the production points of the two identical bosons.

In order to preserve the transverse momenta of the particles in the state $(1, I, 2)$ it is necessary to change the generated $\mathbf{k}_\perp$ at the two internal vertices around the state I during the permutation, i.e. to change the Gaussian weights. Also in this case we may write a formula similar to Eq.(3.9) for the transverse momentum change:

$$\frac{\Delta(\sum \mathbf{k}_{\perp j}^2)}{2\kappa} = \delta \mathbf{p}_\perp \delta \mathbf{x}_\perp \tag{3.10}$$

where $\delta \mathbf{p}_\perp$ is the difference $\mathbf{p}_{\perp 2} - \mathbf{p}_{\perp 1}$ and $\delta \mathbf{x}_\perp = (\mathbf{k}_{\perp b} - (-\mathbf{k}_{\perp a}))/\kappa$. The two neighbouring vertices of the state $(1, I, 2)$ $((2, I, 1))$ are denoted by a and b and $\mathbf{k}_{\perp b} + \mathbf{k}_{\perp a}$ corresponds to the states transverse momentum exchange to the outside. Therefore $\delta \mathbf{x}_\perp$ constitutes a possible estimate of the transverse distance between the production points of the pair.

For the general case when the permutation $\mathcal{P}'$ is more than a two-particle exchange there are formulas similar to equations (3.9) and (3.10), although they are more complex (and the expressions do not vanish when only two of the exchanged particles have the same energy momentum).

It is evident from the considerations leading to equations (3.9) and (3.10) that only particles with a finite longitudinal distance and small relative energy momenta will give significant contributions to the weights. We also note that we are in this way describing longitudinal correlation lengths along the colour fields, inside which a given flavour combination is compensated. The corresponding transverse correlation length describes the tunneling (and in this model it provides a damping chaoticity).

The weight distribution we obtain is discussed in [3] (and with varying kaon and baryon content also below). It is strongly centered around unity although there are noticeable tails to both larger and smaller (even negative) weights.

The total production probability is, however, positive and we find negligible changes in the JETSET default observables (besides the correlation functions) by this extension of the Lund model.

3.3 Results

Two-dimensional Bose–Einstein correlations in e^+e^- annihilation have been analysed at lower energies than LEP by the TASSO collaboration [4]. Although they find that their data is compatible with a spherically symmetric correlation function they conclude that at least one order of magnitude of more data is required to obtain more detailed information. With the large statistics available from LEP we have therefore generated $q\overline{q}$-events at the Z^0 pole to investigate the properties of our model. Short-lived resonances like the ρ and K^* are allowed to decay before the BE-symmetrisation, while more long-lived ones are not affected.

We have analysed two-particle correlations in the Longitudinal Centre-of-Mass System (*LCMS*). For each pair of particles the *LCMS* is the system in which the sum of the two particles momentum components along the jet axis is zero, which of course also means that the sum of their momenta is perpendicular to the jet axis. The transverse and longitudinal momentum differences are then defined in the *LCMS* as

$$\begin{aligned} q_L &= |p_{z2} - p_{z1}| \\ q_\perp &= \sqrt{(p_{x2} - p_{x1})^2 + (p_{y2} - p_{y1})^2} \end{aligned} \tag{3.11}$$

where the jet axis is along the z-axis.

We have taken the ratio of the two-particle probability density of pions, ρ_2, with and without BE weights applied as the two-particle correlation function, R_2

$$R_2(p_1, p_2) = \frac{\rho_{2w}(p_1, p_2)}{\rho_2(p_1, p_2)} \tag{3.12}$$

and the resulting function is shown in Fig.(3.2). It is clearly seen that it is not symmetric in q_L and $q_\perp$ and in particular that the correlation length, as measured by the inverse of the width of the correlation function, is longer in the longitudinal than in the transverse direction. This difference remains for reasonable changes of the width in the transverse momentum generation. For comparison we have also analysed events where the Bose–Einstein effect has been simulated by the LUBOEI algorithm implemented in JETSET [5]. In LUBOEI the BE effect is simulated as a mean-field potential between identical

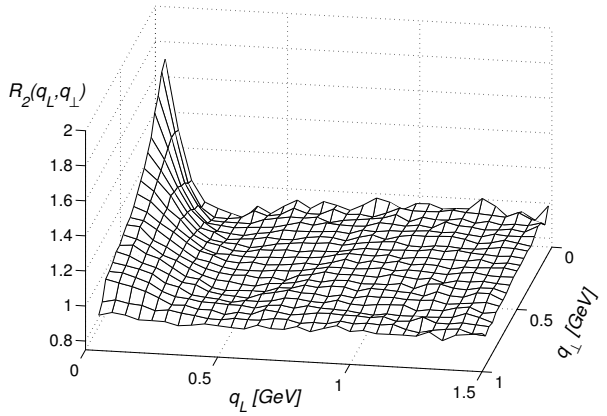

Figure 3.2: The ratio $R_2(q_L, q_\perp)$ of the number of charged pion pairs having relative four-momentum components q_L and $q_\perp$ with and without Bose–Einstein weights applied. The sample consists of particles which are either initially produced or stemming from short-lived resonances.

bosons which is spherically symmetric in Q. Analysing only the initial particles and particles stemming from short-lived decays results for the LUBOEI events in a correlation function with identical transverse and longitudinal correlation lengths. The correlation lengths are in agreement with the source radii input to LUBOEI. Using all the final pion pairs, after all decays, in the analysis results in a small decrease in the transverse correlation length and of course a large decrease in the height for $q_L \simeq q_\perp \simeq 0$, while the longitudinal correlation length is rather unaffected. The pions from long lived decays affect the correlation lengths in the same way both for our model and for LUBOEI.

In [3] it is shown that our model gives rise to genuine three-particle correlations. We will in this letter continue to investigate three-particle correlations and we will in particular use our knowledge of the different contributions to the weight function to study the genuine higher order correlations. We will also exhibit how the genuine higher order terms in the weight function mainly clusters particles in the longitudinal direction.

The total three-particle correlation function is in analogy with Eq.(3.12)

$$R_3^{''}(p_1, p_2, p_3) = \frac{\rho_{3w}(p_1, p_2, p_3)}{\rho_3(p_1, p_2, p_3)} \quad . \tag{3.13}$$

To get the genuine three-particle correlation function, R_3, the consequences of

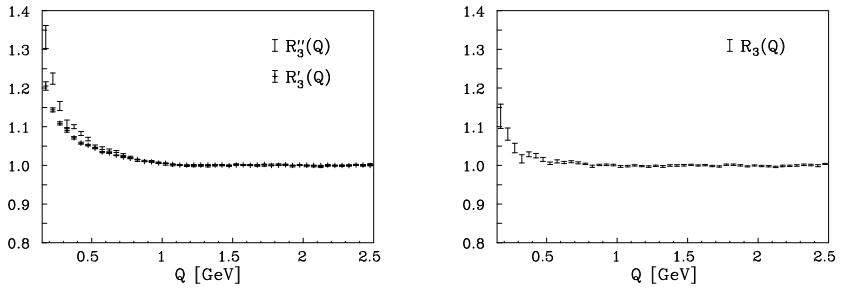

Figure 3.3: $R_3^{''}(Q)$ and $R_3^{'}(Q)$ are shown in the left figure, while the figure to the right shows $R_3(Q)$. The existence of genuine three-particle correlations is apparent.

having two-particle correlations in the model have to be subtracted from $R_3^{''}$. To this aim we have calculated the weight taking into account only configurations where pairs are exchanged, $w^{'}$. In this way the three-particle correlations which only are a consequence of lower order correlations can be defined as

$$R_3^{'}(p_1,p_2,p_3) = \frac{\rho_{3w'}(p_1,p_2,p_3)}{\rho_3(p_1,p_2,p_3)} \quad . \tag{3.14}$$

The genuine three-particle correlation function, R_3, is then given by

$$R_3 = R_3^{''} - R_3^{'} + 1 \quad . \tag{3.15}$$

We have analysed R_3 in one dimension as a function of the kinematical variable

$$Q = \sqrt{Q_{12}^2 + Q_{13}^2 + Q_{23}^2} \quad \text{with} \quad Q_{ij}^2 = -(p_i - p_j)^2 \tag{3.16}$$

and in two dimensions we have used the following variables calculated in the *LCMS* for each triplet of identical bosons

$$\begin{aligned} q_L &= \sqrt{q_{L12}^2 + q_{L13}^2 + q_{L23}^2} \quad \text{with} \quad q_{Lij}^2 = (p_{zi} - p_{zj})^2 \\ q_\perp &= \sqrt{q_{\perp 12}^2 + q_{\perp 13}^2 + q_{\perp 23}^2} \quad \text{with} \quad q_{\perp ij}^2 = (\mathbf{p}_{\perp i} - \mathbf{p}_{\perp j})^2 \end{aligned} \tag{3.17}$$

where the z-axis is along the jet axis. In Fig.(3.3) the correlation functions $R_3^{''}(Q)$, $R_3^{'}(Q)$ and $R_3(Q)$ are shown, and the existence of genuine three-particle correlations in the model is clearly exhibited.

This way of getting the genuine correlations is not possible in an experimental situation, where one has to find other ways to get a $R_3^{'}$ reference sample. We have suggested one possible option in [3] and the results in this letter are in

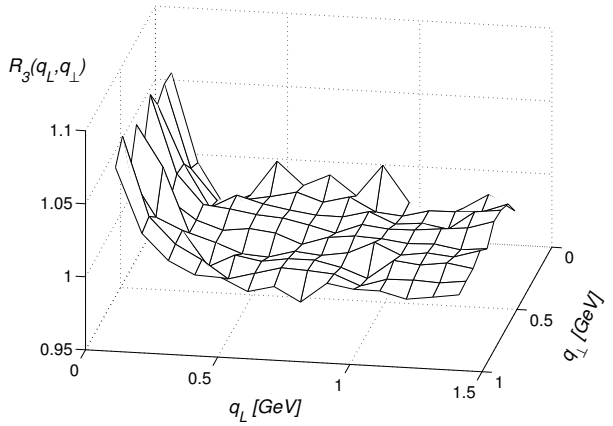

Figure 3.4: The ratio $R_3(q_L, q_\perp)$ of the number of triplets of charged pions with and without Bose–Einstein weights applied.

agreement with the conclusions of that investigation. In the present analysis the contribution to the correlations from higher order configurations in the weight calculation is apparent. We note that R_3 flattens out earlier, i.e. for lower Q-values than $R_3^{''}$. This means that the genuine three-particle correlations have a longer correlation length compared to the consequences of lower order correlations. Performing the same analysis in two dimensions in the *LCMS* for each triplet results in the $R_3(q_L, q_\perp)$ distribution shown in Fig.(3.4). The effect of the higher order terms is to pull the triplets closer in the longitudinal direction while the transverse direction is rather unaffected. This suggests that higher order correlations are more sensitive to the longitudinal stretching of the string field.

We have also studied the correlation length for pion pairs as a function of the final charged multiplicity and the kaon content of the state. Within statistical errors which are relatively large we see no dependence on either the charged multiplicity or the number of kaons. Since one might suspect that events with many pions are premiered by the re-weighting the average baryon and kaon content of the events have been investigated. We find that the changes of the average multiplicity of different kaon species as well as of the average multiplicity of protons and neutrons in the final state are much smaller than the experimental errors as summarised in [6].

References

[1] M.G. Bowler, *Z Phys.* **C29**, 617 (1985)

[2] B. Andersson and W. Hofmann, *Phys. Lett.* **B169**, 364 (1986)

[3] B. Andersson and M. Ringnér, *Nucl. Phys.* **B513**, 627 (1998)

[4] M. Althoff et al. (TASSO Coll.), *Z. Phys.* **C30**, 355 (1986)

[5] L. Lönnblad and T. Sjöstrand, *Phys. Lett.* **B351**, 293 (1995)

[6] Particle Data Group, *Phys. Rev.* **D54**, 187 (1996)

Bose–Einstein and colour interference in W-pair decays

Paper IV

Bose–Einstein and Colour Interference in W-pair Decays

Jari Häkkinen and Markus Ringnér

Department of Theoretical Physics, Lund University,
Sölvegatan 14A, S-223 62 Lund, Sweden

European Physical Journal **C 5**, 275-281 (1998)

We study effects on the W mass measurements at LEP2 from non-perturbative interference effects in the fully hadronic decay channel. Based on a model for Bose–Einstein interference, which is in agreement with LEP1 data, we argue that there are no Bose–Einstein correlations between bosons coming from the different W's. For small reconnection probabilities we rule out the possible experimental signal of colour interference at LEP2, suggested in [1]. The conclusions from this paper are that the theoretical uncertainties in the W mass determination should be smaller than the experimental statistical error.

4.1 Introduction

One of the main goals of LEP2 is to perform high quality precision measurements of the W mass. In order to obtain the projected statistical error of 30–40 MeV, all decay channels – the leptonic, the semi-leptonic, and the hadronic – have to be used. The purely leptonic decays will however be rare and they will not have a large impact on the measurements. In the two cases involving hadronic systems non-perturbative effects, such as colour- and Bose–Einstein interference, can occur and the measured W mass may be affected. The interference effects within the hadronic system can in the semi-leptonic case be estimated from LEP1 studies. From these studies we understand the effects of Bose–Einstein (BE) correlations quite well and we have also learnt that the colour interference (CI) effects are probably small. This means that the semi-leptonic case can be reconstructed using a Monte Carlo tuned to LEP1 data and that the theoretical uncertainties due to interference effects will only influence the fully hadronic channel. These uncertainties arise since the interference effects may have impact on the identity of the two decaying W's. The fully hadronic channel is very nice since we can, in principle, observe all the momentum of the event. However even if LEP2 provides enough statistics for a sub 30 MeV error the interference effects have to be taken into account, or at least be under theoretical control.

That Bose–Einstein correlations might affect the measurement of the mass of the W at LEP2 was first suggested in [2]. The typical separation in space and time between the W^+ and W^- decay vertices is smaller than 0.1 fm in fully hadronic events, i.e. $e^+e^- \to W^+W^- \to q_1\overline{q}_2q_3\overline{q}_4$, at LEP2 energies [3, 4]. Since this distance is much smaller than typical hadronic sizes and the correlation lengths associated with Bose–Einstein effects, pions from different W's are argued to be subject to Bose–Einstein symmetrisation. The effect on the W mass has been estimated in a number of models with widely varying results [2, 5, 6]. In this paper we will based on the model in [7] argue that there are no Bose–Einstein correlations between particles stemming from different W's at LEP2. We will also discuss the consequences of the symmetrisation for various ways of reconstructing the W mass.

Colour interference can occur in the W-pair decays at LEP2 but the probability for reconnections is unknown. In this study we use an improved Monte Carlo implementation of the model described in [1] to address the possibility to experimentally detect effects from CI at LEP2. We will also use it to estimate the effect of CI on the W mass determination.

After a short description of the various mass reconstruction schemes we use, we will in section 4.3 describe the important features of our interference models.

We will in particular review how the correlation length in our BE model arises stressing the parts relevant to understand correlations between particles from different W's. This is followed by the results for the reconstruction of the W mass and conclusions.

4.2 Mass reconstruction

If every final particle in the fully hadronic case can be uniquely and correctly assigned to either the W^+ or the W^- decay, the $W^\pm$ four-momenta can be reconstructed and squared to give the $W^\pm$ masses. There are however many complications which have to be taken into account in practice. It is not our intention to cover these complications here, but a detailed discussion can be found in [3] together with a discussion about various ways to reconstruct the W mass in order to avoid complications. Reconstruction schemes are devised in [3] to study the effects of interference and we have adopted some of them in our analysis. We will only give a brief sketch of how it is done and the reader is referred to the original work for details.

Four jet events are selected using the LUCLUS algorithm [8], with the jet distance parameter $d_{\mathrm{join}} = 8$ GeV. This rejection of events with hard gluon jets is done since they give a much worse W mass resolution. In addition, we require the jets to have energies above 20 GeV and that the angle between any two jets is greater than 0.5 radians, to reduce the number of misassignments. The four jets can be paired in three different ways giving different results for the W mass. We use three different criteria to single out one combination.

1 : The pairs are chosen so that the deviation of the average reconstructed W mass from the used mass is minimized;

$$\min \left| \frac{M_{\mathrm{W}^+} + M_{\mathrm{W}^-}}{2} - M_{\mathrm{W}} \right| \quad .$$

This is not measurable in an experimental situation since we cannot know with which masses the W's were produced, but it is included for comparison.

2 : The pairs are chosen so that the deviation of the sum of the reconstructed masses from a known nominal mass is minimized;

$$\min(|M_{\mathrm{W}^+} - M_{\mathrm{W}}| + |M_{\mathrm{W}^-} - M_{\mathrm{W}}|) \quad .$$

3 : The pairs are chosen so that the sum of their opening angles is maximized. This makes sense close to threshold where the jets from the same W should be almost back-to-back.

To investigate the effects of the interference models we compare the reconstructed W mass with interference with the reconstructed mass without interference.

4.3 Models

Before going into the details of our models we will shortly discuss some general features of $WW \to q_1\overline{q}_2q_3\overline{q}_4$ events, which provide a motivation for some of our assumptions. As will be made clear, our models for the interference effects and in particular some of their major consequences are based upon the picture of singlet strings fragmenting. This may however not be the full story, since there could be an important non-singlet component of hadronization, especially in the scenario when two strings are formed close to each other. The only hadronization model which includes a non-singlet component is that of Ellis and Geiger [5]. In the case of a non-singlet component in $WW \to q_1\overline{q}_2q_3\overline{q}_4$ one would expect that the multiplicity in W-pair events is different from twice the multiplicity in single string events. This is manifested in particular in the colour reconnection scheme of Ellis and Geiger, where not only the W mass shift is much larger than in their singlet models, but it also results in a substantial reduction of the number of hadrons coming from the overlap region of the two W's.

Three of the LEP experiments (DELPHI/L3/OPAL) have measured the mean charged hadronic multiplicity in $W^+W^- \to q_1\overline{q}_2q_3\overline{q}_4$ events, $\langle N_{ch}^{4q}\rangle$, and in $W^+W^- \to q\overline{q}l\overline{\nu}_l$ events, $\langle N_{ch}^{qql\nu}\rangle$ [9, 10, 11]. Summarizing their results give [12]

$$\frac{\langle N_{ch}^{4q}\rangle}{2\langle N_{ch}^{qql\nu}\rangle} = 1.04 \pm 0.03 \tag{4.1}$$

which gives no support for models leading to a reduction of the hadronic multiplicity in W-pair events. This suggests that singlet strings provide a good description of $W^+W^- \to q_1\overline{q}_2q_3\overline{q}_4$ hadronization.

4.3.1 Colour interference at LEP2 energies

The CI model in this paper is an improved Monte Carlo implementation of the model described in [1]. The model for recoupling is quite simple and its features are described in detail in [1]. Here we give a summary of the model with emphasis on the improvements.

The space–time distance between the W decay points in $e^+e^- \to W^+W^- \to q_1\overline{q}_2q_3\overline{q}_4$ is about $1/\Gamma_W$ and hard gluons with energies above Γ_W are therefore

emitted incoherently by the two quark systems early in the event [13]. This means that there are two sets of partons before any possible colour interference can occur. The two sets $q_1 g_1 g_2 \ldots g_n \overline{q}_2$ and $q_3 g_{1'} g_{2'} \ldots g_{m'} \overline{q}_4$ have a lot of different recoupling possibilities since every set of particles $q \ldots g$ is a colour-triplet. Recoupling of a $q \ldots g$ with any $g \ldots \overline{q}$ from the other set can occur with the probability $1/N_c^2$ so the total probability for recoupling can in principle be very large. The estimation of the total recoupling probability is non-trivial. In [1] a discussion is made about what kind of probabilities to expect. No real conclusion was or can be made, and the probability remains a free parameter of the model.

Perturbative QCD favours states which correspond to short strings i.e. parton states which produce few hadrons. The λ measure was introduced in [14] and is a measure of the effective rapidity range inside which the decay products of a particular colour-singlet string are distributed. In this way it is related to the multiplicity. In [1] it is argued that states with smaller λ's could be dynamically enhanced, and that this choice also gives reconnected events that differ most from non-reconnected systems. Reconnected states with the smallest λ measure are therefore chosen in the model.

All of this is still true in the CI model in this paper. We have however made significant improvements in the MC implementation. The Ariadne MC v4.08 [15] allows the user to stop the production of gluons below some given energy. This feature was not available in the original work, where gluons with energy below Γ_W where simply neglected (leading to a 3% loss of energy). Furthermore, the W-pairs were incorrectly generated in the original work since no spin information was preserved and the W's were therefore allowed to decay isotropically. In order to take the full angular correlations into account we now use Pythia v5.7 [8], where the full $2 \to 2 \to 4$ matrix elements are included for the W-pair production and decay.

These improvements will lead to consequences for the results obtained in [1]. In addition to studying possible experimental signals at LEP2 of recoupled events we also extend the analysis of [1] to study CI effects on W mass determination.

4.3.2 Bose–Einstein correlations in W-pair production

A model for Bose–Einstein correlations based upon a possible quantum-mechanical framework for the Lund Fragmentation Model [16] has been proposed [17] and it has been extended to the multi-particle correlations needed at LEP energies [7]. An important feature of the model is that it can be used as an extension of the probability based Lund Model, implementing the correlations as event weights.

The interpretation of the Lund Fragmentation Model in [7] gives an explicit form for the transition matrix element for a string fragmenting into hadrons. The resulting matrix element depends only on the space-time history of the string and the model therefore uniquely predicts the relative amplitudes for different particle configurations, and therefore also the magnitude of the Bose–Einstein effect. To understand how the correlation length between pions arise in the model we will in the following shortly discuss the basic steps leading to the specific form of the transition matrix element.

A unique breakup rule for a string can be derived inside the Lund Model, which results in the following probability for a string to decay into hadrons $(p_1, \ldots, p_n)$,

$$dP(p_1, ..., p_n) = \left[\prod_i (N dp_i \delta(p_i^2 - m_i^2)) \right] \delta(\sum_j p_j - P_{tot}) \exp(-bA) \qquad (4.2)$$

where A is the space-time area spanned by the string during its break-up into $q\overline{q}$-pairs, and N and b are two free parameters.

The production of hadrons from a single string in the Lund Model can be given a quantum mechanical interpretation inside a non-Abelian field theory. The transition matrix element, $\mathcal{M}$, can, to obtain the result in Eq.(4.2) be identified with (note the similarity with Fermi's golden rule)

$$\mathcal{M} = \exp(i\xi A) \quad \text{with} \quad \xi = \frac{1}{2\kappa} + \frac{ib}{2} \qquad (4.3)$$

where the decay surface area, A, is in energy-momentum units in the light-cone metric. The imaginary part of the quantity ξ is related to the pair production probability. As discussed in [7] the phase for $\mathcal{M}$, as given by the real part of ξ, is found by observing how gauge invariance will constrain the production of $q\overline{q}$-pairs along the colour force fields. The main observation is that a final state hadron stems from a q from one vertex and a $\overline{q}$ from the adjoining vertex. This implies that in order to keep gauge-invariance it is necessary that the production matrix element contains at least a gauge connector, $\exp\left(ig \int_j^{j+1} A^\mu dx_\mu\right)$, between the two vertices, denoted j and $j+1$. The total matrix amplitude for a single string must contain at least one gauge connector for each hadron and we get a Wilson Loop Operator as a minimal requirement for gauge invariance

$$\mathcal{M} = \exp(ig \oint A_\mu dx^\mu) \qquad (4.4)$$

where the integral is around the decay surface of the string. Using Wilson's confinement criteria for the behaviour of such a loop operator we get the real part of ξ, as in Eq.(4.3).

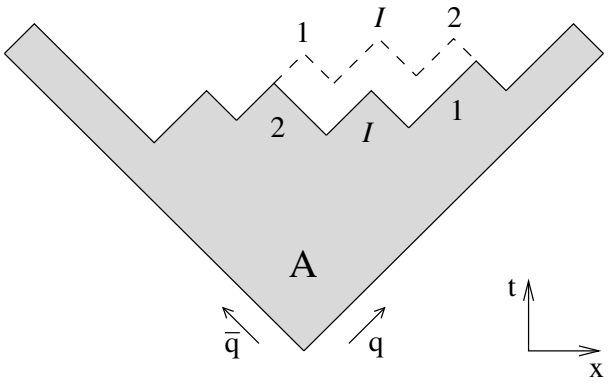

Figure 4.1: The two possible ways, $(1, I, 2)$ and $(2, I, 1)$, to produce the entire state when 1 and 2 are identical bosons. The space-time area, A, spanned by the string during its break-up is shaded.

The transverse momentum generation will also contribute to the total matrix element. This contribution is discussed in detail in [7] and is found to be

$$\propto \exp(-\frac{1}{4\sigma^2}\mathbf{k}_\perp^2) \tag{4.5}$$

where $\pm\mathbf{k}_\perp$ are the compensating transverse momenta generated in a $q\bar{q}$-vertex and σ is the width of the Gaussian supression of the quarks transverse momenta.

In order to see the main mechanism for BE-correlations in the Lund Model we consider Fig.(4.1), in which two of the produced hadrons, denoted $(1, 2)$, are assumed to be identical bosons and the state in between them is denoted I. There are two ways to produce the entire state, corresponding to exchange of the two identical bosons. The two configurations, $(\ldots, 1, I, 2, \ldots)$ and $(\ldots, 2, I, 1, \ldots)$, are shown in the figure and in general they correspond to different areas A.

The area difference, ΔA, depends not only on the energy momentum vectors p_1 and p_2, but also on the four-momentum of the intermediate state, p_I. The difference can be written as

$$\frac{\Delta A}{2\kappa} = \delta p \delta x \tag{4.6}$$

where $\delta p = p_2 - p_1$ and $\delta x = (\delta t, 0, 0, \delta z)$ is a reasonable estimate of the space–time difference, along the string surface, between the production points. This means that the correlation length, which is being measured by the four-momentum difference between pairs, is in the model dynamically implemented as δx [7]. The correlation length is therefore not the direct distance between

production points. Instead it is the distance along the string surface, i.e. the distance along the colour force field. This is not surprising if we consider how the quantum-mechanical process corresponding to the Lund Model was derived; to keep gauge-invariance we got a gauge-connector between adjacent vertices and this is what provides us with the $A/(2\kappa)$ factor in the matrix element, from which the correlation length in the model stems.

In the case of production of two strings, i.e. a $\mathrm{q}_1\overline{\mathrm{q}}_2\mathrm{q}_3\overline{\mathrm{q}}_4$ system, there is no reason for a gauge-connector between vertices belonging to different strings. We will therefore assume that the distance along the gauge-field between them is infinite even though the direct space–time distance may be very small. This implies that there is no interference between production vertices belonging to different strings. This means that in this model each string can be considered a system of its own, with separate Bose–Einstein effects. The resulting event weight is then of course the product of the weights for each system separately. In [7] it is explained how the BE interference can be incorporated in a probabilistic event generation scheme by weighting the produced events. In particular using the amplitudes Eq.(4.3) and Eq.(4.5) results in the weight

$$w = \prod_{n=1}^{2} \left(1 + \sum_{\mathcal{P}'_n \neq \mathcal{P}_n} \frac{\cos \dfrac{\Delta A_n}{2\kappa}}{\cosh\left(\dfrac{b\Delta A_n}{2} + \dfrac{\Delta(\sum^{(n)} p^2_{\perp \mathrm{q}})}{2\sigma^2_{p_\perp}} \right)} \right) \tag{4.7}$$

for a fully hadronic WW event, where Δ denotes the difference with respect to configurations $\mathcal{P}_n$ and $\mathcal{P}'_n$ of the string n and the sum of $p^2_{\perp \mathrm{q}}$ is over all the vertices of string n. We have introduced $\sigma_{p_\perp}$ as the width of the transverse momenta for the generated hadrons, (i.e. $\sigma^2_{p_\perp} = 2\sigma^2$).

It should be emphasized that if only colour-singlet combinations of partons are allowed to be formed there is no model consistent way to get correlations between particles stemming from the different W's. In comparison to most of the models using event weights to implement BE-correlations [6] we have a physical picture of how the correlation length in our model arises and it describes data well in single string fragmentation [7]. Taken together with our previous discussion of multiplicities in WW events this supports our conclusion that there are no correlations between particles from the different W's.

4.4 Results

All the results are for W-pairs generated at 170 GeV. We have checked the effects of our models on the mean charged multiplicity and the results are

shown in Table 4.1. We get small effects on the mean multiplicity and they are compatible with the experimental result, Eq.(4.1).

Model		$\langle N_{ch}^{4q} \rangle$	$\Delta\langle N_{ch}^{4q} \rangle$ (%)
CI	without	38.62 $\pm$0.01	
	100%	36.90 $\pm$0.01	
	10%	38.45 $\pm$0.01	-0.44
BE	without	24.4	
	with	25.1	+2.7$\pm$0.3

Table 4.1: The mean charged multiplicity for the two interference models. For the CI model we show the results for 100% recoupled events and for an admixture of recoupled and non-recoupled events of the order 10%. The lower multiplicities for the BE results are due to that no parton cascade has been used in this case.

4.4.1 Colour interference results

It is natural to divide the CI results into two independent parts. First we discuss the possibility to detect signals of CI at LEP2 in the same way as it was done in [1] and then we will study mass reconstruction effects.

CI signal search at LEP2

The search for signals of CI at LEP2 in [1] give numbers which are very close to what will be statistically significant with the expected number of events from LEP2, when a 10% recoupling probability is assumed. The improvements made here will dilute the signal proposed in [1]. Multiplicity distributions (including π^0) in the central rapidity region, $|y| < 0.5$, for recoupled and non-recoupled events are shown in Fig.(4.2). Comparing these with the original results from [1] we note that the signal-to-background ratio is significantly reduced. In Table 4.2 we have compiled the number of events without particles in a central rapidity region at LEP2 using two different thrust cuts and an expected 5000 fully hadronic events. We note that the signal decreases and if this signal is to be seen at LEP2 there must be a larger recoupling probability than 10%. A larger recoupling probability would increase the number of events without particles in the central rapidity bin. A closer examination of the improvements of the MC implementation in this paper reveals that the conservation of energy will not change the result too much from the original work. Almost all of the suppression of the signal comes from taking the anisotropy of the W decays into account.

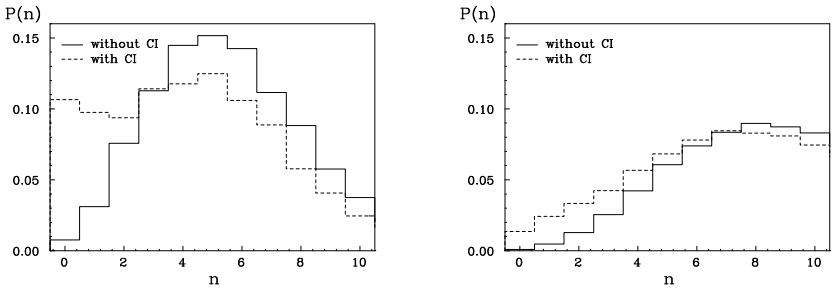

Figure 4.2: Multiplicity distributions for $|y| < 0.5$ for non-recoupled (solid line) and recoupled events (dashed line) with thrust cuts *left)* $T > 0.92$ and *right)* $T > 0.76$. The CI results are for 100% recoupled events.

Model	Thrust	Event fraction	Events with n_{central}=0	background
[1]	0.92	0.04	4.3	0.68
	0.76	0.60	13	1.9
our	0.92	0.01	0.93	0.36
	0.76	0.60	6.4	2.6

Table 4.2: Expected number of events with zero particles in a central rapidity region: $|y| < 0.5$, denoted by n_{central}, for a total of 5000 fully hadronic W-pair events. A 10% recoupling probability is assumed.

From this study we conclude that the statistics from LEP2 will make it hard to use the signal proposed in [1].

W mass reconstruction results

We have studied the effects of CI on the W mass measurement to estimate the size of the theoretical error on the mass implied by our model.

In Fig.(4.3) we show the generated W mass and the reconstructed masses with and without CI interference. We see that the difference between the reconstructed distributions is small. The mass shifts for 100% reconnected events are shown in Table 4.3 and if the reconnection probability is assumed to be 10% the shifts should be scaled down with a factor 10. ΔM denotes the mass shift due to the reconstruction method as compared with the generated W mass and the additional shift due to the interference is denoted by δM.

Assuming a 10% reconnection probability the shifts will be small and negligible

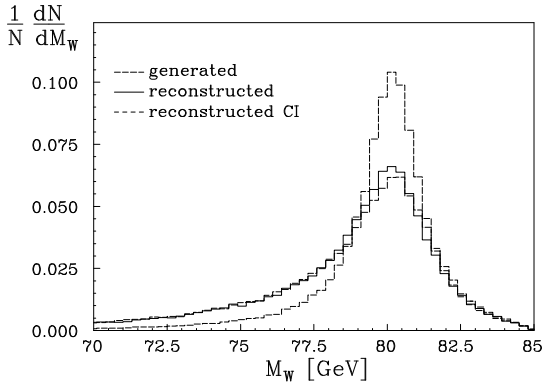

Figure 4.3: The distribution of the generated W mass (dashed) together with the reconstructed mass with (dotted) and without (solid) colour interference. The results are for reconstruction method 2.

Method	ΔM [MeV]	δM [MeV]
1	-279 $\pm$ 15	-3 $\pm$ 21
2	-1238 $\pm$ 19	-90 $\pm$ 27
3	-75 $\pm$ 16	-27 $\pm$ 23

Table 4.3: Shifts in the reconstructed W masses using the different methods from section 4.2. ΔM denotes the mass shift due to the reconstruction method and δM denotes the additional shift due to the colour interference.

from the experimental mass reconstruction point of view. However, in a worse case scenario with a 100% probability the shifts can be quite large but the experimental signal suggested in [1] would then on the other hand be observable.

4.4.2 Bose–Einstein interference results

We have studied how the inclusion of Bose–Einstein correlations, implemented as event weights, affect the results from various mass reconstruction schemes. The main concern in [2] was that the BE effects in the hadronization stage can couple identical particles from the W^+ and the W^-. They used the LUBOEI algorithm [2] in which the momenta of the produced bosons are reshuffled to reproduce a chosen BE-correlation. The momenta are then rescaled by a common factor to keep energy-momentum conservation for the event as a whole. This procedure might result in a redistribution of momenta in such a way that the hadrons which come from the $W^+(W^-)$ decay don't add up to

the same invariant mass as the original $W^+(W^-)$ had. It should be noted that the rescaling procedure needed afterwards introduces shifts in the W mass even if there are no BE-correlations between particles stemming from different W's. After corrections for this 'spurious' mass shift a shift of about +100 MeV at 170 c.m. energy was found in [2].

The main feature of our model is that we don't expect a coupling between particles coming from different W's. The inclusion of correlations may however affect for example multiplicities and event shape variables and therefore it may affect the reconstruction of the W boson mass. Such an artificial mass shift is hoped to be taken into account by the tuning of the JETSET MC [8] to the experimental LEP1 data. Using the MC implementation of our model, we have tuned multiplicity distributions and some event shape variables to the corresponding results as obtained from JETSET for a single string at LEP1 energies. To study the effect of the symmetrisation we have then analysed and compared the reconstructed W mass of W's generated by Pythia with and without symmetrisation included. We have used our tuning to LEP1 energies for the symmetrised events. The events are generated without a parton cascade, i.e. pure $q_1\overline{q}_2q_3\overline{q}_4$ events, in this analysis since the MC implementation of the BE-model has not been extended to general parton configurations. We believe that the inclusion of gluons will affect the mass reconstruction, but it will do it in the same way whether BE symmetrisation is included or not.

The use of event weights introduces statistical fluctuations which require the generation of many events. We have generated a sufficient number of events in order to get reasonable statistical errors for the mass distributions. In Fig.(4.4) we show the reconstructed mass for symmetrised and non-symmetrised events. As can be seen the difference between the distributions is very small.

Method	ΔM $[MeV]$	δM $[MeV]$
1	-306 $\pm$ 1	-6 $\pm$ 8
2	-83 $\pm$ 1	-5 $\pm$ 7
3	-601 $\pm$ 4	-6 $\pm$ 6

Table 4.4: Shifts in the reconstructed W masses using the different methods from section 4.2. ΔM denotes the mass shift due to the reconstruction method and δM denotes the additional shift due to the Bose–Einstein symmetrisation.

Using the same notation for the mass shifts as in section 4.4.1 we have compiled the results for the different reconstruction schemes in Table 4.4. The mass shifts due to BE interference are all very small and compatible with zero. They will therefore not affect the LEP2 measurement and in particular we conclude that the inclusion of Bose–Einstein correlations will compared to a carefully tuned

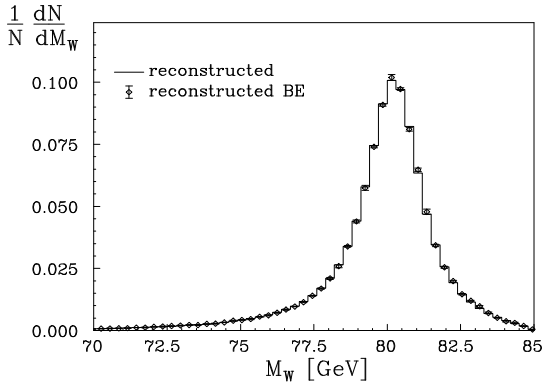

Figure 4.4: The distribution of the reconstructed W mass with (diamonds) and without (solid) Bose–Einstein symmetrisation turned on. The results are for reconstruction method 2.

conventional Monte-Carlo not affect the reconstruction of the W mass. It is important to note that using event weights can in principle affect the W mass even though we don't have any interference between the two W's. This is however not the case with our model.

4.5 Conclusions

The previous work on the effects of BE correlations on the W mass, with the exception of [18], are all based on the observation that the BE effect packs identical particles closer together. The local model [2] as well as the global event weight models [5, 6] are all phenomenological models used to estimate the influence of such a close-packing on the masses of the two $q\overline{q}$ systems, if the two W systems cross-talk. Our model starts from a completely different point of view, i.e. with a quantum mechanical scenario for the particle production dynamics, and at LEP1 energies the results obtained with our model are in agreement with the observables on which the other models are based. A natural consequence of our model is that we do not expect any cross-talk due to BE effects between the W's. The correlations between pions from different W's have been investigated by two of the LEP experiments. The DELPHI experiment has at their present level of statistics found no enhancement of the correlations between pions from different W's, compared to what is expected from a pair of uncorrelated W's [19] (confirmed in [9]) and ALEPH draws a similar conclusion from their data [20]. Their statistics are rather poor but if the results are

confirmed when more data becomes available, it would rule out mass shifts due to cross-talk between the two W's, in agreement with our model.

The reconnection probability of our CI model, as in other models, remains a free parameter. Assuming a moderate probability of 10% the mass shift due to CI will be very small. If we however assume a 100% probability the mass shift can be important, but in this case the experimental signal of [1] should be visible. The magnitude of the signal is a measure of the reconnection probability in our model, and if the signal is found it can be used to estimate the theoretical uncertainty in the mass determination.

To summarize, we conclude that neither colour nor Bose–Einstein interference is expected to affect the W mass reconstruction at LEP2 and in particular that the theoretical uncertainties, as estimated by our models, are much smaller than the expected experimental statistical error.

References

[1] G. Gustafson, J. Häkkinen, *Z. Phys.* **C64**, 659 (1994)

[2] L. Lönnblad and T. Sjöstrand, *Phys. Lett.* **B351**, 293 (1995)

[3] T. Sjöstrand and V.A. Khoze, *Z. Phys.* **C62**, 281 (1994)

[4] T. Sjöstrand and V.A. Khoze, *Phys. Rev. Lett.* **72**, 28 (1994)

[5] J. Ellis and K. Geiger, *Phys. Rev* **D54**, 1967 (1996)

[6] S. Jadach and K. Zalewski, *Acta Phys. Polon.* **B28**, 1363 (1997)
V. Kartvelishvili, R. Kvatadze and R. Møller, *Phys. Lett.* **B408**, 331 (1997)
K. Fialkowski and R. Wit, *Acta Phys. Polon.* **B28**, 2039 (1997)

[7] B. Andersson and M. Ringnér, *Nucl. Phys.* **B513**, 627 (1998)

[8] T. Sjöstrand, *Comp. Phys. Comm.* **82**, 74 (1994)

[9] DELPHI Coll., *Contribution to the EPS conference, Jerusalem, EPS-HEP/97-307, DELPHI 97-84 CONF 70* (1997)

[10] L3 Coll., *Contribution to the EPS conference, Jerusalem, EPS-HEP/97-814, L3 NOTE 2134* (1997)

[11] OPAL Coll., *Euro. Phys. J.* **C1**, 395 (1998)

[12] D.R. Ward, *Talk given at the EPS conference, Jerusalem* (1997)

[13] Yu.L. Dokshitzer, V.A. Khoze, L.H. Orr, W.J. Stirling, *Nucl. Phys.* **B403**, 65 (1993)
T. Sjöstrand, V.A. Khoze, *Z. Physik* **C62**, 281 (1994)

[14] B. Andersson, P. Dahlqvist, G. Gustafson, *Phys. Lett.* **B214**, 604 (1988) , *Z. Phys.* **C44**, 455 (1989)

[15] L. Lönnblad, *Comp. Phys. Comm.* **71**, 15 (1992)

[16] B. Andersson, G. Gustafson, G. Ingelman and T. Sjöstrand, *Phys. Rep.* **97**, 31 (1983)

[17] B. Andersson and W. Hofmann, *Phys. Lett.* **B169**, 364 (1986)

[18] Š. Todorova-Novà and J. Rameš, *hep-ph/9710280* (1997)

[19] DELPHI Coll., *Phys. Lett.* **B401**, 181 (1997)

[20] ALEPH Coll., *Contribution to the EPS conference, Jerusalem, EPS-HEP/97-590* (1997)

Is there screwiness at the end of the QCD cascades?

Paper V

Is there screwiness at the end of the QCD cascades?

Bo Andersson, Gösta Gustafson, Jari Häkkinen,
Markus Ringnér and Peter Sutton

Department of Theoretical Physics, Lund University,
Sölvegatan 14A, S-223 62 Lund, Sweden

Journal of High Energy Physics **09**, 014 (1998)

We discuss what happens at the end of the QCD cascades. We show that, with just a few reasonable assumptions, the emission of soft gluons is constrained to produce an ordered field in the form of a helix. We describe how to modify the Lund fragmentation scheme in order to fragment such a field. Our modified fragmentation scheme yields results which are consistent with current experimental measurements, but predicts at least one signature which should be observable.

5.1 Introduction

In QCD the production of two colour charges which subsequently move apart will lead to the production of further colour radiation. This can be described in terms of the fundamental field quanta, the gluons, but it is also possible to describe the ensuing radiation in terms of dipoles. This property arises because in non-abelian theories the emission of an extra gluon from a gluon-gluon dipole can (to a very good approximation) be modelled as the destruction of the original dipole and the creation of two new dipoles. In this way the change in the colour field can be described as an increasing cascade of dipoles. The end of this cascade occurs when the dipole masses are so small that helicity conservation prevents further real gluon emission. In this paper we examine what happens at the end of this cascade. We find that the conditions are favourable for the field to utilize the azimuthal degree of freedom and wind itself into the form of a helix. This corresponds to a close–packed configuration of gluons in rapidity–azimuthal-angle space.

We begin by describing a toy model which contains the relevant features, namely a tendency to emit as many gluons as possible and the constraint that gluons are not too "close" to each other (which arises from helicity conservation). In this simple model it is clear that at the end of the cascade an ordered field emerges with the characteristics of a helix. To progress beyond this model we use the Lund model of QCD. In the Lund picture hard gluons are represented as excitations of a relativistic string which connects a quark, anti-quark pair. However, the gluons from which the helix is built up are too soft to be modelled in this way. Instead we introduce a helical semi-classical field and thus develop a modifed version of the Lund fragmentation scheme. Our modified fragmentation scheme enables us to study whether the consequences of a screwy field can be detected in the final state particles. We find that if events with hard gluons are excluded then the screwiness of the field may be observed.

5.2 The dipole cascades; increase and decrease of phase space

In order to describe what can happen at the end of the QCD cascades we will provide a brief description of the cascades. We will in particular discuss the consequences of helicity conservation in the emission of partons.

The well-known formula for dipole emission of bremsstrahlung is

$$dn = \bar{\alpha}\frac{dk_\perp^2}{k_\perp^2}dy(\frac{d\phi}{2\pi})\,\Psi \tag{5.1}$$

where $\bar{\alpha}$ is the effective coupling, $k_\perp$, y, and ϕ are the transverse momentum, rapidity and azimuthal angle respectively, although the azimuthal angle dependence is usually neglected. The final factor, Ψ, corresponds to the spin couplings. We will briefly consider the precise definitions before we consider the implications. The effective coupling for QCD in the case of a gluonic dipole is given by

$$\bar{\alpha}_{\rm QCD} = \frac{N_c\alpha_s}{2\pi} \simeq \frac{6}{11\log(k_\perp^2/\Lambda^2)}\ . \tag{5.2}$$

The occurrence of the number of colours, N_c, and the factor $1/2$ in the QCD coupling is due to early conventions, whereas the result that the running is governed by $1/c = 6/11$ is a basic gauge group independent result. It only depends upon the fact that in non-abelian gauge theories there is a three-particle coupling between vector particles, e.g. the colour-8 gluons in QCD. (The four-gluon coupling also occurs to preserve the symmetry, but it does not play a rôle in this connection). We neglect the flavour term $-2n_f/3$ which should accompany 11 in the denominator because it is a small effect related to the possibility of gluon splitting; $\mathrm{g} \to \mathrm{q\overline{q}}$.

The transverse momentum and the (dipole cms) rapidity are defined in a Lorentz invariant way in terms of the squared masses of the final state partons (the emitters are conventionally indexed 1 and 3 and the emitted field quantum 2):

$$\begin{aligned}
s_{ij} &= (k_i+k_j)^2 = 2k_ik_j = 2k_{\perp i}k_{\perp j}\left[\cosh(\Delta y)_{ij} - \cos(\Delta\phi)_{ij}\right] \\
s &= s_{12}+s_{23}+s_{31} \\
s_{12} &= s(1-x_3),\ s_{23} = s(1-x_1) \\
k_\perp^2 &= \frac{s_{12}s_{23}}{s} \\
y &= \frac{1}{2}\log\left(\frac{s_{12}}{s_{23}}\right)
\end{aligned} \tag{5.3}$$

Here x_1 and x_3 are the final state cms energy fractions of the emitters. Requiring energy momentum conservation limits the allowed emittance region to

$$k_\perp\cosh(y) \le \frac{\sqrt{s}}{2}\ . \tag{5.4}$$

This region can conveniently be approximated as $|y| < (L-\kappa)/2$ with the variables $L \equiv \log(s/\Lambda^2)$ and $\kappa \equiv \log(k_\perp^2/\Lambda^2)$. This means that the (approximate)

phase space available for dipole emission is the interior of a triangular region in the (y, κ)-plane with the height and the baselength both equal to L. The inclusive density inside the triangle is, in this Leading-Log Approximation (LLA), given by the effective coupling $\bar{\alpha}$ according to Eq.(5.1). The rapidity range, $L - \kappa$, is of course the length of a hyperbola spanned between the emitters in space-time (or energy-momentum at the scale $k_\perp^2$).

If we consider an initial $q\overline{q}$ dipole emitting a gluon then the probability for the produced $qg\overline{q}$ system to emit a second gluon is a complicated expression [1]. In case the transverse momenta of the first and second gluon are strongly ordered, $k_{\perp 1} \gg k_{\perp 2}$, it is a very good approximation to treat the second emission as independent emission from two dipoles [2]. For an exclusive statement, for example the probability dP to emit the first gluon with a certain (κ_1, y_1), it is necessary to multiply the inclusive formula in Eq.(5.1) with a Sudakov form factor Δ_s containing the probability not to emit above κ_1,

$$\begin{aligned} \Delta_s(L, \kappa_1) &= \exp(-\int_{\kappa_1}^{L} dn), \\ dP(\mathrm{q}, \mathrm{g}_1, \overline{\mathrm{q}}) &= dn(\kappa_1, y_1)\Delta_s(L, \kappa_1) \ . \end{aligned} \tag{5.5}$$

The probability to emit two gluons is then, in the approximation that the second gluon is emitted by two independent dipoles, given by

$$dP(\mathrm{q}, \mathrm{g}_1\mathrm{g}_2, \overline{\mathrm{q}}) = dP(\mathrm{q}, \mathrm{g}_1, \overline{\mathrm{q}})\,[dP(\mathrm{q}, \mathrm{g}_2, \mathrm{g}_1) + dP(\mathrm{g}_1, \mathrm{g}_2, \overline{\mathrm{q}})] \tag{5.6}$$

in easily understood notations. The approximation in Eq.(5.6) results at most in a percentage error over all phase space [3]. Thus, contrary to QED where the chargeless photons still leave the e^+e^--current as the single emitter, the 8-charge gluon (g_1) in QCD changes the original $q\overline{q}$ dipole into two dipole emitters, one between q and g_1 and one between g_1 and $\overline{q}$, and *each can independently emit the second gluon* (g_2). The requirement for the validity of the approximation in Eq.(5.6) is that $k_{\perp 1} \geq k_{\perp 2}$ or else the indices are exchanged.

The two independent dipoles are moving apart (with g_1 as the common parton). This means that they have together a larger effective rapidity range for the emission of g_2, i.e. the original hyperbola length $L = \log(s)$ is exchanged for two hyperbolas with the combined length $\log(s_{\mathrm{qg}_1}) + \log(s_{\mathrm{g}_1\overline{\mathrm{q}}}) = L + \log(k_{\perp 1}^2)$. From any one of the two new dipoles we may then emit the second gluon, thereby producing three independent dipole emitters and the process can be continued towards more dipoles; ordering the process in $k_\perp$ downwards. The available phase space for further emission is increased after each emission, as can be seen from the increased total length, L, after the first emission. This description of the QCD cascades is called the Dipole Cascade Model (DCM) [4].

We will now consider the polarisation sum contribution in Eq.(5.1). Its precise properties depend upon whether we are dealing with a $q\overline{q}$, qg or a gg dipole, but it stems from the spin couplings between the emitter(s) (it is essentially sensitive only to the closest emitter) and the new field quantum. These couplings contain the property that helicity is conserved, which is true for all gauge theories. This means that if a spin-1/2 parton emits a spin-1 parton, the spin-1 parton must go apart from the emitting particle in order to conserve helicity and angular momentum. They have to go even further apart in the case of a spin-1 parton emitting a spin-1 parton. To estimate the separation we consider (for fixed $k_\perp$ (or κ)) the available rapidity range:

$$\int_{y_{\min}}^{y_{\max}} \Psi \, dy = L - \kappa - c + O(k_\perp^2/s) \tag{5.7}$$

where $c = (11/12 + 11/12)$, $(3/4 + 11/12)$ or $(3/4 + 3/4)$ depending on whether the emitters are gg, qg ($g\overline{q}$) or a $q\overline{q}$ dipole [5]. The quantities c are written as sums to show that a spin-1 (g) emitter and a spin-1/2 (q or $\overline{q}$) emitter has an empty region surrounding it in rapidity of size 11/6 and 3/2, respectively. In order to obtain this result we note that in terms of the x-variables introduced in Eq.(5.3) the factor Ψ is $(x_1^{n_1} + x_3^{n_3})/2$ with $x_{1,3} = 1 - k_\perp \exp(\pm y)/\sqrt{s}$ and $n_{1,3}$ equal to 2 or 3 for $q(\overline{q})$ and g, respectively. $y_{\{\max,\min\}}$ are determined from the energy momentum requirement in Eq.(5.4).

A note of caution should be issued at this point. For given s and $k_\perp$ there are two definite limits in rapidity $y_{\min} \leq y \leq y_{\max}$, and there is then a depletion of emissions due to helicity conservation, in regions close to $y_{\min}$ and $y_{\max}$. It is in general a poor approximation to put the factor Ψ to a unit stepfunction for $y_{\min} + c/2 \leq y \leq y_{\max} - c/2$ although it works when the rapidities and azimuth are integrated out. A closer examination provides a y-distribution with similarities to a finite temperature Fermi distribution. We will nevertheless refer to this feature as "the excluded region" around each gluon.

We note that in the process $g \to q\overline{q}$, where the spin-1 parton emits two spin-1/2 partons, that the fermion pair "prefer" to be parallel, since there are no poles in this decay distribution. However the process $g \to q\overline{q}$ is suppressed compared to the process $g \to gg$ and is in general neglected. The DCM will in this way produce a fan-like set of dipoles, which in the LLA increases the phase space (the total available effective rapidity range) for further emissions. However, including the influence from the polarisation sum (which is essentially the approximation scheme called Modified LLA) there is in each emission also a depleted region around an emitted parton, in practice $c = 11/6$, because the gluons completely dominate the process. At large energies, but not too large transverse momenta, one may in general neglect the restrictions but they will be very noticable at the end of the cascades. For example, with a dipole mass of

3 GeV the typical rapidity range available for gluon emission is about 4 units, and it is then very noticable to exclude 11/6 units.

It is interesting that the average region excluded due to helicity conservation also occurs in connection with the properties of the running coupling. To be more precise, we consider a change of scale in the definition of a field quantum and its interaction. A change of scale means that the field operator, which has been normalised to a single quantum at one scale, and the coupling constant, which likewise has been normalised at the original scale, will both change. These changes can be read out from the Callan-Symanzik equations and the β-function contribution, stemming from the change in the coupling constant, can be written as

$$-\beta(\alpha_s)\frac{\partial \mathcal{M}}{\partial \alpha_s} = (\frac{11}{6}\frac{N_c\alpha_s}{2\pi} - \frac{2}{3}\frac{n_f\alpha_s}{4\pi})\alpha_s\frac{\partial \mathcal{M}}{\partial \alpha_s} \tag{5.8}$$

where a change in a quantity $\mathcal{M}$, when the observation scale is decreased from the level $\kappa = \log(k_\perp^2)$ to $\kappa - d\kappa$, is considered. The decrease accounts for the minus sign on the left hand side. According to the DCM there is then at this new scale not only the possibility to emit new gluons but also, at the next order in the coupling α_s, the possibility to reabsorb already emitted gluons.

The operator $\alpha_s\partial/\partial\alpha_s$ works like a number operator, i.e. for any function $\mathcal{M} = \sum \alpha_s^n m_n$ it provides the number n of possible insertions. The quantities $N_c\alpha_s/2\pi$ and $n_f\alpha_s/4\pi$ are the couplings for $gg \to g$ and $q\overline{q} \to g$ (and the inverse processes) while 11/6 and 2/3 corresponds to the effective (generalised) rapidity ranges available in these reabsorption processes for a given κ. It should be noted, however, that this interpretation is gauge-dependent; in almost all gauges there are contributions to the β-function from the vertex corrections. However, for a particular gauge choice with the propagator given by $-(g_{\mu\nu} - 4k_\mu k_\nu/k^2)/k^2$, the vertex contributions vanish. A closer analysis reveals that the major effect stems from the so-called Coulomb gluons, i.e. a charged particle like a field quantum in a non-abelian theory is always accompanied and interacts with its own Coulomb field. The 11/6 can therefore be considered as the region around the gluon containing its accompanying field. This has been utilized for an approximation of the QCD cascades where the available phase space for emission is discretised [6].

5.3 A toy model for the end of the cascades

After several gluon emissions there are a set of dipoles with small masses, and there are in general very many Feynman graphs which may contribute. The largest diagramatic contribution is chosen according to coherence conditions in

the cascade; in the Dipole Model [4] by an ordering of the gluon emissions in transverse momentum, and in the Webber-Marchesini model [7], and the model implemented in JETSET [8], according to a choice of kinematical variables that fascilitates a strong angular ordering of the emitted gluons. Results from the cascade models are essentially equivalent, at least as long as sufficiently hard gluon emission is considered.

The ordering of emissions in the models will lead to dipoles with small masses emitting softer gluons. These soft gluons have a transverse momentum, $k_\perp$, of the same order as their emitter and recoils play an important rôle. At present there exists only a minor knowledge of how the recoils should be distributed among the emitters. A sufficiently large recoil on one of the emitting (soft) gluons will in general imply that the chosen order is no longer in accordance with the coherence conditions. Emitting soft gluons will evidently lead to a situation where several, or even very many, paths to the final state are important, and many different Feynman graphs may contribute and interfere.

To investigate the emission of soft gluons we propose a toy model with the following two properties:

I We assume that the effective coupling $\bar{\alpha}$ is large enough so that there is a tendency to emit as many gluons as possible, essentially with the same $k_\perp$.

II We assume that the emissions fulfil the requirement of helicity conservation; this implies that two colour-connected gluons cannot be closer than a "distance" $d = c$.

We will use the following combination as the probability for a given colour-connected multi-gluon state

$$P = \prod_1^{n-1} \frac{\alpha\beta}{s_{j,j+1}} \tag{5.9}$$

where $s_{j,j+1}$ is the dipole mass between the colour-connected gluons j and $j+1$. The factor α corresponds to the product of the coupling and the relevant phase space region, and β to the restrictions from helicity conservation, i.e. the requirement of a suitable distance between the emitted gluons. Neglecting recoils, we obtain for any order of the emissions in the DCM, that the product of factors $1/s_{j,j+1}$ can be written in terms of the invariant dipole transverse momenta as

$$s_{12}s_{23}\ldots s_{n-1,n} = k_{\perp 2}^2 k_{\perp 3}^2 \ldots k_{\perp n-1}^2 s_{12\ldots n} \tag{5.10}$$

where $k_{\perp j}$ denotes the invariant $k_\perp$ of the dipole from which gluon j is emitted. Eq.(5.9) is therefore a simple generalisation of Eq.(5.1).

The dipole mass can be written as

$$\begin{aligned} s_{j,j+1} &= k_\perp^2\, 2[\cosh(\Delta y) - \cos(\Delta\phi)] \\ &\simeq k_\perp^2 (\Delta y^2 + \Delta\phi^2)[1 + (\Delta y^2 - \Delta\phi^2)/12] \ . \end{aligned} \tag{5.11}$$

For simplicity we have set the transverse momenta of the two gluons to be identical. Δy and $\Delta\phi$ are the differences between the colour-connected gluons in rapidity and azimuthal angle, respectively. We are now in a position to define precisely what we mean by "distance". We therefore introduce a distance measure, d, which is related to the dipole mass by

$$d_{j,j+1} \equiv \sqrt{s_{j,j+1}/k_\perp^2} \ . \tag{5.12}$$

When the dipole mass and the rapidity region are large the azimuthal dependence can be neglected and $d \simeq \Delta y$.

The emission of soft gluons has thus been reduced to the following problem; given a certain rapidity range and the full accompanying azimuthal range $0 \leq \phi < 2\pi$ how are the colour-connected gluons distributed in phase space in order to obtain a maximum of P in Eq.(5.9), keeping in mind that the gluons cannot be too close?

From Eq.(5.9) we see that the magnitude of α controls the relative probability between different gluon number states. If α is sufficiently large the number of emitted gluons will fill the available phase space, and P becomes maximal when the gluons align along a straight line in phase space. This helix-like structure is the optimal configuration irrespective of the size of α, or of the number of emitted gluons. For a given multi-gluon state there are many possible ways to colour-connect the state, where the helix is only one of the possibilities. It is of course possible that the sub-optimal configurations are the important ones and swamp the helix-like contribution, but there are also many contributions close to a perfect helix.

We have carried out a numerical study to test whether the contributions from helix-like structures survive the phase space effects. Our program calculates all possible configurations on a discretized (y, ϕ) phase space taking into account that gluons must not be closer than c to each other. The number of possible configurations grows factorially with the number of gluons, but the number of gluons is restricted by the available phase space. We have studied a reasonable phase space size of three units of rapidity using a closest gluon-to-gluon distance $c = 11/6$ in all the calculations. Since the fluctuations in dipole $k_\perp$ are limited within a narrow range at the end of the cascades and the dependence on dipole $k_\perp$ in Eq.(5.1) is rather weak, we set the transverse momenta of the gluons to be constant. In Fig.(5.1) we show the most probable five and six gluon configurations. The points corresponding to a given

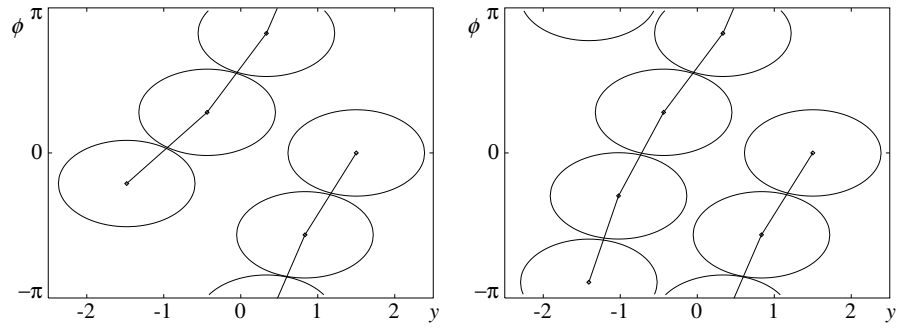

Figure 5.1: The most probable configurations with five and six gluons using $c = 11/6$. (The cylindrical phase space has been mapped onto a plane). The gluon exclusion region for each gluon is indicated with the ellipse-like shapes. The line segments show the colour field and should form a straight line for a perfect helix. The discrepancy is due to the discrete phase space used in our numerical analysis.

mass correspond to ellipse-like shapes ($\sqrt{(\cosh(\delta y) - \cos(\delta\phi))}$) and in order to minimize the distance between adjacent gluon emissions these ellipses must be displaced so that they correspond to a helix-shaped configuration. The case shown corresponds to the optimal situation where it is favourable to "close pack" the gluons irrespective of the size of α.

Taking into account all possible configurations we obtain a distribution in $D^2 \equiv \sum d_{jj+1}^2$ which is very broad, cf. Fig.(5.2), but weighting each D^2 with the corresponding P from Eq.(5.9) we obtain a large and narrow peak close to the most probable colour-connected configuration indicating that the gluon configurations have short strings close to the optimal helix structure.

Now that we have established that short strings are preferred we investigate in more detail if they are helix-like in general. To this aim we will introduce a new possible observable, "screwiness". At this point it is only a theoretical observable, but later on we will show how to use it for the final state hadrons. We define screwiness $\mathcal{S}$ from the values of (y_j, ϕ_j) for the emitted gluons in accordance with the toy model,

$$\mathcal{S}(\omega) = \sum_e P_e \left| \sum_j \exp(i(\omega y_j - \phi_j)) \right|^2 \quad . \tag{5.13}$$

The first sum is over all the configurations e found in the phase space and the second goes over the gluons in the configuration. For ω-values close to zero, screwiness must be small if the gluons are emitted isotropically in the

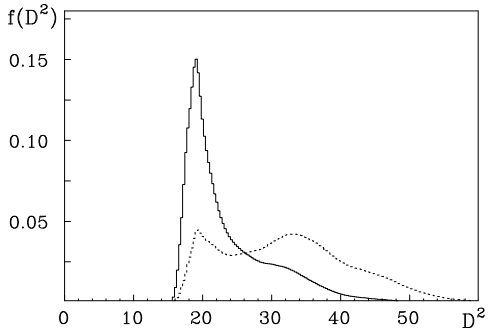

Figure 5.2: The unweighted (dashed line) and weighted (solid line) squared length distributions, f, of configurations with six gluons.

azimuthal angle. For large values of ω the phases should be close to chaotic and then screwiness only depends on the mean number of emitted gluons.

In Fig.(5.3) we show the screwiness distribution including contributions from all configurations with a specific number of gluons. Two cases are shown, firstly configurations with the maximum possible number of gluons (in a three unit rapidity phase space this is six gluons), and secondly those corresponding to five gluon states (the contributions corresponding to even smaller number of gluons show similar distributions). There are two noticable broad peaks with their mean values close to $\omega = \pm 2\pi/c$. Since the helix structure has no preferred rotational direction the distributions should be even. The small apparent asymmetry is due to numerical effects. We have also analysed the configurations for $c = 1.5$ and 3 and these results are independent of the minimum gluon-to-gluon distance.

From this toy model we see that if we fill the phase space with soft gluons, which are forbidden to be too close to one another, then they tend to line up along a helix structure, since the colour-connection between the gluons prefer to be as short as possible.

5.4 Modelling the helix as an excited string

In order to consider the consequences of the helix-like colour field which we obtained in Section 5.3 it is necessary to provide observables in terms of the final state hadrons. A first attempt to model such a field is to approximate it by the emission of a set of colour-connected gluons with the same transverse

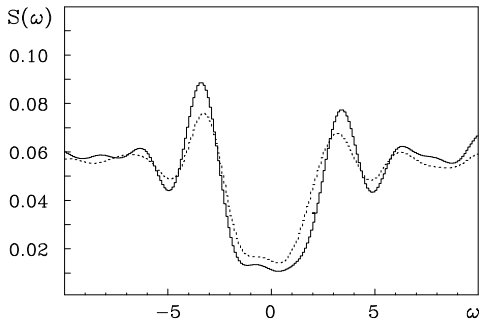

Figure 5.3: Screwiness in the toy model for five (dashed line) and six (solid line) gluon states in a rapidity region of three units with c=11/6.

momentum $k_\perp$. We may then consider the properties of the final state hadrons, as produced by the Lund string fragmentation model. We very quickly find that in the competition between increasing the multiplicity versus increasing the transverse momentum of the hadrons the model uses the first possibility only. In this section we will be content with giving the basic argument for why the helix cannot be described as gluonic excitations on the string field.

Suppose that a gluon with transverse momentum $k_\perp$ is moving transversely to the constant (κ) force field, then it is possible for the gluon to drag out the string field the distance $\ell = k_\perp/2\kappa$ (a gluon experiences twice the force acting on a quark). On the other hand, in a quantum mechanical setting such a gluon is only isolated from the field if the wave-length of the gluon $\lambda \simeq 2\pi/k_\perp$ is smaller than ℓ and therefore

$$\begin{aligned} k_\perp^2 &\geq 4\pi\kappa \\ \ell_{min}^2 &= \frac{\pi}{\kappa} \end{aligned} \tag{5.14}$$

(this is similar to the Landau-Pomeranchuk formation time arguments). From the first line in Eq.(5.14) we obtain the requirement that a "real" gluon must have a transverse momentum larger than $k_{\perp 0} = 1.6$ GeV.

We conclude that the helix field cannot be described in terms of a finite number of gluon excitations on the Lund string. The many small-$k_\perp$ excitations in the model tend to increase the final state particle multiplicity (with small fluctuations) rather than to produce transverse momentum for the particles. The interested reader can find a more thorough investigation of the problems associated with the fragmentation of soft gluons in appendix 5.A.

5.5 A semi-classical field at the end of the cascades

We will now consider the possibility that a (semi-)classical colour field is produced at the end of the perturbative QCD cascades that cannot be described solely in terms of gluonic excitations on the Lund Model string field. The properties of this field should be in accordance with the toy model that was described in section 5.3. Thus the internal colour quantum number should be correlated to the external space-time (energy-momentum space) behaviour so that the colour field has a helix structure, i.e. the colour field lines are turning around a spacelike direction, from now on called the 1-axis.

We may describe the expected field in terms of a wave-packet of energy-momentum space four-vectors, k_θ, corresponding to the colour current (the index θ stands for the parameters describing the wave-packet). We will assume that the vectors k_θ always have a constant virtuality $k_\theta^2 = -m^2$. We further assume that the helix colour field is itself emitted from the current as a continuous stream of gluons dk, colour-connected along each emission vector, k_θ. They should be obtained by differentiating the vector k_θ (we are generalising the physics picture from a ladder-diagram as in Fig.(5.4), where the "propagator" vectors $\{k\}_j$ are emitting the gluons $dk_j = k_j - k_{j-1}$).

The most general description of such a vector is (we use lightcone coordinates along the 01-direction and transverse coordinates in the 23-plane and we do not worry about the initial values):

$$\begin{aligned} k_\theta &= m[cos(\theta)(\exp(y), -\exp(-y), 0, 0) + \sin(\theta)(0, 0, \cos(\sigma\phi), \sin(\sigma\phi))] \\ &\equiv m[\cos(\theta)e_1(y) + \sin(\theta)\vec{e}_{\perp 1}(\sigma\phi)] \ . \end{aligned} \tag{5.15}$$

Here m is a constant parameter, y is the rapidity and ϕ the azimuthal angle. We have introduced σ as a constant describing the relative motion in rapidity and azimuth. We will put $\sigma = 1/2$ later in order to get ϕ as the azimuthal angle of dk. Finally θ is the variable describing, on the one hand, the size of the fluctuations in the longitudinal and transverse parts, and on the other hand, the properties of the wave-packet.

Assuming that the emitted field quanta dk are massless, we get,

$$\begin{aligned} dk^2 = 0 \quad &\Rightarrow \quad \left(\frac{d\theta}{d\ell}\right)^2 + \left(\frac{1 - cos(2\theta)}{2}\right) = \left(\frac{dy}{d\ell}\right)^2 , \\ \text{small } \theta \quad &\Rightarrow \quad \left[\left(\frac{d\theta}{d\ell}\right)^2 + \theta^2\right] = \left(\frac{dy}{d\ell}\right)^2 . \end{aligned} \tag{5.16}$$

We have used the differential $d\ell \equiv \sqrt{dy^2 + d(\sigma\phi)^2}$. Therefore, the assumptions

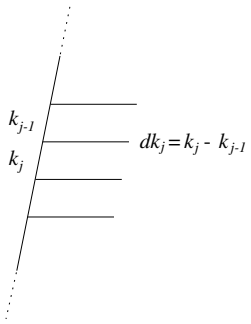

Figure 5.4: A current with constant virtuality, $k_j^2 = -m^2$, emitting massless field quantas, $dk_j^2 = 0$.

of constant virtuality of k and the masslessness of dk imply that the variable θ should fulfil the pendulum equation according to the first line of Eq.(5.16). In the limit of small $|\theta|$-values this becomes a harmonic oscillator equation, assuming that the quantity $dy/d\ell$ is a (small) constant along each vector k_θ. For consistency we will then make the change $d\ell \to \sigma d\phi$. This is the second line of Eq.(5.16) and using the notation $dy/d\phi \equiv \tau$ we obtain as a classical description (again neglecting the boundary values):

$$\theta = \frac{\tau}{\sigma} cos(\sigma\phi) \quad . \tag{5.17}$$

If we choose $\sigma = 1/2$ to make ϕ the azimuthal angle of dk, then we find that the field emission vectors $dk/d\phi$ and the corresponding current vector k_θ are (in the approximation of small oscillations):

$$\begin{aligned} \frac{dk}{d\phi} &= m\tau[e_0(y) + \vec{e}_{\perp 0}(\phi)] \\ k_\theta &= m[e_1(y) + \tau(\vec{e}_{\perp 1}(\phi) + \vec{e}_{\perp 1}(0))] \quad . \end{aligned} \tag{5.18}$$

Here we have introduced the vectors $e_0 = de_1/dy$ and $\vec{e}_{\perp 0} = d\vec{e}_{\perp 1}/d\phi$ (note that all the occurring vectors are orthogonal). We may evidently use the quantity τ (together with suitable boundary values) to label the wave packet for the current. That is to say, we may assume that there is a distribution $h(\tau)$ which describes the occurrence of the different current lines, each with a well-defined direction τ. This distribution, $h(\tau)$, should be similar to a Gaussian. A single current line with fixed τ may also be described in the transverse plane. The current turns around the 1-axis with the azimuthal angle and the corresponding field quanta are emitted transversely to the current at every emission point

according to Eq.(5.18). There is one reasonable restriction: the field energy emitted by the current in a small angular segment should not exceed the energy which should be available in the Lund Model string. If we use the string radius as calculated in Eq.(5.14), $\ell_{min} = \sqrt{\pi/\kappa}$, then we find that

$$m\tau \leq \kappa \ell_{min} \simeq 0.8 \text{ GeV} \quad . \tag{5.19}$$

It is interesting to note that these fields have similarities to those studied in connection with dimensional reduction in [9].

5.6 Fragmentation and screwiness

We have in the previous section described the emission of a continuous stream of colour-connected gluons having the property that the azimuthal angle of the stream is proportional to the rapidity, i.e. it is of a helical character. As previously discussed we cannot implement this as individual gluonic excitations of the Lund string. We will in this section instead describe a possible way to take the transverse properties of the continuous helix into account whilst keeping the major properties of the Lund fragmentation model. In order to do this we will begin by presenting a few relevant parts of the Lund model. This model has been described several times and a recent investigation can be found in [10].

5.6.1 The Lund fragmentation process

The following (non-normalised) probability to produce a set of hadrons has been derived using semi-classical arguments in [11]

$$dP(\{p\}_j; P_{tot}) = \left[\prod_1^n N_j dp_j \delta(p_j^2 - m_j^2)\right] \delta(\sum p_j - P_{tot}) \exp(-bA) \quad . \tag{5.20}$$

Here N_j are normalisation constants, A the decay area, cf. Fig.(5.5), and b a basic colour-dynamical parameter; from comparison to experimental data we know that $b \simeq 0.6 \text{ GeV}^{-2}$ if the area A is expressed in energy-momentum space quantities.

The constant force field spanned between a colour-3 quark and a colour-$\overline{3}$ anti-quark is a simple mode of the massless relativistic string. The process has been generalised into a situation with multigluon emission in [12] using the Lund interpretation that the gluons are internal excitations on the string field.

The area decay law in Eq.(5.20) can be implemented as an iterative process, in which the particles are produced in a stepwise way ordered along the positive

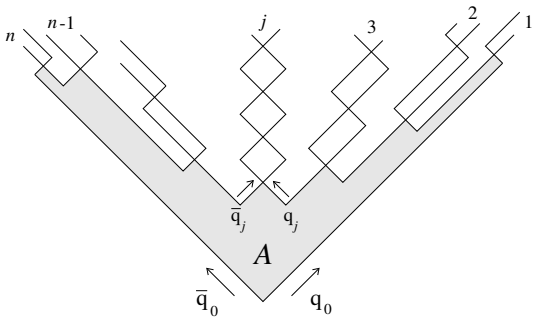

Figure 5.5: The break-up of a Lund string.

(or negative) light-cone. If a set of hadrons is generated, each one takes a fraction z of the remaining light-cone component $E + p_l$ (or $E - p_l$, if they are generated along the negative light-cone), with z given by the distribution

$$f(z) = N\frac{(1-z)^a}{z}\exp(-bm_\perp^2/z) \quad . \tag{5.21}$$

The parameters N, a and b are related by normalisation, leaving two free parameters. The transverse mass parameter in the fragmentation function is $m_\perp^2 = m^2 + \vec{p}_\perp^{\,2}$, with the transverse momentum obtained as the sum of the transverse momenta stemming from the q and $\overline{\mathrm{q}}$ particles generated at the neighbouring vertices, $\vec{p}_\perp = \vec{k}_{\perp 2} - \vec{k}_{\perp 1}$. In the Lund model a $\mathrm{q}\overline{\mathrm{q}}$-pair with transverse momenta $\pm k_\perp$ is produced through a quantum mechanical tunneling process. It results in a Gaussian distribution for the transverse momenta

$$d^2k_\perp \exp(-\pi k_\perp^2/\kappa) \quad . \tag{5.22}$$

The whole process is implemented in the Monte Carlo program JETSET [8].

Consider the production of a particle with transverse mass $m_\perp$. Given that one vertex has the rapidity y_1, the rapidity difference Δy is not enough to specify the position of the other vertex. One must also know the proper-time of the first vertex. This is shown in energy-momentum space in Fig.(5.6) where the first vertex is specified by Γ which is the squared product of the proper-time and κ. Of course there are two solutions in this case, but one is strongly favoured by the area dependence in Eq.(5.20). In the Lund model the vertices, on average, lie on a hyperbola given by a typical Γ. That is to say, the steps in rapidity in the particle production are related to the scale $\langle\Gamma\rangle$ as given by the model. There is a similar situation in the transverse momentum generation. The squared

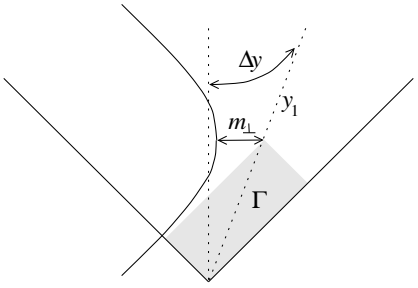

Figure 5.6: The longitudinal energy scale in the Lund model is $\langle\Gamma\rangle$. The figure shows the production of a particle with transverse mass $m_\perp$. The difference in rapidity between the constituent vertices has to be related to the Γ of one of the vertices in order for the vertices to be specified.

transverse momentum of a particle is not only given by the azimuthal angle $\Delta\phi$ between the break-up points that generate the particle. The lengths of the transverse momenta of the q and the $\overline{\mathrm{q}}$ that make up the particle are also needed. In the tunneling process in Eq.(5.22) these sizes are given by the scale κ/π.

Thus the Lund fragmentation model provides two different energy scales; one longitudinal to relate to the rapidity difference between vertices and one transverse to relate to their difference in azimuthal angle.

5.6.2 A modified fragmentation process with screwiness

The main idea in the screwiness model is that the transverse momentum of the emitted particles stems from the piece of screwy gluon field that is in between the two break-up points producing the particle. Therefore we begin by summing up the transverse momentum that is emitted between two points along the field line, cf. Eq.(5.18):

$$\int_1^2 \frac{d\vec{k}_\perp}{d\phi} d\phi = \vec{k}_{\perp 2} - \vec{k}_{\perp 1} = m\tau[\vec{e}_{\perp 1}(\phi_2) - \vec{e}_{\perp 1}(\phi_1)] \quad . \tag{5.23}$$

We note that the quantity $m\tau$ also occurs here. We will always consider the parameter m to be a suitable fixed mass parameter but according to the assumed wave function for the current the direction τ may vary between the different break-up points. To keep the presentation clear we will start off keeping τ fixed. In the end we will present the generalisation to the case of a varying τ.

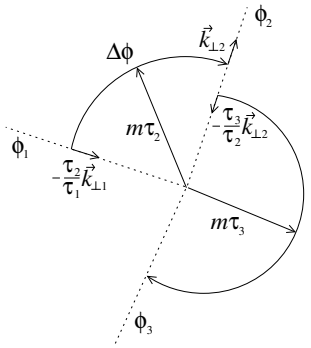

Figure 5.7: A $q\overline{q}$-pair is produced in a break-up point with azimuthal angle ϕ. The figure illustrates how the screwy gluon field between ϕ_1 and ϕ_2 is associated with the transverse momentum $(-k_{\perp 1}, k_{\perp 2})$ of the quarks produced at the two break-up points. This association has the property that the produced transverse momentum is conserved locally in each break-up point.

If we associate $\pm\vec{k}_{\perp i}$ with the transverse momenta of the $q\overline{q}$-pair produced at vertex i, the transverse momenta of the produced particles are given by Eq.(5.23). The corresponding squared transverse momentum is then

$$p_{\perp i}^2 = 2m^2\tau^2[1 - \cos(\Delta\phi)] \tag{5.24}$$

where $\Delta\phi = \phi_i - \phi_{i-1}$. Since $\Delta\phi$ is proportional to the rapidity difference between vertices Δy, it can be written as a function of the particle's light-cone fraction z

$$\Delta\phi = \frac{\Delta y}{\tau} = \frac{1}{2\tau}\log\left(\frac{z + m_\perp^2/\Gamma}{z(1-z)}\right) \tag{5.25}$$

where Γ is defined as in Fig.(5.6) and with respect to the previous break-up point $i-1$. Taken together this means that we can write the transverse momentum of a particle as a function of z and τ

$$p_\perp^2(z) = 2m^2\tau^2\left[1 - \cos\left(\frac{\Delta y(z)}{\tau_i}\right)\right] \quad . \tag{5.26}$$

As explicitly manifested in Eq.(5.26) this means that the transverse and longitudinal components are connected in this model. Inserting $p_\perp^2(z)$ in the Lund fragmentation function gives

$$f(z) = N\frac{(1-z)^a}{z}\exp\left(-\frac{b}{z}\left(m_h^2 + p_\perp^2(z)\right)\right) \quad . \tag{5.27}$$

In this way Eq.(5.27) gives the distribution of light-cone fractions for a given direction τ.

This model keeps the longitudinal properties of the ordinary Lund fragmentation model, but the azimuthal properties are changed. Rapidity differences are still related to $\langle\Gamma\rangle$ but steps in the azimuthal angle are now correlated with steps in rapidity. The azimuthal angles are no longer related to κ/π as given by the tunneling process, but instead to $m^2\tau^2$ as given by the screwy gluon field.

When going from one vertex to the next in the case of varying τ one has to keep in mind that the transverse momentum produced at the first vertex has been specified by the previous step. In order to conserve the transverse momenta generated at each vertex we therefore modify the association in Eq.(5.23), as follows

$$\int_{i-1}^{i} \frac{d\vec{k}_\perp}{d\phi} d\phi = \vec{k}_{\perp i} - \frac{\tau_i}{\tau_{i-1}} \vec{k}_{\perp i-1} \tag{5.28}$$

where τ_i denotes the direction between break-up points $i-1$ and i, cf. Fig.(5.7). The transverse momenta of the produced particles are then given by

$$\begin{aligned} \vec{p}_{\perp i} &= \vec{k}_{\perp i} - \vec{k}_{\perp i-1} = m\left[\tau_i \vec{e}_{\perp 1}(\phi_i) - \tau_{i-1}\vec{e}_{\perp 1}(\phi_{i-1})\right] \\ p_{\perp i}^2 &= m^2\left[\tau_i^2 + \tau_{i-1}^2 - 2\tau_i\tau_{i-1}\cos(\Delta\phi)\right] \quad . \end{aligned} \tag{5.29}$$

The $p_\perp^2$ given by Eq.(5.29) can then be put into the fragmentation function. Varying τ results in larger variations in the emitted transverse momenta of the particles. We have used a Gaussian distribution of τ-directions and we have approximated $m_\perp^2$ in Eq.(5.25) with $m_\perp^2 \simeq m_h^2 + \langle p_{\perp min}^2\rangle = m_h^2 + 2m^2\sigma_\tau^2$. Where m_h is the hadron mass and σ_τ denotes the width in the distribution of τ-directions. The equations can be solved iteratively without this approximation, but we find that our results are unaffected by this approximation.

5.7 Is screwiness observable?

In this section we will address the question of whether introducing a correlation between y and ϕ of the string break-up vertices has observable consequences for the produced particles. There are two processes which in principle can destroy such a correlation. Firstly, there is the initial particle production and secondly, there are resonance decays. The initial particle production spoils things because even if the vertices lie on a perfect helix the produced particle will usually not lie on the line between its two constituent vertices in the (y,ϕ)-plane. The particle production fluctuations are mainly in rapidity, i.e. a particle is produced with an azimuthal angle which roughly corresponds to the average

angle of its constituent vertices, while its rapidity is distributed with width unity around the average of the vertices.

To study the consequences of the screwiness model we have generated events with three different values $\langle\tau\rangle = 0.3, 0.5$ and 0.7. For each value we have tuned the parameters of the model to agree with the multiplicity, rapidity and transverse momentum distributions of default JETSET. In this way we can study the correlations introduced by the model as compared to the ordinary Lund string model. We have tuned m to get the default average $p_\perp$ of the produced particles, utilizing the fact that the product $m\tau$ is the important factor. The parameter b has been changed from the default JETSET value to tune the multiplicity, and σ_τ has been tuned to get the final charged $p_\perp$ fluctuations. Tuning with different $\langle\tau\rangle$ values results in the parameter values shown in Table 5.1. We note in particular that to get the multiplicity distributions of default JET-

$\langle\tau\rangle$	0.3	0.5	0.7
m	1.0	0.71	0.61
b	0.64	0.68	0.7
σ_τ	0.2	0.3	0.35

Table 5.1: Parameter values. The model has been tuned to the multiplicity and charged final $p_\perp$ distributions of default JETSET ($b = 0.58$).

SET only minor changes of the b-parameter are needed. We also note that the restriction in Eq.(5.19) is satisfied for all the cases since in this model only a fraction of the energy available in the Lund string is used to produce transverse momenta.

We have generated pure $q\overline{q}$ events and the particles in the central rapidity plateau have been included in the analysis. The plots shown are for four units of rapidity, but the qualitative results for observable screwiness are unaffected for values as low as approximately three units of central rapidity. We have analysed the properties of the generated events by means of the screwiness measure, defined in Eq.(5.13). Here, the second sum in the measure instead goes over the hadrons or over the break-up vertices. The weight P_e is of course unity for all events.

In Fig.(5.8) the screwiness for the break-up vertices is shown. It has a clear peak for the different values of $\langle\tau\rangle$, and the ω-values for the peaks correspond to the average τ values used. The screwiness for the initially produced particles is shown in Fig.(5.9). We note that the peak vanishes for small values of τ. A helix where the windings are separated by two units of rapidity corresponds to $\tau = 1/\pi$. The vanishing of the signal for small τ values is therefore in agreement

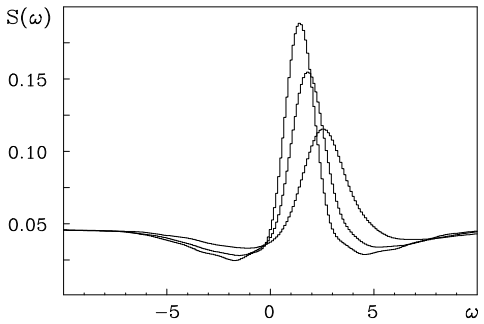

Figure 5.8: Screwiness for the string break-up vertices. The three curves shown are for $\langle\tau\rangle = 0.3,\ 0.5$ and 0.7, respectively. There is a clear peak at $\omega \simeq 1/\langle\tau\rangle$ in all the cases.

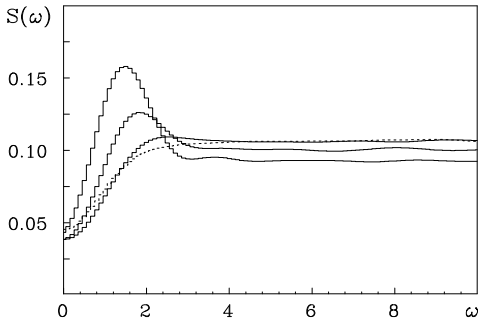

Figure 5.9: Screwiness for the directly produced particles. The three solid curves are for $\langle\tau\rangle = 0.3,\ 0.5$ and 0.7, respectively. The peak decreases as $\langle\tau\rangle$ is reduced. For $\langle\tau\rangle = 0.3$ the peak has vanished due to the fluctuations in particle production. The screwiness for default JETSET (dashed line) has been included for comparison.

with our findings for the rapidity fluctuations in the particle production. For comparison we have included the screwiness for the initial particles produced by default JETSET in Fig.(5.9). As expected no signal is found in this case. The screwiness is further diluted by resonance decays, but it is still visible for not too small τ values as shown in Fig.(5.10).

To try to enhance the signal we have investigated how the screwiness measure depends on multiplicity and the transverse momentum of the particles. Selecting events with large initial multiplicity enhances the signal. However, analysing events with different final multiplicities separately does not give an

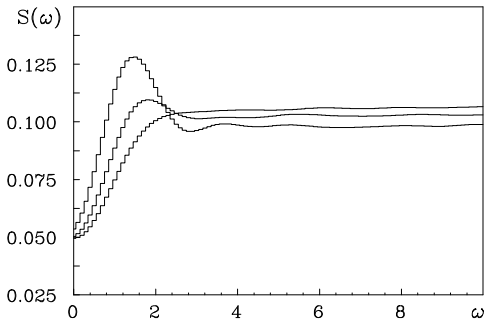

Figure 5.10: Screwiness for the final particles (π^0's are set stable). The three curves shown are for $\langle\tau\rangle = 0.3,\ 0.5$ and 0.7, respectively. For not too small $\langle\tau\rangle$-values there is a peak at $\omega \simeq 1/\langle\tau\rangle$.

enhancement of the signal. The influence of resonance decays on the multiplicity is too large.

Selecting events where $\langle p_\perp^2 \rangle$ is large enhances the signal when decays are not included. This is shown for $\langle\tau\rangle = 0.3$ in the left part of Fig.(5.11) where events with $\langle p_\perp^2 \rangle > 0.3$ GeV^2 for the initial particles have been selected. As shown in the figure this event selection results in the signal surviving particle production even for small $\langle\tau\rangle$-values. This event selection is also profitable when it comes to decreasing the effects of resonance decays since events with many decay products are not likely to be selected. In the right part of Fig.(5.11) we show the screwiness for the final state particles in events where $\langle p_\perp^2 \rangle > 0.25$ GeV^2. The curves shown are for $\langle\tau\rangle = 0.3$ to show that with event selection a signal can be obtained *even for this case*. Using the same event selection of course enhances the signal for larger $\langle\tau\rangle$-values, but in those cases it was clearly visible in the total sample.

A total of 50000 $q\overline{q}$ events have been used in the analysis, except in the event selection analysis in Fig.(5.11) where 250000 events are analysed. To be able to observe screwiness for such a small $\langle\tau\rangle$-value one needs to increase the number of events by a factor of about five compared to the larger values. Since we have only used positive $\langle\tau\rangle$-values, events with a preferred rotational direction are generated. We could have included both rotational directions in the event generation which would add a signal for negative ω, but reduce the statistics by a factor of two.

The effects on the screwiness from hard gluons stemming from the parton cascade will be investigated in future work. However, since only a fairly small

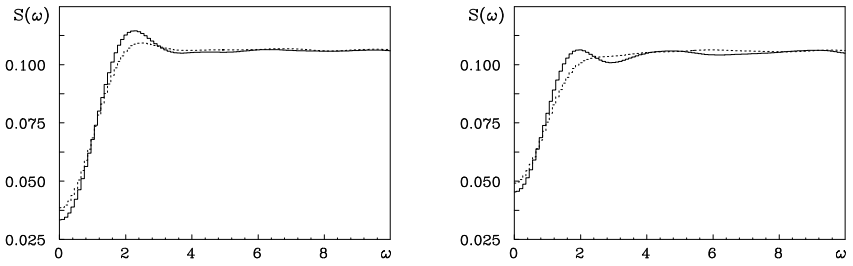

Figure 5.11: Screwiness for $\langle\tau\rangle = 0.3$. To enhance the signal events where $\langle p_\perp^2\rangle$ is large have been selected (solid lines). We have included the corresponding curve with no event selection (dashed lines) to indicate the improvement. Left) Initially produced particles. $\langle p_\perp^2\rangle > 0.3$ GeV^2. Right) The final particles. π^0's are set stable. $\langle p_\perp^2\rangle > 0.25$ GeV^2.

number of events are needed for the results in this paper we expect that investigations of experimental data, in which hard gluon activity is excluded, can be profitable.

A specific property of our model is that $\langle p_\perp^2\rangle$ for directly produced pions is smaller than $\langle p_\perp^2\rangle$ for heavier particles. This feature appears to be in agreement with experimental data on two-particle correlations [13]. A model for correlations in $p_\perp$ in the string hadronization process with similar consequences was introduced in [14]. The $p_\perp$ for directly produced pions and ρ's are shown for the screwiness model in Fig.(5.12) and the distributions are clearly different. In the figure we also show the $p_\perp$ distribution of the final pions and compare it to the default JETSET distribution. As seen the secondary pions wash out the differences. The $\langle p_\perp\rangle$ for various flavours at the initial production level depend on the screwiness parameters, but the qualitative difference remains.

5.8 Conclusions

It is perhaps surprising that such an ordered structure as a helix could emerge at the end of the QCD cascade. However, when we consider the constraint imposed by helicity conservation, we see that purely random configurations of gluons are disfavoured. This is because the exclusion region around each gluon restricts the maximum number of allowed gluons. Instead we see that the gluons can achieve the maximum concentration by close packing themselves into the form of a helix. The fragmentation of this screwy field has consequences for the final state particles. Although the fragmentation cannot be described in

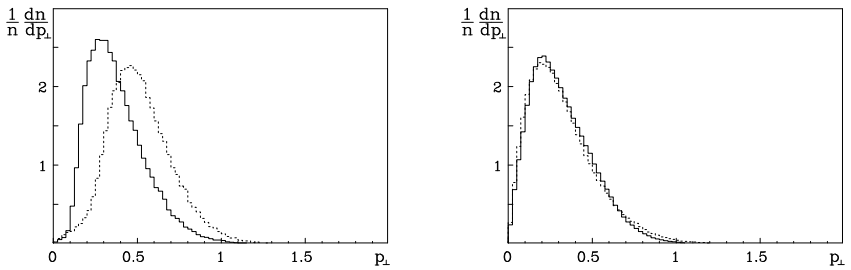

Figure 5.12: Left) The $p_\perp$ (GeV) distributions for the directly produced π's (solid) and ρ's (dashed). The curves shown are for $\tau = 0.5$. Right) The $p_\perp$ (GeV) distributions for the all final pions (solid), π^0's are set stable, as compared with default JETSET (dashed).

terms of gluon excitations of the Lund string, we have instead modified the Lund fragmentation scheme. If the winding is within reasonable limits then we expect "screwiness" to be an observable feature of the QCD cascade.

Acknowledgments

We thank Patrik Edén for very many valuable discussions. This work was supported in part by the EU Fourth Framework Programme 'Training and Mobility of Researchers', Network 'Quantum Chromodynamics and the Deep Structure of Elementary Particles', contract FMRX-CT98-0194 (DG 12 - MIHT).

5.A Problems with fragmenting soft gluons

In section 5.4 we claimed that the helix colour-field cannot be implemented as an excited string, since gluons softer than $k_{\perp 0} = 1.6\,\mathrm{GeV}$ cannot be considered as excitations of the string.

To illustrate the problems with fragmentation of soft gluons we have investigated JETSET fragmentation of parton configurations with soft gluons emitted according to the Dipole Cascade Model as implemented in the ARIADNE Monte Carlo [15]. The allowed $k_\perp$ range for emissions from the colour dipoles is normally between an upper value, given by phase-space limits, and a lower infra-red cut-off, $k_{\perp c}$. We have instead used a small maximum allowed $k_\perp$ value (denoted $k_{\perp \max}$) to restrict the hardness of the emitted gluons. This

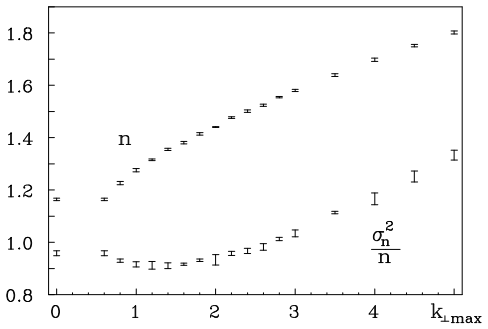

Figure 5.13: The multiplicity in central rapidity per unit of rapidty n and the corresponding variance σ_n^2 depends on the upper cut-off in the cascade $k_{\perp\max}$ (GeV) as shown. Default JETSET has been used for fragmentation and σ_n^2/n does not start to increase until $k_{\perp\max}$ is roughly 1.6 GeV

soft cascade has been applied to $q\overline{q}$-dipoles oriented along the z-axis. The soft gluons have a negligible impact on the event topology and for our purposes it therefore makes sense to define rapidity with respect to the z-axis. We have analysed the resulting hadrons in the central rapidity plateau of the events. To emphasize the features of fragmentation of soft gluons we have not included resonance decays in our analysis.

In Fig.(5.13) we show how the average and the squared width of the central multiplicity distribution depend on $k_{\perp\max}$. The effect of the soft gluons is an increase of the average multiplicity while the multiplicity fluctuations remain constant or even decrease until $k_{\perp\max}$ is above $k_{\perp 0}$. The $\langle p_\perp \rangle$ with respect to the z-axis of the hadrons only increases from 0.46 GeV for a flat string with no gluon excitations to 0.56 GeV for $k_{\perp\max} = 3$ GeV. Changing the generated $\langle p_\perp \rangle$ by such a small factor has a minor effect ($\sim 5\%$) on the average multiplicity in pure $q\overline{q}$ events whilst adding the soft gluons increases the average multiplicity by roughly 40%, as shown in the figure. As mentioned in section 5.4, we find that the soft gluons essentially only increase the hadron multiplicity. The number of gluons per rapidity unit varies from 0.25 for $k_{\perp\max} = 1$ GeV to 0.7 for $k_{\perp max} = 5$ GeV. The situation is even worse in the case of the helix field where the expected number of soft gluons per unit of rapidity is significantly larger. We conclude that gluons softer than $k_{\perp 0}$ cannot be implemented inside the Lund Model as individual gluonic excitations of the string.

We will end this appendix with an interpretation of the Lund fragmentation model, which provides us with the possibility to relate $k_{\perp 0}$ to the b-parameter in

the model. The result in Eq.(5.20) (although derived semi-classically) can be interpreted quantum-mechanically by a comparison to Fermi's Golden Rule. It equals the final state phase space times the square of a transition matrix element $|\mathcal{M}|^2 = \exp(-bA)$. There are two such quantum-mechanical processes, Schwinger tunneling and the Wilson loop integrals, which can be used in this connection (and they result in very similar interpretations of the parameters). For the Schwinger tunneling case we note that if a constant (κ) force field is spanned across the longitudinal region X during the time T with a transverse size $A_\perp$ then the persistence probability of the vacuum (i.e. the probability that the vacuum should not decay by the production of new quanta) is [16]

$$|\mathcal{M}|^2 = \exp(-\kappa^2 X T A_\perp \Pi) \quad . \tag{5.30}$$

Here the number Π only depends upon the properties of the quanta coupled to the field; for two massless spin 1/2 flavours it is $\Pi = 1/12\pi$. Comparing the result in Eq.(5.30) to Eq.(5.20) we find that the parameter $b = A_\perp/24\pi$ (taking into account that the Lund model area is counted in lightcone units). From Eq.(5.14) we obtain the minimum transverse size of the field from which it then follows that the b-parameter in the Lund model must be $b \geq \pi/24\kappa \simeq 0.6$ GeV^{-2}. This is evidently just in accordance with the phenomenological findings in the Lund model for the parameter b. Further, considering the distribution in Eq.(5.22) for the transverse momentum of a produced $q\overline{q}$-pair breaking the string we recognise the quantity ℓ^2_{min} in the exponential fall-off. We may conclude that there is a wave-function for the Lund string in transverse space with just the right transverse size to allow the "ordinary" transverse fluctuations in momenta.

References

[1] R.K. Ellis, D.A.Ross and A.E. Terrano, *Nucl. Phys.* **B178**, 421 (1981)

[2] Ya.I. Azimov, Yu.L. Dokshitzer, V.A. Khoze and S.I. Troyan, *Phys. Lett.* **B165**, 147 (1985)

[3] B. Andersson, G. Gustafson and C. Sjögren, *Nucl. Phys.* **B380**, 391 (1992)

[4] G. Gustafson, *Phys. Lett.* **B175**, 453 (1986)
G. Gustafson and U. Pettersson, *Nucl. Phys.* **B306**, 746 (1988)

[5] G. Gustafson, *Nucl. Phys.* **B392**, 251 (1993)

[6] B. Andersson, G. Gustafson and J. Samuelsson, *Nucl. Phys.* **B463**, 217 (1996)

[7] G. Marchesini, B.R. Webber, *Nucl. Phys.* **B238**, 1 (1984)

[8] T. Sjöstrand, *Comp. Phys. Comm.* **82**, 74 (1994)

[9] N.K. Nielsen, *Nucl. Phys.* **B167**, 249 (1980)

[10] B. Andersson, G. Gustafson, M. Ringnér and P. Sutton, *hep-ph*/9808436 and *LU TP* 98-15, (1998)

[11] B. Andersson, G. Gustafson and B. Söderberg, *Z. Phys.* **C20**, 317 (1983)

[12] T. Sjöstrand, *Nucl. Phys.* **B248**, 469 (1984)

[13] TASSO coll. W. Braunschweig et. al., *Phys. Lett.* **B231**, 548 (1989)

[14] B. Andersson, G. Gustafson and J. Samuelsson, *Z. Phys.* **C64**, 653 (1994)

[15] L. Lönnblad, *Comp. Phys. Comm.* **71**, 15 (1992)

[16] J. Schwinger, *Phys. Rev.* **82**, 664 (1951)
N.K. Glendenning and T. Matsui, *Phys. Rev.* **D28**, 2890 (1983)